Dissertation

submitted to the

Combined Faculties for the Natural Sciences and for
Mathematics

of the Ruperto-Carola University of Heidelberg,
Germany

for the degree of

Doctor of Natural Sciences

put forward by

Benjamin John King MSci.

born in Leeds, United Kingdom

Oral examination: 2$^{\text{nd}}$ June 2010

Vacuum Polarisation Effects in Intense Lasers Fields

Referees: Prof. Dr. Christoph H. Keitel

Prof. Dr. Jan M. Pawlowski

Zusammenfassung

Die Polarisation des Vakuums durch ein externes elektromagnetisches Feld ist gemäß theoretischer Vorhersagen die Ursache verschiedener nichtlinearer Prozesse. Angesichts zukünftiger Laseranlagen mit Intensitätsbereichen, die um Größenordnungen jenseits der heutigen experimentellen Grenzen liegen, wird eine konkrete Untersuchung von Vakuumpolarisationseffekten erforderlich. Anhand der Streuung von Photonen eines Probelichtstrahls an zwei ultrastarken Laserstrahlen beschreiben wir ein neues experimentelles Szenario, in dem das Vakuumsignal durch Interferenzeffekte vom Probehintergrund getrennt werden kann. Durch die Betonung experimenteller Aspekte stellen wir ein realistisches Szenario vor, mit dem man erstmals eine reelle, elastische Photon-Photon-Streuung beobachten könnte. Dadurch zeigen wir außerdem, wie man prinzipiell mit starken Laserstrahlen einen Doppelspalt aufbauen kann, der ausschließlich aus Licht besteht. Darüber hinaus weisen wir nach, dass ein solcher Aufbau die Erwartungswerte der Vakuum-Doppelbrechung und des Dichroismus im Vergleich zu konventionellen Zweistrahl-Stoßexperimenten erhöht. Dies wird durch eine theoretische Methode ergänzt, die sowohl eine endliche Temperatur als auch die Vakuumpolarisation gemeinsam beschreibt. Indem wir diese Methode auf den Fall eines sogenannten „constant crossed" Feldes anwenden, berechnen wir, wie sich der thermische Vakuumdruck unter dem Einfluss dieses externen Feldes ändert.

Abstract

Polarisation of the vacuum by an external electromagnetic field is predicted to lead to an array of non-linear processes. In light of upcoming laser facilities that will access intensity ranges orders of magnitude above current limits, the continued study of vacuum polarisation effects is both necessary and timely. By considering how photons from a probe laser field are scattered by two ultra-intense laser beams, we present a novel experimental scenario in which interference effects separate the vacuum signal from the probe background. By placing emphasis on experimental considerations, we demonstrate a realistic arrangement that could be used to observe, for the first time, real, elastic, photon-photon collisions. In doing so, we also show how strong-field lasers can in principle be used to generate a double-slit experiment consisting entirely of light. Moreover, such a set-up is also shown to modestly increase vacuum birefringence and dichroism over traditional two-beam collisions. We complement this by expounding an original theoretical method that incorporates both finite temperature and vacuum polarisation in a common setting. By employing this method on the case of a constant crossed field, we calculate the resulting change in the pressure of the vacuum in an external field.

In connection with work performed during the thesis, the following paper was published in a refereed journal:

- B. King, A. Di Piazza, C. H. Keitel, *A matterless double slit*, Nature Photonics **4** (2), 92–94 (2010).
  See also:

  - Cover of the February 2010 issue of Nature Photonics
    http://www.nature.com/nphoton/journal/v4/n2/covers/
    index.html

  - M. Marklund, *Fundamental optical physics: Probing the quantum vacuum*,
    Nature Photonics **4** (2), 72–74 (2010)
    (news and views article on the above paper)

  - Press release by the Max Planck Society (in German)
    http://www.mpg.de/bilderBerichteDokumente/dokumentation/
    pressemitteilungen/2010/pressemitteilung20100108/index.html

  - Press release at the IDW
    http://idw-online.de/de/news350807

  - Physik Journal 3, 24 (2010) - Pro Physik (in German)
    http://www.pro-physik.de/Phy/leadArticle.do?laid=12547.

The following paper is to be submitted after completion of the thesis (April 2010):

- B. King, A. Di Piazza and C. H. Keitel, *Double-slit vacuum polarisation effects in ultra-intense laser fields.*

Results from work on the thesis currently in preparation:

- B. King, A. Di Piazza and C. H. Keitel, *Thermal effects in vacuum polarisation.*

Contents

Appendices

Chapter 1

Introduction

Does the concept of a vacuum, a region of empty space, have any real-world existence? This and similar questions have preoccupied thinkers since antiquity with exchanges between Parmenides and Leucippus culminating in Aristotle's definitive remark *horror vacui* or "nature abhors a vacuum". Indeed, the question has persisted with the famous Michelson-Morley experiments arguing against a classical aether or preferential co-ordinate system, only to be re-questioned a century later with concepts such as ,,dark energy" and quintessence to explain cosmological expansion. Even without mentioning the role of a quantised vacuum on spontaneous emission of atoms and the Casimir force, questions of the vacuum remain a vehicle for theoretical enquiry.

Soon after Dirac developed a wave equation for spin-1/2 particles, Klein calculated that when electrons, mass m, impinge on a square electromagnetic barrier of height $V_0 \gtrsim 3mc^2$, for speed of light in vacuo c, not only are more reflected than were incident, a large proportion is also transmitted through the barrier with a negative mass. Sauter then refined this calculation for smooth potentials and achieved the key result that only if the rise distance was less than the reduced Compton wavelength, $\lambda = \hbar/mc$, for $\hbar$ equal to Planck's constant over 2π, would electrons penetrate. Resolution of *Klein's paradox* comes when one permits a second continuum of particle states for negative energies $E < -mc^2$, the *Dirac sea* in Dirac's *hole theory*, which is now associated with the positron ensemble. In light of these findings, Euler and Heisenberg and independently Weisskopf then calculated, in an effective theory, the correction to Maxwell's equations brought about by a *polarisation of the vacuum* by a constant electromagnetic (EM) field, the results of which still form the basis of many applications to detect vacuum polarisation effects (VPEs) [104, 156, 84, 181].

The modern interpretation of the vacuum is rooted in quantum field theory (QFT), which describes particles using an analogy of excitations of a harmonically oscillating field which permeates spacetime. In the absence of particles, instead of being devoid of energy, in this picture, the vacuum comprises the lowest energy or vacuum- modes of the field, also known as "zero-point" fluctuations. QFT then envisages the vacuum as a bath of "virtual" particles which can mediate interactions between real ones. In line with the uncertainty principle these particles are suitably ephemeral and obey other fundamental symmetries of the QFT at hand, such as charge conjugation. Sufficiently strong external fields can then promote virtual particles out from the quantum vacuum into existence, reproducing the results of Dirac's hole theory.

Owing to the light degrees of freedom, the relativistic and gauge-invariant theory of quantum electrodynamics (QED) has been the most successful in posing and answering questions of the quantum vacuum. Virtual electron-positron pairs, in line with Sauter's calculations, are regarded to be active over the length scale of the reduced Compton wavelength. These virtual loops couple to photons and can be regarded as giving the photon a finite size and mass, affecting its dispersion. The virtual fermion loops can be polarised by external electromagnetic fields, which by Le Chatelier's principle must act to damp the field in a manner similar to Lenz's law. Virtual photons on the other hand, are emitted and reabsorbed by electrons and can be thought to smear out the charge distribution and correct the electrons' mass, taking into account its EM field and being responsible for the anomalous magnetic dipole moment not being exactly equal to two as predicted by the Dirac equation. As the coupling scales in an external Coulomb field with $\sim Z\alpha$, for a charge Z and fine-structure constant $\alpha = e^2$ (using the cgs system of units), around heavy nuclei such as uranium ($Z\alpha \approx 0.67$) the effect can become appreciable. As the $2s_{1/2}$ wavefunction has a non-zero overlap with the nucleus, due to either "screening of the nuclear charge" from vacuum polarisation (Uehling potential) or "smearing of the electron charge", the energy is shifted 1057 MHz higher than the $2p_{1/2}$ which has no nuclear penetration, known as the *Lamb shift* or *hyperfine splitting*, one of the experimental results not predicted by the Dirac equation and key to the formulation and success of QED due to Dyson, Feynman, Tomonaga and Schwinger at the end of the 1940s [109, 55, 65, 157].

The study of effects of the polarised vacuum proceeds in *strong field QED* in which the usual external fields treated are either i) constant (or slowly-varying); ii) Coulombic; iii) wave-like. In all cases, the coupling can become so large that representing the action of the external field perturbatively fails, with the only solution being to use the exact solution for propagators in the external field where just the interaction between quantised particles is seen as perturbative - the so-called *Furry picture* [70]. This emphasises the *non-perturbative* nature of strong-field QED and when the coupling to the external field becomes large enough, processes involving multiple field interactions can be significant, hence making the problem also *non-linear*. If we imagine the typical situation of an incoming particle, electron or photon, with momentum p^μ in an external field of frequency ω and electric and magnetic field strength E and B respectively, effects of the polarised vacuum can be quantified using two gauge-invariant Lorentz scalars ξ and χ. First, the degree of non-linearity can be quantified by the invariant *classical* parameter $\xi = eE/mc\omega$ for electron charge $-e < 0$, equal to the work the field can perform over the reduced Compton wavelength $eE\lambda$ in units of field energy quantum and therefore represents the mean number of external field photons involved in a typical process. To what degree the effects are *quantum*, can be ascertained with a second invariant parameter $\chi = e\hbar\sqrt{|(F_{\mu\nu}p^\nu)^2|}/(mc)^3$, for field strength tensor $F_{\mu\nu}$. For massive particles, this is equal to the work done by the field over the reduced Compton wavelength in the particle's rest-frame in units of the electron rest energy mc^2. The $\hbar$ factor emphasises that the conversion of radiation to matter and vice versa has no classical analogue.

When the external field becomes strong enough, the vacuum undergoes a phase transition and becomes conducting, through spontaneous generation of electron-positron pairs. If one consider just photons, this can occur either i) when the photon energy $\hbar\omega \geq 2mc^2$ in some QED background (required for energy-momentum conservation) decay; or ii) when the photon energy flux reaches the *critical intensity*

$I_{cr} = (m^2 c^3/e\hbar)^2/8\pi = 2.3 \times 10^{29}$ Wcm^{-2} as already shown by Euler and Heisenberg in the case of a constant EM field, corresponding to critical electric and magnetic fields $E_{cr} = m^2 c^3/e\hbar = 1.3 \times 10^{16}$ Vcm^{-2}, $B_{cr} = m^2 c^3/e\hbar = 4.4 \times 10^{13}$ G.

Vacuum polarisation effects can be classified as either i) dissipative, involving real pair creation or ii) refractive, where only virtual particles mediate interactions. Dissipative effects are perhaps the most dramatic manifestation of a polarised vacuum, but as Schwinger showed with his famous expression for the rate of pair creation in a constant EM field per unit volume per unit time, which for weak fields $eE \ll m^2$ becomes $(eE_0/\pi)^2 \exp(-\pi E_{cr}/E_0)$, the exponential dependence on $-E_{cr}/E_0$ represents a large technical barrier, which has yet to be overcome. However, recent results show that for non-trivial field configurations, even intensities as low as $10^{-5} I_{cr}$ can in principle lead to prolific pair-creation [135, 20, 103, 53]. The single measurement of radiation converted into particle pairs in a vacuum remains the elegant 144d experiment conducted more than a decade ago at SLAC National Accelerator Laboratory [34] in which photons, back-scattered by a beam of electrons collided with other background photons via the Breit-Wheeler process ($\gamma_1 \gamma_2 \rightarrow e^+ e^-$) and decayed into ~ 106 particle pairs. Refractive VPEs by contrast, allow elastic photon collisions, the non-linearity of which provides for a rich spread of phenomena. Alongside photon-photon scattering (vacuum diffraction, or ray-bending), photon-splitting, photon-merging (high-harmonic generation) as well as photon polarisation rotation (vacuum dichroism) and photon ellipticity effects (vacuum birefringence) are all predicted to occur [102, 169, 63, 26, 32, 141, 62, 129, 82, 142]. Collective effects such as photon acceleration (continual change of frequency of photons in a laser beam), EM wave collapse, photon bullets and light wedges have also been predicted to occur [126, 123, 121, 161, 122]. Although such effects have been calculated in a variety of situations, with calculations having been performed in the field of magnetars (where $B_0 \gtrsim 10^{13} G$ can cause light-ray bending and photon acceleration) [138], heavy-ion collisions (in which superheavy nuclei are formed and the total $Z > Z_{cr} = 170$), proton-proton collisions [96], the field of heavy nuclei, constant laboratory magnetic fields and also in lasers, of these, only photon-photon scattering in the field of a heavy nucleus (Delbrück scattering) [183] and photon-splitting in atomic fields [6] have been experimentally observed.

An example typical scaling of $\exp(-\pi E_{cr}/E_0)$ in the case of dissipative or I_0/I_{cr} in the case refractive VPEs highlights the experimental challenge in investigating effects of the polarised vacuum. The HERCULES laser currently holds the record for the highest laser intensity, which stands at 2×10^{22} Wcm^{-2}, some seven orders of magnitude lower than the critical value [187]. However, in light of the forthcoming ELI and HiPER laser facilities, both of which expect to offer intensities of the order $\sim 10^{26}$ Wcm^{-2} or $\xi \approx 690$, ($\chi \approx \times 10^{-7}$ for head-on photon-photon scattering), signatures of the polarised vacuum should be detectable [60, 86]. Lasers offer an advantage over many other EM backgrounds in that they are i) readily tunable and ii) "clean" without signatures from hadrons or QCD (quantum chromodynamics). The prospect of using lasers to probe for the first time the unexplored low-energy regime of our hitherto most accurate theory of nature has triggered interest in hypothetical particles which could explain any unexpected deviations from QED. The veritable menagerie includes *WISPs* (Weakly-Interacting Sub-eV Particles) such as axions or *ALPs* (Axion-Like Particles) including scalar and pseudo-scalar particles, as well as *MCPs* (Mini-Charged Particles), which often arise in theories containing extra spacetime dimensions as well as *unparticles*, which unlike particles, would have a

continual mass spectrum [75, 4, 3, 80, 170, 39]. These exotic scenarios are possible outcomes of photon-photon scattering and pair-creation experiments, both of which appear in this work.

Whilst it can be phrased in the terminology of high-energy physics, the polarised vacuum can also be used to generate interference effects, finding application in quantum optics [101, 102]. The famous double-slit experiment, first recorded by Thomas Young in 1804 using two pinholes in a slip of card [188], and later recreated by Geoffrey Ingram Taylor using very weak light sources [165], has been central to the interpretation of quantum mechanics as it exhibits wave-particle duality in a clear manner, leading to Dirac's statement that "each photon then interferes only with itself"[47]. This phenomenon continues to be challenged [159, 184, 116, 100] and demonstrated in a broad range of set-ups using neutrons, helium atoms, C_{60} fullerenes, Bose-Einstein condensates and biological molecules [190, 36, 11, 9, 81]. In addition, whilst first being shown to diffract in crystals in the 1920s, electrons have also been shown to generate interference effects, even with only one particle in the apparatus at a time [45, 94, 127, 171]. All previous examples however, have only displayed how light or matter diffract on interaction with matter in the double-slit. Using the polarised vacuum, it is in principle possible to construct a double-slit comprising ultra-intense lasers and hence demonstrate the diffraction of light with light.

Polarisation of the vacuum can be caused by other particles such as quarks and light mesons [64] as well as in other settings such as in non-trivial spacetimes, strong gravitational fields around e.g. black holes and neutron stars [87, 144, 35, 88, 76], in QCD [106], as well as in a hot radiation plasma [182, 123]. Finite temperature vacua are particularly interesting as they offer typically i) broadband radiation ii) more realistic calculation iii) the possibility of measuring the effect of the polarised vacuum from thermodynamic quantities. Moreover the rate of production of real electron-positron pairs can be increased not only by using stronger fields but also by increasing temperature [49]. However, neither for inhomogeneous external fields nor for non-equilibrium systems do there exist definitive results and clarity of method in four-dimensional QED at finite temperature, with it requiring a decade to ascertain even whether pair-creation occurred at all in the one-loop effective Lagrangian [41, 117, 71, 57, 49]. Finite temperature, strong-field QED, being a gauge theory with large coupling constant ($Z\alpha$ for nuclei or $\sim \alpha\chi^{2/3}$ for lasers [151]) could also be used to better understand the mechanisms at play in the formation of the QGP (quark-gluon plasma), especially when studied in non-equilibrium situations, undergoing a phase transition at a critical temperature $T_{cr} \sim 10^{10}$ K.

The current thesis expounds upon a realistic scenario to detect VPEs. We envisage scattering probe laser photons off of two ultra-intense laser beams, using the interference between the signals to spatially separate the intensity of the vacuum signature from the probe background, resulting in a "matterless double-slit" effect. An additional outcome of this set-up is that vacuum birefringence and dichroism are also increased over standard two-laser collisions. Moreover, considering experimental application, we show that the effect should be measurable at upcoming laser facilities to be completed by the end of the decade. In addition, we also consider the polarisation of the vacuum by a constant crossed field in a finite temperature setting, which we show changes macroscopic thermodynamical quantities by calculating the resulting increase in pressure.

After some useful preliminary notes on nomenclature and units, we begin in **chapter 2** by introducing effective field theory, in particular applied to QED, including details of the heat kernel method of evaluating resulting functional determinants which is applied by way of example to the case of a constant magnetic field. The chapter is then concluded with a discussion of the Euler-Heisenberg Lagrangian, the weak-field expansion of which will form the basis of calculations for our photon scattering scenario.

Calculations for photon-photon scattering are then presented in **chapter 3**, in which a weaker probe field is diffracted by two separated ultra-intense laser beams in two different set-ups with both optical and X-ray frequencies investigated. We first derive the field scattered by the polarised vacuum, and then study two intensity terms that come from this vacuum signal, the pure signal itself and the interference with the probe background, and conclude with numerical results for the corresponding number of diffracted probe photons. Calculations for the rotation of the probe polarisation and the induced ellipticity are then detailed, and the corresponding improvement over the typical probe + strong-beam collision investigated. A comprehensive discussion of the validity of employed approximations and measurability of the effects then concludes the chapter.

We outline the derivation of the polarisation operator that describes photon scattering in an external plane wave in **chapter 4**, which is supplemented by calculations and identities given in **appendix A**. The result is then specialised to the case of a constant crossed field, for which the modified refractive indices are derived and their asymptotic limits. Details of the form of relevant special functions as well as the derivation of asymptotic limits are contained in the supplement in **appendix B**.

Averaging the photon scattering solution summed over a thermal ensemble, initial calculations investigating the effect of temperature on vacuum polarisation effects in a constant crossed field are presented in **chapter 5**. We calculate the change in pressure induced by elastic photon-photon scattering between the thermal photons and the external field and also include tentative calculations for how the rate of pair-creation scales with temperature. We detail the various approaches to thermal and non-equilibrium field theory which are complementary to this direct averaging approach in **appendix C**.

1.1 Conventions and Nomenclature

In order to reduce confusion, we explain notational issues here. Throughout the thesis we use cgs units, unless otherwise stated, and we will often use natural units, in which $c = \hbar = 4\pi\epsilon_0 = 1$.

In natural units, we will give energies and hence frequencies and inverse distances in electron volts (eV). The mass of the electron is in these units 0.511 MeV. Some useful conversion factors when dealing with lasers are:

When we use the terminology four-vector we are referring to Lorentz-invariant objects. Three-vectors are emboldened **k** and the components of four-vectors k will

Notation guide	
$-e < 0$	electron charge
$\alpha = e^2$	fine-structure constant (cgs units)
$\eta^{\mu\nu} = \mathrm{diag}(+,-,-,-)$	Minkowski metric
$g^{\mu\nu}$	general metric
ω	frequency
k_{B}	Boltzmann constant
c	speed-of-light in vacuo
$\hbar$	Planck's constant
ϵ_0	Permittivity of free space
$\dagger$	Hermitian conjugate
T	transpose
$\gamma^\mu,\ \gamma_\mu$	Gamma matrices
$\not{a}$	$\gamma^\mu a_\mu$
$\dot{\mathbf{v}}$	$d\mathbf{v}/dt$

$$
\begin{aligned}
1.60 \times 10^{-19}\ \mathrm{J} &= 1\ \mathrm{eV} \\
1 \times 10^{-15}\ \mathrm{s} = 1\ \mathrm{fs} &= 0.66\ \mathrm{eV}^{-1} \\
1 \times 10^{-6}\ \mathrm{m} = 1\ \mu\mathrm{m} &= 5.07\ \mathrm{eV}^{-1}.
\end{aligned}
$$

be denoted by normal sub- and super- scripts whereas powers will be denoted with a superscript slightly displaced to the right and dot products could be explicitly defined with a $\cdot$ so that for a photon in vacuum with four-momentum k we have $k^2 = k \cdot k = (k^0)^2 - \mathbf{k} \cdot \mathbf{k}$.

Whenever vector labels are dropped, the result applies to all such vectors e.g. for four-vectors a_1, a_2, $\varkappa \cdot a = 0$ implies $\varkappa \cdot a_1 = \varkappa \cdot a_2 = 0$. We will often refer to objects without explicitly writing spacetime indices, i.e. Π will represent the polarisation operator when taken in context.

When we want to emphasise the operator nature of an object, we will use a hat e.g. $f(\hat{p})|p\rangle = f(p)|p\rangle$ and a state $|p\rangle$ is an eigenfunction of the operator $\hat{p}$. In addition, we use ∂_μ to mean partial differentiation with respect to the μth spacetime co-ordinate as well as $g'(x)$ to mean differentiation of the function with respect to its argument, x. Also for fermions, $\bar{\psi} := \psi^\dagger \gamma_0$ and the gamma matrices satisfy $\{\gamma^\mu, \gamma^\nu\} = 2g^{\mu\nu}$.

Chapter 2

Effective field theory in the context of vacuum polarisation

We introduce EFT (effective field theory) as a means to describe a system whose heavier degrees of freedom have little influence on the dynamics. A method of evaluating the resulting functional determinants that occur in the theory is presented, and employed in the pedagogical example of a constant external magnetic field. We make some remarks on the Euler-Heisenberg Lagrangian and give its weak-field expansion, which will be the basis for calculations of photon-photon scattering in Ch. 3.

One of the first examples of an effective field theory was constructed by Euler and Heisenberg as they considered the collision photons in vacuum [84, 83]. Following the elegant rederivation of Schwinger in the 50s [158], the Euler-Heisenberg Lagrangian has found many applications in describing QED vacuum polarisation processes. The weak field expansion $E \ll E_{\mathrm{cr}}$ is particularly useful as it provides the leading-order quantum correction to classical quantities. It has been employed to describe a multitude of refractive vacuum polarisation effects such as the modified refractive index [82] (photon dispersion), photon splitting in arbitrary slowly-varying electromagnetic fields [26, 2], vacuum four-wave mixing [118], vacuum birefringence and dichroism [85, 142, 82], photon-photon scattering [142, 169, 63, 102] and in the context of laser pulse propagation in plasmas [123, 121, 161, 122]. Moreover as the imaginary part of the Lagrangian is directly related to dissipative effects, the EH Lagrangian has also been used extensively to describe pair creation [172, 54, 123], often in the form of the famous pair-production formula in constant external fields derived by Schwinger [158]. In addition, the EH Lagrangian has also found application at finite temperatures [48], again applied to pair-production [41, 117, 71, 57, 49] as well as to photon splitting [58] and photon-photon scattering [168]. Other examples of highly successful effective field theories include *Fermi theory* for low-energy weak nuclear interactions, *BCS theory* used to describe properties of superconductors and *general relativity* which is believed to be an effective theory of quantum gravity. In the current thesis, we focus on the case of QED.

2.1 Effective Field Theory

One of the key elements of EFT is that it represent physics occurring on some low energy scale with respect to other degrees of freedom in the field theory. The heavier degrees of freedom are "integrated out" and the object of study is a function only of the lighter fields. In QED, the mass of the electron defines a clear separation between low and high energy phenomena – in electroweak theory it is the mass of the $W^{\pm}$ and Z^0 particles. Effective field theory is simply a rewriting of the original theory in an expression valid at lower momentum scales.

Since we wish to explain processes in a laser, which can typically produce photons with frequencies from the infra-red (energies of the order eV) to the X-ray (keV energies), we are comfortably in a region much lower than that required for spontaneous photon decay into pairs $\omega \ll 2m$, using a system of units $\hbar = c = 4\pi\epsilon_0 = 1$. Therefore, an effective theory of QED should give reliable results.

Let us consider a classical field theory containing a light and a heavy scalar field $\phi_l(x)$, $\phi_h(x)$ and at the end assume the straightforward generalisation to quantum field theory [140]. Labelling the action $S[\phi_l, \phi_h]$, the transition amplitude for this system, for initial and final spacetime co-ordinates $(\mathbf{x}_i, t_i)$, $(\mathbf{x}_f, t_f)$, then becomes:

$$\langle\phi_l(\mathbf{x}_f, t_f), \phi_h\mathbf{x}_f, t_f)|\phi_l(\mathbf{x}_i, t_i), \phi_h(\mathbf{x}_i, t_i)\rangle = \int \mathcal{D}\phi_l \int \mathcal{D}\phi_h \ \mathrm{e}^{iS[\phi_l, \phi_h]}, \qquad (2.1)$$

where:

$$S[\phi_l, \phi_h] = \int_{(\mathbf{x}_i, t_i)}^{(\mathbf{x}_f, t_f)} d^4x \ \mathscr{L}[\phi_l, \phi_h], \qquad (2.2)$$

and where $\mathcal{D}\phi$ defines a path integral measure. A description of the low-energy physics should depend only on the light degrees of freedom so we define a functional $W[\phi_l]$ fulfilling:

$$\langle\phi_{l,f}, \phi_{h,f}|\phi_{l,i}, \phi_{h,i}\rangle \quad = \quad \int \mathcal{D}\phi_l \ \mathrm{e}^{-iW[\phi_l]}, \qquad (2.3)$$

$$\mathrm{e}^{-iW[\phi_l]} \quad := \quad \int \mathcal{D}\phi_h \ \mathrm{e}^{iS[\phi_l, \phi_h]}, \qquad (2.4)$$

where $|\phi_{s,i(f)}\rangle$ are initial (final) configurations of a field ϕ_s. We notice that the right-hand side of Eq. (2.4) can just be written as the transition amplitude of the ϕ_h field given a coupling $J[\phi_l]\phi_h$ for some functional J, typically a polynomial. Let us rewrite the action as:

$$S[\phi_l, \phi_h] = \int_{(\mathbf{x}_i, t_i)}^{(\mathbf{x}_f, t_f)} d^4x \left\{ \mathscr{L}_l + \mathscr{L}_h + J[\phi_l]\phi_h \right\}, \qquad (2.5)$$

for $\mathscr{L}_l = \mathscr{L}_l(\phi_l)$ and $\mathscr{L}_h = \mathscr{L}_h(\phi_h)$. We then define $W[J]$ as the *energy functional* through:

$$Z[J] = \mathrm{e}^{-iW[J]} \quad = \quad \int \mathcal{D}\phi_h \ \mathrm{e}^{i\int d^4x \left(\mathscr{L}_h + J\phi_h\right)} \qquad (2.6)$$

$$= \quad \langle\phi_{l,f}|\phi_{l,i}\rangle, \qquad (2.7)$$

where $Z[J]$ is the quantum-mechanical partition function (briefly reviewed in the context of quantum statistical mechanics in App. C.1), being regarded as a normalisation for expectation values of the field that occur in e.g. Green's functions. Inserting a factor $\mathbb{1} = \exp(-i\hat{H}t)\exp(i\hat{H}t)$ and evolving the states $|\phi_{h,i(f)}\rangle$ to the distant past (future), we can consider slightly rotating the t co-ordinate in the complex plane, to generate a factor $\exp(-\varepsilon\hat{H}|t|)$ for arbitrarily small ε. This can be applied by expanding the field states $\phi_{h,i(f)} = \sum_n |n\rangle\langle n|\phi_{h,i(f)}\rangle$, in a sum of energy eigenstates $\{|n\rangle\}$, and applying the evolution operator for arbitrary large t. This famous adiabatic switching on (off) of the interactions justifies reducing the field states to their vacuum values as the overlap with all higher energy eigenstates dies away, finally giving:

$$\mathrm{e}^{-iW[J]} \rightarrow \langle 0^+|0^-\rangle. \tag{2.8}$$

This relation is the usual starting definition of the energy functional [158]. The energy functional $W[J]$ can be regarded as the (quantum) free energy, and from Eq. (2.8), like the free energy, must tend to 0 in the absence of external perturbations, so that $\langle 0^+|0^-\rangle \rightarrow 1$. We can interpret $W[J]$ better by expanding in terms of a functional Taylor series in J, with each successive term generated by differentiating Eq. (2.6):

$$W[J] = \sum_{n=1}^{\infty} \frac{1}{n!} \int c_n(x_1,\dots,x_n) \prod_{j=1}^{n} J(x_j) d^4 x_n, \tag{2.9}$$

where the coefficients are given by:

$$c_n(x_1,\dots,x_n) = \left[\Big(\prod_{j=1}^{n} \frac{\delta}{\delta J(x_j)}\Big)W[J]\right]_{J=0} \tag{2.10}$$

$$= \frac{\langle 0^+|\phi_h(x_1)\dots\phi_h(x_n)|0^-\rangle}{\langle 0^+|0^-\rangle}. \tag{2.11}$$

One can then show by iteration [140] that:

$$\frac{\delta^n W[J]}{\delta J(x_1)\cdots\delta J(x_n)} = C(x_1,\dots,x_n), \tag{2.12}$$

where $C(x_1,\dots,x_n)$ are the n-point connected correlators. So the free energy $W[J]$ contains all 1PI (one-particle irreducible) connected diagrams and is simply a rewriting of the field theory. Knowing the free energy to all orders is therefore equivalent to the exact theory. We will investigate the one-loop correction, $C(x_1,x_2)$, which is the leading-order correction to the classical theory $C(x_1)$. We denote by ϕ_h^c the classical solution:

$$\phi_h^c = \frac{\delta W[J]}{\delta J} = \frac{\langle 0^+|\phi_h|0^-\rangle}{\langle 0^+|0^-\rangle}, \tag{2.13}$$

which is in some way the "mean-field" in a quantum sense. Now following [140], we can split the Lagrangian up into a piece which is a function of renormalised parameters and one which contains counterterms $\delta\mathscr{L}_h$, $\delta J\phi_h$:

$$\mathscr{L}_h + J\phi_h = \mathscr{L}_h' + \delta\mathscr{L}_h + J'\phi_h + \delta J\phi_h, \tag{2.14}$$

where $J'\phi_h$ is so defined that:

$$\left.\frac{\delta\mathscr{L}'}{\delta\phi_h}\right|_{\phi=\phi_h^c} = -J'. \tag{2.15}$$

We now wish to expand the right-hand side of Eq. (2.6) in a Taylor series around this classical solution. Setting $\phi_h(x) = \phi_h^{\mathrm{c}}(x) + \eta(x)$, we have:

$$\int d^4x \Big(\mathscr{L}' + J'\phi_h \Big) = \int d^4x \Big(\mathscr{L}'[\phi_h^{\mathrm{c}}] + J'\phi_h^{\mathrm{c}} \Big)$$
$$+ \sum_{n=2}^{\infty} \frac{1}{n!} \prod_{j=1}^{n} \left[\int d^4x_j \, \eta(x_j) \frac{\delta}{\delta\phi(x_j)} \right] \mathscr{L}'. \qquad (2.16)$$

Neglecting terms $n \geq 3$, substituting Eq. (2.16) back into Eq. (2.6) and performing the functional integration over $\mathcal{D}\eta$, gives:

$$W[J] = -\int d^4x \Big[\mathscr{L}'[\phi_h^{\mathrm{c}}] + J'\phi_h^{\mathrm{c}} \Big] - \frac{i}{2} \ln\det \left[-\frac{\delta^2 \mathscr{L}'}{\delta\phi_h \delta\phi_h} \right] + \dots$$
$$+ \int d^4x \Big[\delta\mathscr{L}[\phi_h^{\mathrm{c}}] + \delta J \phi_h^{\mathrm{c}} \Big], \qquad (2.17)$$

where ... signify higher-order terms in the expansion and $\delta^2/\delta\phi_h\delta\phi_h$ represents functional differentiation of the field at two different spacetime points. The term $\delta^2\mathscr{L}'/(\delta\phi_h\delta\phi_h)$ will be related to the two-point Green's function as we show for the case of QED in Sec. 2.1.1. The higher-order terms will then be a function of higher derivatives, which are related to higher-order Green's functions and can be neglected in our treatment at zero temperature[1].

The effective action $\Gamma[\phi_h^{\mathrm{c}}]$ can be defined:

$$\Gamma[\phi_h^{\mathrm{c}}] = -W[J] - \int d^4x \, J(x)\phi_h^{\mathrm{c}}(x), \qquad (2.18)$$

which by definition as an action, satisfies:

$$\lim_{J \to 0} \frac{\delta\Gamma[\phi_h]}{\delta\phi_h}\bigg|_{\phi_h = \phi_h^{\mathrm{c}}} = 0. \qquad (2.19)$$

Then the one-loop quantum correction from EFT to the classical Lagrangian becomes:

$$\frac{i}{2} \ln\det \left[-\frac{\delta^2 \mathscr{L}'}{\delta\phi_h\delta\phi_h} \right] = \frac{i}{2} \mathbf{Tr} \ln \left[-\frac{\delta^2 \mathscr{L}'}{\delta\phi_h\delta\phi_h} \right]. \qquad (2.20)$$

2.1.1   Application to QED

A suitable Lagrangian for QED would be [120]:

$$\mathscr{L}_{\mathrm{QED}} = -\frac{1}{2} \partial_\mu A_\nu \, \partial^\mu A^\nu + \bar{\psi}\Big(i\big[\gamma(\partial - ieA)\big] - m \Big)\psi. \qquad (2.21)$$

The heavy degrees of freedom are fermions and the light ones bosons, so we associate $\phi_h \to \psi, \bar{\psi}$ and $\phi_l \to A$ with the coupling $J[\phi_l, \phi_h] = J[\psi, \bar{\psi}, A] = -e\bar{\psi}\gamma A\psi$.

---

[1]Interestingly, it has been shown in finite temperature QED, the two-loop contribution of Eq. (2.16) dominates the effective action Eq. (2.18) for $T \ll m$ [74].

The functional derivative we have to evaluate in this case is:

$$\frac{\delta^2 \mathscr{L}_{\mathrm{QED}}}{\delta\psi(x_1)\delta\bar{\psi}(x_2)} = \Big[\pm i\gamma(\partial - ieA) - m \Big] \delta^{(4)}(x_1 - x_2), \tag{2.22}$$

where the $\pm$ sign indicates that since this occurs inside a trace, the sign of the differential is irrelevant to the physics. This can be shown by inserting a factor $\mathbb{1} = \gamma^5\gamma^5$ and using trace cyclicity, which results in:

$$\mathbf{Tr}\ln\left(i\slashed{D} - m\right) = \mathbf{Tr}\ln\left(-i\slashed{D} - m\right). \tag{2.23}$$

Eq. (2.22) demonstrates a general property of $-\delta^2\mathscr{L}'/(\delta\phi_h\delta\phi_h)$ that for a free-field Lagrangian (here with classical field) this object corresponds to the inverse propagator for the theory, as in our case for QED Eq. (2.22). As the action is defined up to a total derivative, we can write the EFT term as:

$$\frac{i}{2}\mathbf{Tr}\ln\left[\frac{S_F^{-1}(p+eA)}{S_F^{-1}(p)}\right] = \frac{i}{2}\mathbf{Tr}\ln\left[\frac{i\gamma D - m}{i\gamma\partial - m}\right], \tag{2.24}$$

where S_F is the fermion propagator and the external field propagator is subtracted by the free-field propagator, just like the typical renormalisation performed in external fields (discussed briefly in App. A.1.3). There are various methods for evaluating this *functional determinant*, and we discuss one in Sec. 2.1.2, which we then apply on the case of a constant magnetic field. We notice the consistency that when the photon field is set to zero, the one-loop contribution to the field equations also disappears, as should be the case.

As explained in Sec. 4.1, the polarisation operator in a strong external field can be represented as an expansion of even photon exchanges with the field, given by the first line of Fig. 2.1 **a**.

In the EFT case as the fermions have been integrated out, the one-loop functional determinant then represents the situation given by the second line of Fig. 2.1 **b**, i.e. where fermion loops have been shrunk to effective vertices. A particularly interesting
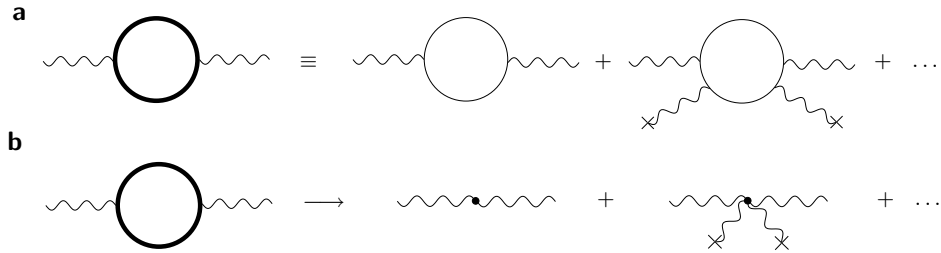
Figure 2.1: The polarisation operator and effective polarisation operator where ⨯ represents photon exchange with a classical external field.

result for us, is shown by considering Eq. (2.8). As the free energy is related to the vacuum-persistence amplitude, the probability for any other process must be $1 - |\langle 0^+|0^-\rangle|^2$. But "any other process" corresponds to pair creation, whose probability per unit time and volume $P_{e^+e^-}$, for $P_{e^+e^-} \ll 1$ is then:

$$P_{e^+e^-} = 2\mathfrak{Im}\,\mathscr{L}_{\mathrm{QED}} + O\Big[\big(\mathfrak{Im}\mathscr{L}_{\mathrm{QED}}\big)^2\Big] \tag{2.25}$$

$$\approx \mathfrak{Im}\left\{i\mathbf{Tr}\ln\left[\frac{i\gamma D - m}{i\gamma\partial - m}\right]\right\}. \tag{2.26}$$

This can be thought of as a shortcut to the optical theorem, which relates twice the imaginary part of the one-loop diagram to the square of its matrix element, which is in turn related by Fermi's Golden Rule [152] to a rate per unit volume (elaborated in Ch. A.1.3).

2.1.2   Heat Kernels

We now wish to introduce some tools in order to deal with objects such as Eq. (2.26), required for evaluation of effective actions. The study of the spectrum of Laplace operators (the divergence of the gradient) is greatly aided by the use of heat kernels. The name originates from a generalised solution to the heat equation and they are typically used to reconstruct the geometry of a manifold given the spectrum of a differential operator, eloquently captured by Kac's famous question "can one hear the shape of a drum?"[95]. Other applications include studying quantum anomalies, the Casimir effect and as we shall see here, vacuum polarisation. Our aim is to calculate the effective action given in Eq. (2.24) for QED, which can be efficiently computed with the use of the heat kernel method.

The general heat equation with boundary condition:

$$\left(\frac{\partial}{\partial t} - \hat{M}\right) K(t; \vec{x}, \vec{y}) \;\; = \;\; 0, \tag{2.27}$$

$$\lim_{t \to 0} K(t; \vec{x}, \vec{y}) \;\; = \;\; \delta(\vec{x} - \vec{y}), \tag{2.28}$$

for an operator $\hat{M}$ is solved by the heat kernel $K(t; \vec{x}, \vec{y})$:

$$K(t; \vec{x}, \vec{y}) \;\; := \;\; \langle \vec{x} | e^{-\hat{M}t} | \vec{y} \rangle, \tag{2.29}$$

$$K(t) \;\; = \;\; \int dx \; K(t; \vec{x}, \vec{x}) = \text{Tr}\{e^{-\hat{M}t}\}, \tag{2.30}$$

where we already recognise a link with EFT. Taking the Mellin transformation of both sides, one can see how the traced heat kernel is closely related to zeta-function renormalisation:

$$\int_0^\infty dt \; t^{s-1} K(t) = \sum_n \int_0^\infty dt \; t^{s-1} e^{-\lambda_n t}, \tag{2.31}$$

where we have written the trace as a sum over eigenvalues λ_n of $\hat{M}$. Performing the substitution $t \to t' = \lambda_n t$ and using definition of the gamma function $\Gamma(s) := \int_0^\infty t^{s-1} \exp(-t) dt$, we arrive at the following relation:

$$\zeta_E(s) = \frac{1}{\Gamma(s)} \int_0^\infty dt \; t^{s-1} K(t), \tag{2.32}$$

where the zeta function $\zeta_E(s)$ is the *Epstein* zeta function allowing eigenvalues with quadratic dependence on n: $\lambda_n = an^2 + bn + c$ for constants a, b, c:

$$\zeta_E(s) := \sum_{n=0}^\infty \frac{1}{\lambda_n^s}. \tag{2.33}$$

We mention for later reference the *Hurwitz* zeta function, which is a special case of the Epstein version with $a = 0, b = 1$:

$$\zeta_H(s; c) := \sum_{n=0}^\infty \frac{1}{(n+c)^s}, \tag{2.34}$$

with the relation $\zeta_H(s;0) = \zeta(s)$, with $\zeta(s)$ the Riemann zeta function.

The crucial link to the effective action comes when taking the differential of the above expression Eq. (2.33). Let us consider a more general zeta function of the following form:

$$\zeta(s) = \sum_{n=0}^{\infty} \frac{\mu_n^{ls}}{\lambda_n^s}, \tag{2.35}$$

where l is a constant. Rewriting μ^{ls}/λ_n^s as $\exp(-s \ln \lambda_n + ls \ln \mu)$, differentiating and setting s = 0 we find:

$$\zeta'(s) = \sum_{n=0}^{\infty} \frac{1}{\lambda_n^s} \Big(-\mu_n^{ls} \ln \lambda_n + l\mu_n^{ls} \ln \mu \Big), \tag{2.36}$$

$$-\zeta'(0) = \sum_{n=0}^{\infty} \ln \left(\frac{\lambda_n}{\mu_n^l} \right) = \ln \left(\prod_{j=1}^{\infty} \frac{\lambda_j}{\mu_j^l} \right). \tag{2.37}$$

For an operator $\hat{M}_1$ with eigenvalues $\{\lambda_j\}$ and an operator $\hat{M}_2$ with eigenvalues $\{\mu_k^l\}$ we then have:

$$-\zeta'(0) = \mathbf{Tr} \ln \left(\frac{\hat{M}_1}{\hat{M}_2} \right). \tag{2.38}$$

Hence using heat kernels, we have built a link between the generalised zeta function Eq. (2.35) and the one-loop effective field theory correction Eq. (2.24). This allows us to evaluate functional determinants by differentiating the zeta function formed by the function's eigenvalues and setting the argument equal to zero rather than forming a complicated sum of logarithms.

2.2   Constant Magnetic Field

One practical application of heat kernels is in calculating the effective action for charged fermions in a constant external magnetic field[2]. Through the Lorentz law, a charged particle feels a constant electric field completely differently to how it experiences a constant magnetic one. An electric field will exert a force on a positively (negatively) charged particle parallel (antiparallel) to the applied field. In contrast, the effect of a constant magnetic field will be to force the charged particle on helical paths whose orbital plane is perpendicular to the direction of the applied field in a fashion given by $m\dot{\mathbf{v}} = q\,\mathbf{v} \wedge \mathbf{B}$ for a charge, q, velocity $\mathbf{v}$ and mass m. If we again consider the one-loop EFT correction, with judicious insertion of γ^5 matrices, one can again rewrite the determinant in a more manageable form:

$$\mathbf{Tr} \ln (i\slashed{D} - m) = \frac{1}{2}\mathbf{Tr} \left[\ln (\slashed{D}^2 + m^2) \right]. \tag{2.39}$$

Now we know from QFT that the eigenvalues of $-\gamma_i D_i^2 + m^2$ are given by $m^2 + k_{\parallel}^2 + eB(2n + 1 \pm 1)$ [92], $n \in \mathbb{N}_0$ correspond to the discretised orbital motion in a plane perpendicular to magnetic field lines, the so-called *Landau levels*, where

---

[2]This section was inspired by Gerald V. Dunne's "Functional Determinants in Quantum Field Theory" lectures at the 14th Saalburg Summer School on Mathematical Physics [52], but with all calculations performed independently.

$k_\parallel$ is the momentum of the fermions parallel to field flux lines, and $+eB$ $(-eB)$ corresponds to energies for particles aligned with spins anti-parallel (parallel) to the field direction. To this we add $\gamma_0 D^2$, which also has continuous, positive semi-definite eigenvalues. Therefore, eigenvalues for the whole operator can be written $\lambda_n^\pm = m^2 + k_1^2 + k_2^2 + eB(2n + 1 \pm 1)$. In addition, we bear in mind the typical degeneracy factor $eBL^2/2\pi$, which comes from considering the orbits of the electrons to be constrained to a finite area, L^2.

We can utilise the preceding heat kernel formalism by calculating the general zeta function Eq. (2.35) with these eigenvalues. In a frame where particle motion is only in the plane perpendicular to applied magnetic field, we first define the Klein-Gordon eigenvalue in the absence of an external field to be a constant μ^2 (which will be later set equal to the rest energy squared m^2). Our zeta function becomes:

$$\zeta_H(s) = \mathbf{Tr}\, \frac{\mu^{2s}}{\lambda^s} = \frac{eBVt}{2\pi} \int d^2k \sum_{n=0}^{\infty} \sum_{\pm} \frac{\mu^{2s}}{\left[m^2 + k^2 + eB(2n + 1 \pm 1)\right]^s}, \qquad (2.40)$$

where Vt is a four-volume composed of the L^2 degeneracy factor and another area coming from letting the sum over discrete frequencies tend to an integral and we have also multiplied by the other degeneracy factor $eB/2\pi$ and sum over $\pm$ spins and explicitly noted that we are dealing with a Hurwitz zeta function $\zeta_H(s)$ as in Eq. (2.34). We deal with the four-volume factor by taking it to the other side and absorbing it in the constant μ. To integrate out k^2, we can transform to polar co-ordinates and then reverse differentiate to acquire:

$$\int d^2k \frac{1}{\left(k_\perp^2 + c\right)^s} = \frac{\pi}{s - 1} \frac{1}{c^{s-1}}, \qquad (2.41)$$

where c is a constant. Using this Eq. (2.41) result in Eq. (2.40) and dropping the label on the zeta function gives us:

$$\begin{aligned}
\zeta(s) = \mathbf{Tr}\, \frac{\mu^{2s}}{\lambda^s} &= \frac{eB}{(2\pi)^3} \sum_{n=0}^{\infty} \sum_{\pm} \frac{\pi}{s - 1} \frac{\mu^{2s}}{\left[m^2 + eB(2n + 1 \pm 1)\right]^{s-1}} \\
&= \frac{eB}{(2\pi)^3} \frac{\mu^{2s}}{(2eB)^{s-1}} \frac{\pi}{s - 1} \sum_{n=0}^{\infty} \sum_{\pm} \frac{1}{n + \frac{1}{2} \pm \frac{1}{2} + \frac{m^2}{2eB}}. \qquad (2.42)
\end{aligned}$$

We can then evaluate the sum over $\pm$ modes by using:

$$\sum_{n=0}^{\infty} \left[\frac{1}{(n + c)^{s-1}} + \frac{1}{(n + c + 1)^{s-1}} \right] = 2 \sum_{n=0}^{\infty} \frac{1}{(n + c)^{s-1}} - \frac{1}{c^{s-1}} \qquad (2.43)$$

$$= 2\zeta(s - 1; c) - \frac{1}{c^{s-1}}. \qquad (2.44)$$

Inserting this into Eq. (2.42) we have:

$$\zeta(s) = \frac{e^2 B^2}{(2\pi)^2} \left(\frac{\mu^{2s}}{2eB} \right)^2 \frac{1}{s - 1} \left[\zeta\left(-1; \frac{m^2}{2eB} \right) - \frac{1}{2} \left(\frac{m^2}{2eB} \right)^{1-s} \right]. \qquad (2.45)$$

Labelling $m^2/2eB = z$ and using $dc^s/ds = d\exp(s\ln c)/ds = c^s\ln c$, one acquires:

$$\zeta'(s) = \frac{e^2B^2}{(2\pi)^2}\left[\quad -\frac{2}{(s-1)^2}\left(\frac{\mu^2}{2eB}\right)^s\zeta(s-1;z) + \frac{2}{s-1}\left(\frac{\mu^2}{2eB}\right)^s\zeta'(s-1;z)\right.$$

$$+\frac{2}{s-1}\left(\frac{\mu^2}{2eB}\right)^s\ln\left(\frac{\mu^2}{2eB}\right)\zeta(s-1;z) + \frac{z}{(s-1)^2}\left(\frac{\mu}{m}\right)^{2s}$$

$$\left.+\frac{z}{s-1}\left(\frac{\mu}{m}\right)^{2s}\ln z - \frac{z^{1-s}}{s-1}\left(\frac{\mu^2}{2eB}\right)^s\ln\left(\frac{\mu^2}{2eB}\right)\right]. \tag{2.46}$$

After a little manipulation and setting $\mu = m$ and $s = 0$ we have:

$$\zeta'(0) = \frac{e^2B^2}{(2\pi)^2}\left[-2\zeta(-1;z) - 2\zeta'(-1;z) - 2\zeta(-1;z)\ln z + z\right]. \tag{2.47}$$

Using the following identities [52]:

$$\zeta(-1;z) = \frac{z}{2} - \frac{z^2}{2} - \frac{1}{12}, \tag{2.48}$$

$$\zeta'(-1;z) = \frac{1}{12} - \frac{z^2}{4} - \zeta(-1;z)\ln z$$
$$-\frac{1}{4}\int_0^\infty \frac{dt}{t^2}\,e^{-2zt}\left(\coth t - \frac{t}{3} - \frac{1}{t}\right), \tag{2.49}$$

inserted into Eq. (2.46) we achieve:

$$\zeta'(0) = \frac{e^2B^2}{(2\pi)^2}\left[\frac{3}{2}z^2 + \frac{1}{2}\int_0^\infty \frac{dt}{t^2}\,e^{-2zt}\left(\coth t - \frac{t}{3} - \frac{1}{t}\right)\right]. \tag{2.50}$$

The first term in the brackets is a field-independent constant as $e^2B^2z^2 = m^2/4$, which will therefore not appear in the corresponding dynamics of this effective Lagrangian and can be dropped. We then have the effective or Euler-Heisenberg Lagrangian in a constant magnetic field [92]:

$$-\zeta'(0) = -\frac{e^2B^2}{8\pi^2}\int_0^{i\infty}\frac{dt}{t^2}\,e^{-m^2t/eB}\left(\coth t - \frac{t}{3} - \frac{1}{t}\right). \tag{2.51}$$

2.3   The Euler-Heisenberg Lagrangian

The Euler-Heisenberg Lagrangian is simply the one-loop effective QED Lagrangian in a constant electromagnetic field:

$$\delta\mathscr{L}_{\text{EH}} = \frac{i}{2}\mathbf{Tr}\ln\left[\frac{i\gamma D - m}{i\gamma\partial - m}\right] = \frac{i}{4}\mathbf{Tr}\ln\left[\frac{(\gamma D)^2 + m^2}{\partial^2 + m^2}\right]. \tag{2.52}$$

After rewriting in terms of Klein-Gordon operators, the logarithm can be partially dealt with by differentiating $\delta\mathscr{L}_{\text{EH}}$ with respect to the photon field, and since kinetic momentum is not conserved in an external field, the trace can be evaluated over all position eigenstates, i.e. an integral over d^4x, sandwiched between $\langle x|$ and $|x\rangle$. This trace can be performed numerous ways, i) being regarded as an evolution between

initial and final position states (proper-time method) [158] ii) if specialised to constant fields then also with the WKB method which gives exact solutions when the potential in the Lagrangian is at most quadratic in the co-ordinates [22] iii) solving the Green's function equation via Fourier transformation [49], all of which give the final result:

$$
\begin{aligned}
\delta\mathscr{L}_{\mathrm{EH}} \;=\;& \frac{1}{8\pi^2}\int_0^\infty \frac{ds}{s^3}\mathrm{e}^{-im^2 s} \\
& \times\;\Bigg\{(es)^2\mathcal{G}\,\frac{\cos\left[es\big(\sqrt{\mathcal{F}^2+\mathcal{G}^2}+\mathcal{F}\big)^{1/2}\right]\cosh\left[es\big(\sqrt{\mathcal{F}^2+\mathcal{G}^2}-\mathcal{F}\big)^{1/2}\right]}{\sin\left[es\big(\sqrt{\mathcal{F}^2+\mathcal{G}^2}+\mathcal{F}\big)^{1/2}\right]\sinh\left[es\big(\sqrt{\mathcal{F}^2+\mathcal{G}^2}-\mathcal{F}\big)^{1/2}\right]} \\
& \;+\frac{2}{3}(es)^2\mathcal{F}-1\Bigg\},
\end{aligned}
\tag{2.53}
$$

with $\mathcal{F}, \mathcal{G}$ the electromagnetic invariants (see App. A.1.1). A usual way of rewriting this (see e.g. [92]) is in terms of the positive semi-definite functions a and b:

$$
a = \sqrt{\mathcal{F}^2+\mathcal{G}^2}+\mathcal{F}; \quad b = \sqrt{\mathcal{F}^2+\mathcal{G}^2}-\mathcal{F},
$$

which gives, after rotating in the complex plane:

$$
\delta\mathscr{L}_{\mathrm{EH}} \;=\; \frac{e^2}{8\pi^2}\int_0^\infty \frac{ds}{s}\,\mathrm{e}^{-im^2 s}\left[ab\coth eas\cot ebs - \frac{a^2-b^2}{3}-\frac{1}{(es)^2}\right].
\tag{2.54}
$$

After a change of variable $t \to t/eB$ in Eq. (2.51), in the limit $E \to 0$ one can rotate the complex contour to an integral along the imaginary axis to reproduce constant magnetic field expression Eq. (2.51). Considering current and near-future maximum laser intensity values, we will only require a weak-field expansion in E/E_{cr}, $E_{\mathrm{cr}} = m^2/e$, which corresponds to an expansion in powers of $\mathcal{F}, \mathcal{G}$. This also gives us insight into the meaning of the second and third terms. The -1 term is due to subtraction of the free field case to ensure that the quantum correction vanishes in this limit (see App. A.1.3 and [27]). The term proportional to $\mathcal{F}$ then ensures that for very weak fields the correction remains finite, cancelling the first order expansion terms and is important in charge renormalisation [92]. After solving a simple remaining integral, the weak-field expansion then becomes:

$$
\delta\mathscr{L}_{\mathrm{EH}} = \frac{\alpha^2}{360\pi^2 m^4}\left[4\mathcal{F}^2 + 7\mathcal{G}^2\right],
\tag{2.55}
$$

or in terms of observable quantities for $\mathscr{L} = \mathscr{L}_{\mathrm{classical}} + \delta\mathscr{L}_{\mathrm{EH}}$:

$$
\mathscr{L}_{\mathrm{EH}} = \frac{1}{8\pi}(E^2 - B^2) + \frac{\alpha^2}{360\pi^2 m^4}\left[(E^2 - B^2)^2 + 7(\mathbf{E}\cdot\mathbf{B})^2\right].
\tag{2.56}
$$

We note that if the two electromagnetic invariants $E^2 - B^2$ and $\mathbf{E}\cdot\mathbf{B}$ are zero, such as is the case for a single plane wave, there is no polarisation of the vacuum. We also note that even without having derived Eq. (2.53), we could have imagined what form the weak-field expansion would have taken by making the observations i) $\delta\mathscr{L}_{\mathrm{EH}}d^4x$ is a dimensionless Lorentz scalar ii) $\delta\mathscr{L}_{\mathrm{EH}}$ is gauge invariant iii) corrections from the polarisation operator start at order α^2. Using only these arguments, we see that $\delta\mathscr{L}_{\mathrm{EH}}$ must be of the form:

$$
\delta\mathscr{L}_{\mathrm{EH}} = \frac{\alpha^2}{m^4}\left[c_1(E^2 - B^2)^2 + c_2(\mathbf{E}\cdot\mathbf{B})^2\right],
\tag{2.57}
$$

where $c_{1,2}$ are constants.

In the following chapter, we use the weak-field Euler-Heisenberg Lagrangian Eq. (2.56) to calculate vacuum polarisation effects in ultra-intense lasers.

Chapter 3

Light-light diffraction in the polarised vacuum

We present results for two possible experimental set-ups that could be used to detect photon-photon scattering and vacuum birefringence effects in lasers. By polarising regions of the vacuum with two separate ultra-intense lasers, we can form a "matterless" double-slit, which can be probed with a third, weaker laser. One can utilise the interference between photons scattered in each of the strong beams to spatially separate this vacuum signal from the probe background, for which we calculate the expected number of detectable photons. Moreover, we discuss the effect of beam-geometry and show that the double-slit configuration even leads to a modest increase of vacuum birefringence results over single-slit values.

The race to experimentally verify a collection of vacuum polarisation effects and perhaps even more exotic physics has already begun. Upcoming laser facilities such as ELI and HiPER are planning by the end of the decade, to offer such colossal intensities of 10^{26} Wcm^{-2}, which should already be sufficient for pair creation [135, 20, 103] and mark a vast improvement over the current world record of 2×10^{22} Wcm^{-2} [187] at the HERCULES facility in Michigan. *Refractive* vacuum polarisation effects are also mostly lacking experimental verification and, as they by definition only involve virtual fermions, do not require the high intensities required for pair creation and are therefore particularly desirable to study. In the current chapter, we focus on an example of elastic photon-photon scattering, a particularly hot topic of the last five years. Although having long been measured in the Coulomb field of a heavy nucleus as Delbrück scattering [183], the theory [50] of which being already intensely studied [70, 130], in other, fundamentally different environments such as a constant magnetic field [14], the effect is still to be experimentally confirmed. It should be mentioned that the PVLAS (Polarizzazione del Vuoto con Laser)[189] collaboration have been searching for almost a decade to detect vacuum birefringence (change in ellipticity) and dichroism (rotation of polarisation vector) as laser photons pass through an effectively constant magnetic field, which with a still negative result [31], gives an indication of the experimental challenges involved. Moreover, as any particle-antiparticle pair can in principle appear in the virtual loop, photon scattering has also been discussed as a probe for new physics [80, 4, 3, 75, 170, 39]. In the present case of strong

lasers, photon-photon scattering has been investigated theoretically through such effects as the phase difference one laser beam acquires when passing through another [169, 63], vacuum birefringence in a head-on collision of strong laser and X-ray probe [82, 142] or scattering of photons in four-wave mixing in which three lasers impinge on one another [118]. Current tentative experimental limits on the minuscule elastic photon-photon scattering cross-section of $\sigma_{\gamma\gamma}[\text{ cm}^2] = 7.3 \times 10^{-66} \big(\hbar\omega[eV]\big)^6$ in the optical region [176], include a limit of 1.5×10^{-48} cm^2 using three-wave mixing and 0.8 eV centre-of-mass photons [24] as well as 4.6×10^{-58} cm^2 and 2.7×10^{-56} cm^2 for 1.2 and 2.4 eV photons respectively [31].

We propose two original experimental scenarios involving a weaker probe laser crossing two ultra-intense (defined to be $\geq 10^{23}$ Wcm^{-2}) laser beams and take the novel step of investigating the generated diffraction pattern from the polarised vacuum (see [102]) as well as calculating more conventional quantities such as vacuum birefringence and dichroism which we can compare to the literature.

The Euler-Heisenberg approach

Our primary interest consists of calculating effects of the polarised vacuum which could be probed experimentally. Regarding current laser capabilities, we are therefore working in the dual limit: $\omega \ll m$, $E \ll E_{cr}$. The first of these constraints allows us to use the Euler-Heisenberg effective field theory approach outlined in Sec. 2.1, and the latter constraint allows us to use the weak-field expansion of this Lagrangian Eq. (2.56), derived in Sec. 2.3. This region of parameter space is then particularly tractable mathematically and suitable for calculation of the quantum alterations to classical quantities. We outline in the following, a couple of consequences of these corrections.

Since alterations to the classical Lagrangian are of the order $O(E^4)$, we note that field equations will contain corresponding source terms of the order $O(E^3)$. So we can observe how, on interaction with an EM field, the non-vanishing vacuum current from the polarised vacuum generates non-linear waves in measurable quantities such as the electric field, which we will often term the "diffracted" field, $\mathbf{E}_d$.

In his autobiographical work "Das Teil und das Ganze" (The part and the whole), Werner Heisenberg recalls a talk with his student Leonhard Euler, which precipitated the calculation of the modified Lagrangian. Originally discussing the idea of an energetic photon as a composite particle, they form a useful analogy also for processes in which intense EM fields, say two colliding laser beams, interact with one another. Euler commented, wrote Heidelberg:

> "Wenn in dem einen Lichtstrahl virtuell, das heißt als Möglichkeit, Paare von Elektronen und Positronen vorhanden sind, so könnte der andere Lichtstrahl doch an diesen Teilchen gestreut werden . . . " [83] (If in a beam of light, virtual, in the sense of "possible", electron-positron pairs were present, another beam of light would surely be scattered by these [virtual] particles.)

In the spirit of Heisenberg's uncertainty principle: $\Delta p \Delta x \geq \hbar/2$, it is possible to rigorously define a lower bound on the uncertainty in the energy density for a given

length of time, similar to the above relation [46]. For short enough times Δt, the uncertainty in the corresponding energy density can be large enough that "virtual" particles can be brought into existence, interact and then disappear, all within Δt. Therefore the quantum vacuum can be thought to manifest itself as a sea of virtual particles that can be activated in the passage of ultra-intense laser beams. It is possible in principle, to consider all imaginable forms of particle creation that obey the usual conservation laws of charge and species number. The Euler-Heisenberg approach can be applied to e.g. QCD where the fluctuation of the lightest virtual mesons $\pi_0, \pi^{\pm}$ as well as quark-antiquark pairs $q\bar{q}$ both in the quark condensate and at higher energies have been calculated. In line with the energy uncertainty relation however, these contributions prove to be negligible[1] compared to those from the lightest known charged pair [64], the electron-positron pair. Concentrating entirely on QED, these virtual particles can then be thought to be "polarised" by the intensity of the EM field and we can form the useful comparison to e.g. the polarisation of dipoles in solids due to an external field. This allows us to develop our analogy as regarding strongly polarised regions of the vacuum as a solid-state medium with non-linear response.

The aptness of the non-linear solid-state perspective is demonstrated on return to the weak-field Lagrangian Eq. (2.56). We first bear in mind that $\mathbf{D} = \mathbf{E} + 4\pi\mathbf{P}$ and $\mathbf{H} = \mathbf{B} - 4\pi\mathbf{M}$, where $\mathbf{D}$, $\mathbf{H}$ are the electric displacement and magnetic inductance and $\mathbf{P}$, $\mathbf{M}$ are the polarisation and magnetisation respectively. Using:

$$\mathbf{D} = 4\pi\frac{\partial\mathscr{L}}{\partial\mathbf{E}}, \qquad \mathbf{H} = -4\pi\frac{\partial\mathscr{L}}{\partial\mathbf{B}}, \tag{3.1}$$

we can then show[2]:

$$\mathbf{P} = \frac{\partial\,\delta\mathscr{L}_{\mathrm{EH}}}{\partial\mathbf{E}}, \qquad \mathbf{M} = \frac{\partial\,\delta\mathscr{L}_{\mathrm{EH}}}{\partial\mathbf{B}}. \tag{3.2}$$

This then gives:

$$\mathbf{P} = \frac{\alpha^2}{45\pi^2 m^4}\big[2(E^2 - B^2)\mathbf{E} + 7(\mathbf{E}\cdot\mathbf{B})\mathbf{B}\big] \tag{3.3}$$

$$\mathbf{M} = -\frac{\alpha^2}{45\pi^2 m^4}\big[2(E^2 - B^2)\mathbf{B} - 7(\mathbf{E}\cdot\mathbf{B})\mathbf{E}\big], \tag{3.4}$$

these quantities satisfy the following relation as required for them to be considered the straightforward quantum analogue of the classical counterpart:

$$\nabla^2\mathbf{E} - \partial_t^2\mathbf{E} = 4\pi\mathbf{J}_{\mathrm{vac}}(t, \mathbf{r}) \tag{3.5}$$
$$\mathbf{J}_{\mathrm{vac}}(t, \mathbf{r}) = \nabla\wedge(\partial_t\mathbf{M}) + \partial_t^2\mathbf{P} - \nabla(\nabla\cdot\mathbf{P}),$$

which can be derived extremising the Lagrangian with respect to the vector potential. Eq. (3.5) clearly displays both aforementioned additions due to a polarised vacuum: the vacuum current, J_{vac} as well as the solid-state-like polarisation. All required electrodynamical quantities can then be derived from these polarisation properties Eq. (3.3), Eq. (3.4). Moreover, now that we have made this correspondence, from this point onward, all EM experimental quantities can be calculated using classical

---

[1]Either photons in the TeV range are required, or an energy density of 300MeV/fm^3 $\approx$ 10^{37}Wcm^{-2}, perhaps relevant to supernovae or intense gamma ray bursts.

[2]The expressions for the magnetisation appear here with the correct sign, unlike in [142] which suffers from a printing error.

electrodynamics.

In the following experimental scenarios, we will consider time-dependent electromagnetic fields which must then lead to a non-stationary vacuum polarisation. We are however, still justified in using the Euler-Heisenberg Lagrangian for "constant" fields as this constancy is with respect to the physical phenomenon at large, namely the spontaneous appearance and disappearance of virtual electron-positron pairs which occurs over a reduced Compton wavelength $\lambda = 1/m = 3.9 \times 10^{-11}$ cm. Therefore as regards vacuum-polarisation effects, optical and X-ray wavelengths relevant to upcoming scenarios, $\lambda_{\text{optical}} > 10^{-5}$ cm $\gg \lambda$, $\lambda_{\text{X-ray}} > 4 \times 10^{-10}$ cm $\gg \lambda$, vary slowly enough to be felt by the quantum vacuum as constant.

Laser description

Electromagnetic fields obey a wave equation which describe their propagation through spacetime. In vacuum, in the Lorentz gauge $\partial A = 0$, we have the traditional homogeneous wave equation $\Box F(x) = 0$, where F represents A^μ, E^i and B^i. With a general solution of the form $F = C_1 f(t - \mathbf{k} \cdot \mathbf{x}) + C_2 g(t + \mathbf{k} \cdot \mathbf{x})$ for constants C_1, C_2, the homogeneous wave equation admits a plethora of phenomena, even the propagation of undifferentiable initial conditions such as cusps and Heaviside field shapes [21]. We simplify our life but also restrict ourselves to one domain of solutions by making a separation ansatz $F(x^\mu) = f(t)g(x, y, z)$ or superposition thereof for f, g $\in \mathbb{C}$, and by doing so map the initial hyperbolic PDE onto the subspace of elliptic PDEs[3] and form the simple harmonic oscillator and Helmholtz equations for the temporal and spatial parts of the electromagnetic wave respectively: $\ddot{f}(t) - \omega^2 f(t) = 0$; $\nabla^2 g(x, y, z) - \omega^2 g(x, y, z) = 0$. Even with this simplification there are a multitude of possibilities to fulfil the latter inhomogeneous Laplace equation for the wave's spatial dependence, which can be classified by the following steps taken in solving the equation. Employing various co-ordinate transformations one can expand g in terms of a series of Hermite polynomials, Laguerre, Ince or hypergeometric functions, thereby allowing for a great wealth of possible wave shapes (for a review of Hermite modes see [59]; for Laguerre-Ince see [13]; for hypergeometric [108] and hypergeometric-Gaussian [98]). No matter the basis, all these solutions are equal to the Gaussian beam at zero-order which will suffice to calculate the leading-order vacuum polarisation effect. Moreover, by assuming a simple power series ansatz [155], one can then show for our considered geometries that successive corrections scale $\approx (1/\pi)^n$ for the nth correction to a beam focused at the diffraction limit (as explained in the discussion section of the current chapter) and therefore by placing observation instruments close to the relevant laser propagation axis within the paraxial approximation $\sin\theta \approx \theta$, $\cos\theta \approx 1$, our results will be accurate to within a factor of around $1/\pi \approx 30\%$. With regard to temporal dependence, photons from intense laser beams are delivered in a pulse, typically modelled as Gaussian, $\exp(-t^2/\tau_s^2)$ with a duration τ_s. This also leads to a perturbative expansion, in the parameter $1/\omega_0\tau_s$, for central frequency of radiation ω_0. As long as our pulse length is sufficiently larger than the interaction length, we can regard our pulse as being flat. Assuming only natural broadening, monochromaticity is also equivalent to the the condition $\omega_0\tau_s \gg 1$.

---

[3]Partial differential equations of the form $Au_{xx} + Bu_{xy} + Cu_{yy}$ can be classified similar to quadratic equations with the determinant $D = B^2 - 4AC$: $D > 0$ determines a hyperbolic equation, $D = 0$ a parabolic and $D < 0$ an elliptic equation.

In addition, we implicitly mitigate possible reductions in the signal from temporal corrections by choosing less than the absolute limits of values for envisaged laser systems.

Experimental scenarios

As with all processes in strong-field QED, the degree of vacuum polarisation is dictated by the relativistic invariants $\mathbf{Tr}\, F^2 = 2(E^2 - B^2)$ and $\mathbf{Tr}\, F^*F = 4\,\mathbf{E} \cdot \mathbf{B}$. For a single plane EM wave, both of these vanish indicating that single plane EM waves (which are in any case, an idealistic construction) cannot feel the effect of their own polarisation of the vacuum. Therefore any interesting experimental scenarios will have to involve multiple fields or focusing effects such that the these invariants are non-trivial.

We will focus on two main types of geometry given in Fig. 3.1. Both involve two ultra-intense monochromatic Gaussian laser beams with wavevectors, electric and magnetic fields given respectively by $k_{s,i}, \mathbf{E}_{s,i}, \mathbf{B}_{s,i}, i \in \{1, 2\}$, whose centres are separated by $(2x_0, 2y_0, 2z_0)$, with a waist $\mathrm{w}_{s,0}$ and Rayleigh length depending on the geometry $\{y_{r,s}, z_{r,s}\} = k_s \mathrm{w}_{s,0}^2/2$, giving a transverse "width" (standard deviation over $\sqrt{2}$) $\mathrm{w}_s(x, x_{r,s}) = \mathrm{w}_{s,0}\sqrt{1 + (x/x_{r,s})^2}$. A subscript p in place of s then indicates corresponding quantities of the probe laser. We take the probe laser to also be monochromatic and Gaussian, characterised by being much weaker in amplitude $|\mathbf{E}_p| \ll |\mathbf{E}_s|$ and broader in extent $\mathrm{w}_{p,0} \gg \mathrm{w}_{s,0}$. We calculate results for idealised geometries, the accuracy of which will be discussed in Sec. 3.4.

In the first scenario, the two parallel ultra-intense plane-wave Gaussian laser beams centred at $(\pm x_0, 0, \pm z_0)$ counterpropagate into an *optical* Gaussian probe beam and will be referred to as the *double-shaft* set-up[4]. In the second scenario, two antiparallel ultra-intense plane-wave Gaussian beams centred at $(\pm x_0, \pm y_0, 0)$ counterpropagate into one another, perpendicular to the weaker *X-ray* Gaussian probe beam of broader waist in a manner shown and will be referred to as the *double-slit* set-up. These set-ups are depicted in Fig. 3.1 and typical parameters given in Tab. 3.2. Indices on observables will denote the relevant experimental configuration with ^{h} for the double-**sh**aft arrangement[5] and ^{l} for the double s**l**it one.

When it comes to evaluating our expressions, we have in mind experimental parameters that correspond to the upcoming generation of laser facilities. For our strong-field laser, we use, in both cases, quoted parameters from the ELI [60] and HiPER [86] projects, modifying only the pulse duration whilst maintaining values within the total attainable energy. The probe-field laser can be chosen to satisfy the observable being measured. Diffraction maxima from a double-slit satisfy $n\lambda_p = d \sin \vartheta$ for slit separation d and maxima labelled by integer $n \in \mathbb{Z}$ and at observation angle $\vartheta < \pi/2$ that increases monotonously with the wavelength of light λ_p. We may therefore choose parameters from the optical VULCAN [178] laser in the Rutherford Appleton Laboratory (RAL). Complementary to this is the measurement of polarisation effects in the probe which are inversely proportional to wavelength and for this

---

[4]This is a different labelling to the one used in [102], where the current *double-shaft* was labelled *double-slit* instead.

[5]We will also discuss, where suitable, the single-shaft arrangement which is similar to the double-shaft case, but with both beams on top of one another, displaced from the origin at $(x_0, 0, z_0)$. This will also be signified with a ^{h} superscript.

purpose we will typically choose parameters from the XFEL [185] laser being built at DESY, with values from the FLASH FEL [68] at DESY or the LCLS FEL [37] at the SLAC National Accelerator Laboratory used as a comparison. A summary of laser parameters is given in Tab. 3.1:

Strong-Field Lasers			
	PFS	ELI	HiPER
Peak av. power	0.5 PW	1 EW	1 EW
Wavelength	800 nm	800 nm	800 nm
Min. Pulse duration	5 fs	10 fs	10 fs
Date of Completion	2010	2015	2020

Probe Lasers				
	VULCAN	FLASH	LCLS	XFEL
Peak av. power	100 TW	1–5 GW	10 GW	80 GW
Wavelength	1054 nm	6.8–47 nm	0.15 nm	1.6-0.1 nm
Pulse duration	700 fs	10–70 fs	230 fs	100 fs
Shot Frequency [Hz]	>1/60	500	120	10
Date of Completion	2005[6]	2005	2010[7]	2009

Table 3.1: Current possible strong and probe lasers that could serve vacuum polarisation experiments

In accordance with the planned or current laser values in Tab. 3.1, we will evaluate expressions with the parameters given in Tab. 3.2. In addition to laser parameters,

Set-up	P_s[PW]	I_s[Wcm^{-2}]	λ_s[μm]	τ_s[fs]
shaft	150	5×10^{24}	0.8	30
slit	100(-500)	$1(-5) \times 10^{24}$	0.8	100

Set-up	P_p[GW]	λ_p[μm]	$w_{p,0}$[μm]
shaft	80	1.054/0.527[9]	$100 - 400$
slit	80	$4(-16) \times 10^{-4}$	$(8-)100$

Table 3.2: Default parameters used in the two experimental scenarios. All powers are peak. Values in brackets denote other possibilities for particular situations which we will declare in the text.

focusing widths will also govern interactions. As the strong field intensity should be as high as possible, we anticipate the diffraction limit will be almost met and set the strong-field focal spot width equal to its wavelength, $w_{s,0} = \lambda_0$. The probe in contrast, should be wide enough to capture both strong fields but also intense enough that diffraction effects are measurable. The detector will then typically be placed in the far-field region, which is defined more accurately in the following chapter.

We rely upon the assumption $c\tau_s > l_s \gg \lambda_s/2\pi$, where l_s is the effective strong-field pulse length, to neglect temporal corrections to the Gaussian pulse and assume

---

[6]The Vulcan laser has been active since the 1980s, the next upgrade to 10 PW is scheduled to begin in 2010.

[7]LCLS was completed in August 2009 but first runs with X-ray beam will begin in 2010.
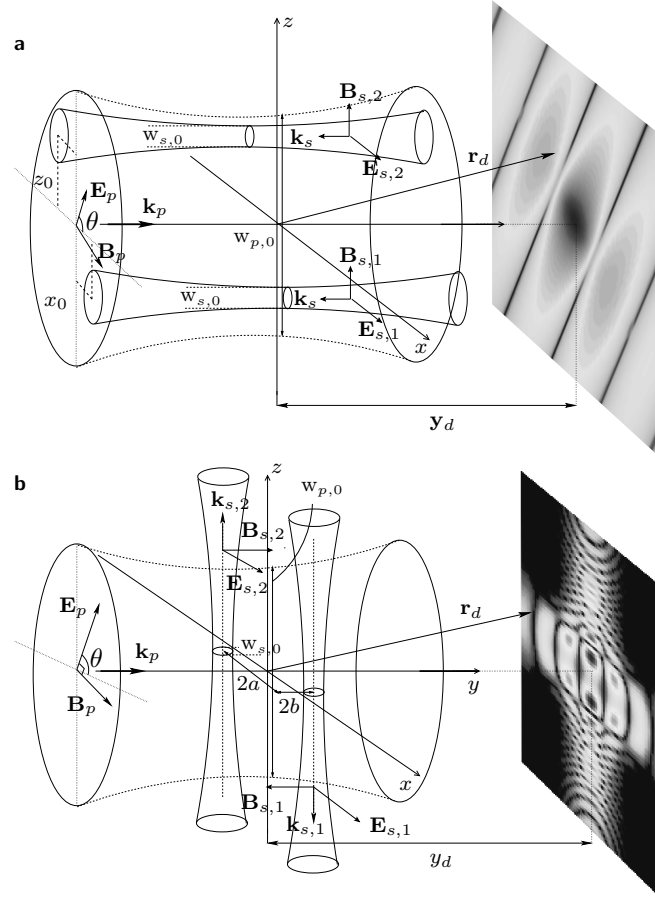
Figure 3.1: The double-shaft **a** and double-slit **b** experimental scenarios, showing the passage of a focused, monochromatic Gaussian probe laser beam, wavevector $\mathbf{k}_p$ passing through two ultra-intense monochromatic Gaussian beams, wavevectors $\mathbf{k}_s$, $\mathbf{k}_{s,1}$, $\mathbf{k}_{s,2}$, with the diffracted probe photons being imaged on a detector at a distance y_d along the probe-axis from the interaction centres.

monochromaticity. For the double-shaft configuration, as the ultra-intense beams travel through the probe, their movement during passage is not as important as for the double-slit configuration, in which the "shape" of the aperture changes with probe passage. Therefore, in the double-shaft case we take l_s^h to simply be equal to the strong-field Rayleigh length and impose $c\tau_s^h \approx 3.5 y_{r,s}$, with a pulse length of $\tau_s^h = 30$ fs. In the double-slit case, we choose to restrict l_s^l more and define it as the distance from the centre of the pulse at which the intensity falls to below a tenth of its initial value, $l_s^l = 3z_{r,s}$. Then to ensure $c\tau_s^l > 2l_s^l$, we choose $c\tau_s^l \approx 2 \times 2l_s^l$ with $\tau_s^l = 100$ fs. This then explains why different intensities are considered in the double-slit case (Tab. 3.2), being limited through $I_0\tau_0 A = \mathcal{E}$ for a fixed laser energy $\mathcal{E}$ and focus area A.

3.1 Diffracted electric field

In the solid-state perspective, we consider photons from the probe laser to be *diffracted* by regions of the polarised vacuum. Employing Babinett's principle [115] which states

that the inverse of an aperture will give exactly the same diffraction pattern as the aperture itself, we anticipate the two experimental geometries Fig. 3.1 will exploit the interference between the two sources of diffracted field to produce a series of alternating bright and dark fringes in the far-field. However we have here three-dimensional "apertures" which, instead of being sharply defined like apertures, will have along two dimensions smooth Gaussian and along the other $1/(1 + x^2)$ transmission behaviour. We bear in mind that this will bring a deviation from the over-simplified slit and circular aperture diffraction picture.

Derivation of the diffracted electric field proceeds according to the familiar Green's function solution to the inhomogeneous wave equation Eq. (3.5) $\mathbf{E}_d(\mathbf{r}, t) = -\int d^3r' |\mathbf{r} - \mathbf{r}'|^{-1} \mathbf{J}_{\text{vac}}(\mathbf{r}', t - |\mathbf{r} - \mathbf{r}'|)$, (see e.g. [93] for derivation of this method). As we are interested in how the probe is diffracted we Fourier-transform in time in order to be able later to focus on the frequency $\omega = \omega_p$:

$$\mathbf{E}_d(\mathbf{r}, \omega) = -\int d^3r' \, dt \Big[\nabla \wedge \partial_t \mathbf{M} - \nabla(\nabla \cdot \mathbf{P}) + \partial_t^2 \mathbf{P} \Big]$$
$$\times \frac{\exp\big[-i\omega\big(|\mathbf{r} - \mathbf{r}'| + t\big)\big]}{|\mathbf{r} - \mathbf{r}'|}. \tag{3.6}$$

Assuming detection instruments will have to be placed much further from the radiation-intense diffraction region i.e. that $\mathrm{w}_{s,0}, \mathrm{w}_{p,0} \ll r$, such that:

$$\frac{\mathrm{w}_{s,0}}{\lambda_p} \frac{\mathrm{w}_{p,0}}{r}^2 \ll 1, \qquad \frac{\mathrm{w}_{p,0}}{\lambda_p} \frac{\mathrm{w}_{p,0}}{r}^3 \ll 1, \tag{3.7}$$

we can curtail the exponential of Eq. (3.6) to:

$$\frac{\exp\big[-i\omega\big(|\mathbf{r} - \mathbf{r}'| + t\big)\big]}{|\mathbf{r} - \mathbf{r}'|} \approx \frac{1}{r} \exp\Big\{-i\omega\Big[\big(r - \hat{\mathbf{r}} \cdot \mathbf{r}' + \frac{1}{2r}|\hat{\mathbf{r}} \wedge \mathbf{r}'|^2\big) + t\Big]\Big\}. \tag{3.8}$$

By retaining the quadratic co-ordinate terms, we are implicitly working within the *Fresnel* regime. We can then integrate Eq. (3.6) by parts to acquire a more manageable form:

$$\mathbf{E}_d(\mathbf{r}, \omega) \approx \frac{\omega^2 \exp(-i\omega r)}{r} \int d^3r' \, dt \, \big(\mathbf{M} \wedge \hat{\mathbf{r}} + \mathbf{P} - \mathbf{P} \cdot \hat{\mathbf{r}} \, \hat{\mathbf{r}}\big) \times \tag{3.9}$$
$$\exp\Big[i\omega\big(\hat{\mathbf{r}} \cdot \mathbf{r}' - \frac{1}{2r}|\hat{\mathbf{r}} \wedge \mathbf{r}'|^2 - t\big)\Big].$$

So far, this analysis is quite general. Let us specify the fields first to our experimental scenarios; for both we have the following:

$$\mathbf{E}(x, y, z, t) = \mathbf{E}_s(x, y, z, t) + \mathbf{E}_p(x, y, z, t), \tag{3.10}$$
$$\mathbf{E}_s(x, y, z, t) := \big[E_{s,1}(x, y, z, t) + E_{s,2}(x, y, z, t)\big]\hat{\mathbf{x}}, \tag{3.11}$$
$$\mathbf{E}_p(x, y, z, t) := E_p(x, y, z, t)\big[\hat{\mathbf{x}}\cos\theta + \hat{\mathbf{z}}\sin\theta\big], \tag{3.12}$$
$$E_p(x, y, z, t) := E_p(x, y, z)\sin\big[\psi_p + \omega_p t - k_p y + f_p(x, y, z)\big]. \tag{3.13}$$

Then for each scenario, the strong-fields are different:

$$E_{s,\{1,2\}}^h(x, y, z, t) := E_s^h(x \mp x_0, y, z \mp z_0)\sin\big[\psi_{s,\{1,2\}} + \omega_s t + k_s y$$
$$- f_s^h(x \mp x_0, y, z \mp z_0)\big], \tag{3.14}$$
$$E_{s,\{1,2\}}^l(x, y, z, t) := E_s^l(x \mp x_0, y \mp y_0, z)\sin\big[\psi_{s,\{1,2\}} + \omega_s t \pm k_s z$$
$$\mp f_s^l(x \mp x_0, y \mp y_0, z)\big], \tag{3.15}$$

where:

$$E_s^h(x,y,z) \quad := \quad \frac{E_s}{\sqrt{2}} \frac{\mathrm{e}^{-(x^2+y^2)/\mathrm{w}_s^2(y)}}{\sqrt{1+(y/y_{r,s})^2}}, \tag{3.16}$$

$$E_s^l(x,y,z) \quad := \quad \frac{E_s}{\sqrt{2}} \frac{\mathrm{e}^{-(x^2+z^2)/\mathrm{w}_s^2(z)}}{\sqrt{1+(z/z_{r,s})^2}}, \tag{3.17}$$

$$E_p(x,y,z) \quad := \quad E_p \frac{\mathrm{e}^{-(x^2+z^2)/\mathrm{w}_p^2(y)}}{\sqrt{1+(y/y_{r,p})^2}}, \tag{3.18}$$

and:

$$f_s^h(x,y,z) \quad = \quad \tan^{-1}\left(\frac{y}{y_{r,s}}\right) - \frac{k_s y}{2}\frac{x^2+z^2}{y^2+y_{r,s}^2}, \tag{3.19}$$

$$f_s^l(x,y,z) \quad = \quad \tan^{-1}\left(\frac{z}{z_{r,s}}\right) - \frac{k_s z}{2}\frac{x^2+y^2}{z^2+z_{r,s}^2}, \tag{3.20}$$

$$f_p(x,y,z) \quad = \quad \tan^{-1}\left(\frac{y}{y_{r,p}}\right) - \frac{k_p y}{2}\frac{x^2+z^2}{y^2+y_{r,p}^2}. \tag{3.21}$$

From these initial geometries, using Faraday's law we can derive the corresponding magnetic fields (dropping terms much smaller than our working accuracy):

$$\mathbf{B}_s^l(x,y,z,t) \quad = \quad -\left(E_{s,1}^l - E_{s,2}^l\right)\hat{\mathbf{y}} \tag{3.22}$$

$$\mathbf{B}_s^h(x,y,z,t) \quad = \quad \left(E_{s,1}^h + E_{s,2}^h\right)\hat{\mathbf{z}} \tag{3.23}$$

$$\mathbf{B}_p^h(x,y,z,t) \quad = \quad E_p\left[\sin\theta\,\hat{\mathbf{x}} - \cos\theta\,\hat{\mathbf{z}}\right]. \tag{3.24}$$

We would now like to insert these fields into our expressions for the vacuum polarisation and magnetisation Eqs. (3.3) and (3.4). Since we are only interested in the scattered probe photons, the relevant part of these expressions will be those containing terms in which the probe field occurs to just a single power. Higher powers E_p^j for $j \in \mathbb{N}_1$ will eventually lead to delta-functions in $\omega \pm j\omega_p$ which correspond to off-shell photons, which can be neglected [93]. The remaining terms form the relevant polarisation and magnetisation contributions:

$$\mathbf{P}^h(\mathbf{r},t) \quad = \quad \frac{\alpha^2}{45\pi^2 m^4}\Big[4(\mathbf{E}_s^h\!\cdot\!\mathbf{E}_p-\mathbf{B}_s^h\!\cdot\!\mathbf{B}_p)\mathbf{E}_s^h+7(\mathbf{E}_s^h\!\cdot\!\mathbf{B}_p+\mathbf{B}_s^h\!\cdot\!\mathbf{E}_p)\mathbf{B}_s^h\Big], \tag{3.25}$$

$$\mathbf{M}^h(\mathbf{r},t) \quad = \quad -\frac{\alpha^2}{45\pi^2 m^4}\Big[4(\mathbf{E}_s^h\!\cdot\!\mathbf{E}_p-\mathbf{B}_s^h\!\cdot\!\mathbf{B}_p)\mathbf{B}_s^h-7(\mathbf{E}_s^h\!\cdot\!\mathbf{B}_p+\mathbf{B}_s^h\!\cdot\!\mathbf{E}_p)\mathbf{E}_s^h\Big], \tag{3.26}$$

$$\mathbf{P}^l(\mathbf{r},t) \quad = \quad \frac{\alpha^2}{45\pi^2 m^4}\Big[2\big((E_s^l)^2-(B_s^l)^2\big)\mathbf{E}_p+4\mathbf{E}_s^l\!\cdot\!\mathbf{E}_p\,\mathbf{E}_s^l+7\mathbf{E}_s^l\!\cdot\!\mathbf{B}_p\,\mathbf{B}_s^l\Big], \tag{3.27}$$

$$\mathbf{M}^l(\mathbf{r},t) \quad = \quad -\frac{\alpha^2}{45\pi^2 m^4}\Big[2\big((E_s^l)^2-(B_s^l)^2\big)\mathbf{B}_p+4\mathbf{E}_s^l\!\cdot\!\mathbf{E}_p\,\mathbf{B}_s^l-7\mathbf{E}_s^l\!\cdot\!\mathbf{B}_p\,\mathbf{E}_s^l\Big]. \tag{3.28}$$

(where co-ordinates $\mathbf{r}, t$ have been suppressed in vectors on the right-hand side). Now let us try and insert these expressions into that for the diffracted electric field Eq. (3.9). By having $\mathbf{E}_d$ already as a function of frequency, the relevant physical components become clear. Bearing in mind the typical exponential time-dependence of the fields, the probe field occurs to the single power $\pm\exp(i\omega_p t)$, and the strong fields therefore to the quadratic power $\pm\exp(2i\omega_s t)$, one can see how integration over the t co-ordinate in Eq. (3.9) will supply a variety of delta-functions in ω with arguments: $\omega - \omega_p$, $\omega - (\omega_p \pm 2\omega_s)$. The final two delta-functions again represent

evanescent waves and can be neglected. When we then Fourier-transform $\mathbf{E}_d$ back into the time-domain, these unmeasurable terms can then be neglected. We note that the on-shell terms retained then correspond to the constant terms in the strong-field squared which, considering the sinusoidal time dependence, are therefore also the values achieved by time-averaging all quadratic strong field combinations. Then after this strong-field time-averaging and the Fourier transform in ω (essentially evaluating the $\omega = \omega_p$ delta function), and keeping in line with the definition given in [142], we have:

$$\mathbf{E}_d(\mathbf{r}, t) = \mathbf{E}_d^*(\mathbf{r}) \frac{\exp\left[i(-\omega_p r + \omega_p t + \psi_p)\right]}{2i} + \text{c.c.}, \tag{3.29}$$

$$\mathbf{E}_d(\mathbf{r}) = \frac{\omega_p^2}{r} \int d^3 r' \Big(\mathbf{M}(\mathbf{r}) \wedge \hat{\mathbf{r}} + \mathbf{P}(\mathbf{r}') - \mathbf{P}(\mathbf{r}') \cdot \hat{\mathbf{r}} \; \hat{\mathbf{r}} \Big) \times \tag{3.30}$$
$$\exp\left[i\omega_p\Big(-y + \hat{\mathbf{r}} \cdot \mathbf{r}' - \frac{1}{2r}|\hat{\mathbf{r}} \wedge \mathbf{r}'|^2\Big)\right],$$

where c.c. is the complex conjugate, $\mathbf{P}(\mathbf{r}) = \langle \mathbf{P}(\mathbf{r}, t) \rangle$, $\mathbf{M}(\mathbf{r}) = \langle \mathbf{M}(\mathbf{r}, t) \rangle$ and $\langle \rangle$ denotes averaging over t. This time averaging leads to the generation of four different types of term in the integral corresponding to the exponential function generated from $\langle E_{s,1}^2 \rangle$, $\langle E_{s,2}^2 \rangle$ and two originating from the cosine cross-term $\langle E_{s,1} E_{s,2} \rangle$. Insertion of Eqs. (3.25-3.28) into Eq. (3.30) then yields the following formulae:

$$\mathbf{E}_d^h(\mathbf{r}) = \frac{I_{s,0}}{I_{cr}} \frac{4\alpha E_p \mathbf{v}^h}{45\lambda_p^2 r} \sum_{k=1}^{4} \mathcal{V}_k^h(\mathbf{r}), \tag{3.31}$$

where $I_{s,0} = E_{s,0}^2/8\pi$ is the time-averaged strong field intensity, $\mathbf{v}$ is the polarisation vector with:

$$\mathbf{v}^h = \begin{pmatrix} (1/2)\big[1 + (y/r)\big]\cos\theta \\ -(1/2)\big[1 - (y/r)\big]\big[(x/r)\cos\theta + (7z/4r)\sin\theta\big] \\ (7/8)\big[1 + (y/r)\big]\sin\theta \end{pmatrix} + O\left[\left(\frac{x}{r}\right)^2, \left(\frac{z}{r}\right)^2\right], \tag{3.32}$$

and $\mathcal{V}_k^h(\mathbf{r})$ are the four integration volumes:

$$\mathcal{V}_k^h(\mathbf{r}) = \int_{-\infty}^{\infty} d^3 r' \frac{e^{\mathscr{F}_k^h}}{(1 + (y'/y_{r,s})^2)\sqrt{1 + (y'/y_{r,p})^2}} \tag{3.33}$$

$$\mathscr{F}_k^h = -i\omega_p\Big(y' + \frac{x'^2 + y'^2 + z'^2}{2r} - \frac{xx' + yy' + zz'}{r}$$
$$- \frac{(xx' + yy' + zz')^2}{2r^3} \Big) - \frac{2}{\mathrm{w}_s^2(y')}(x'^2 + z'^2 + x_0^2 + z_0^2)$$
$$- \frac{x'^2 + z'^2}{\mathrm{w}_p^2(y')} + \tan^{-1}\frac{y'}{y_{r,p}} - \frac{\omega_p y'}{2}\frac{x'^2 + z'^2}{y'^2 + y_{r,p}^2}$$
$$+ (x'x_0 + z'z_0)\Big(\frac{4\beta_k}{\mathrm{w}_s^2(y')} + \frac{2i\Gamma_k\omega_s y'}{y'^2 + y_{r,s}^2}\Big) + i\Gamma_k\Delta\psi_s, \tag{3.34}$$

$$\beta_k = \begin{cases} 1 & \text{if } k = 1 \\ -1 & \text{if } k = 2 \\ 0 & \text{if } k = 3, 4, \end{cases} \quad \text{and} \quad \Gamma_k = \begin{cases} 0 & \text{if } k = 1, 2 \\ 1 & \text{if } k = 3 \\ -1 & \text{if } k = 4. \end{cases} \tag{3.35}$$

$$\mathbf{E}_d^l(\mathbf{r}) \quad := \quad \frac{I_0}{I_{cr}} \frac{\alpha E_p}{45\lambda_p^2 r} \left((\mathcal{V}_3^l + \mathcal{V}_4^l)\mathbf{u}_1^l + (\mathcal{V}_1^l - \mathcal{V}_2^l)\mathbf{u}_2^l + \sum_{i=1}^{4} \mathcal{V}_i^l \mathbf{u}_3^l \right), \qquad (3.36)$$

where the vectors, $\mathbf{u}_i$ and the volumes $\mathcal{V}_k$ are defined as following:

$$\mathbf{u}_1^l \quad := \quad \begin{pmatrix} 0 \\ (z/r)\sin\theta + (x/r)\cos\theta - (y/r)\big[(x/r)\cos\theta + (z/r)\sin\theta\big] \\ 0 \end{pmatrix},$$

$$\mathbf{u}_2^l \quad := \quad \begin{pmatrix} (z/r)\cos\theta + (7xy/4r^2)\sin\theta \\ 0 \\ -(x/r)\cos\theta + (7yz/4r^2)\sin\theta \end{pmatrix},$$

$$\mathbf{u}_3^l \quad := \quad \begin{pmatrix} \cos\theta \\ -(7z/4r)\sin\theta - (xy/r^2)\cos\theta \\ (7y/4r)\sin\theta \end{pmatrix} + \mathrm{O}\left[\left(\frac{x}{r}\right)^2, \left(\frac{z}{r}\right)^2 \right], \qquad (3.37)$$

$$\mathcal{V}_k^l := \int_{-\infty}^{\infty} d^3 r' \, \frac{\exp(\mathscr{F}_k^l)}{1 + (z'/z_r)^2}, \qquad (3.38)$$

$$\begin{aligned}
\mathscr{F}_k^l \quad = \quad & -i\omega_p \Big(\frac{x'^2 + y'^2 + z'^2}{2r} - \frac{xx' + yy' + zz'}{r} - \frac{(xx' + yy' + zz')^2}{2r^3} + y' \Big) \\
& - \frac{x'^2 + z'^2}{\mathrm{w}_{p,0}^2} - \frac{2}{\mathrm{w}_0^2} \Big(x'^2 + y'^2 + x_0^2 + y_0^2 + 2\beta_k(x'x_0 + y'y_0) \Big) \\
& + 2i\Gamma_k \Big(k_0 z' - \tan^{-1}\frac{z'}{z_{r,s}} + \frac{k_0 z'(x'^2 + y'^2 + x_0^2 + y_0^2)}{2(z'^2 + z_r^2)} \Big) \Big].
\end{aligned} \qquad \begin{aligned} (3.39) \\ (3.40) \end{aligned}$$

After integration in the plane perpendicular to strong-field propagation, we are left with the remaining one-dimensional integrals:

$$
\mathcal{V}_k^h = \int_{-\infty}^{\infty} dy' \; \frac{\pi \mathrm{w}_{s,0}^2 y_{r,s}}{\sqrt{\alpha_{x'}^h \alpha_{y'}^h}} \frac{1}{1+y'^2} \frac{1}{1+(y_{r,s}/y_{r,p})^2 y'^2} \exp\left\{ \frac{4}{\alpha_{x'}^h} \left[\frac{x_0 \beta_k}{\mathrm{w}_{s,0}(1+y'^2)} \right. \right.
$$

$$
\left. + \frac{i\Gamma_k \pi x_0 \mathrm{w}_{s,0}}{\lambda_s y_{s,0}} \frac{y'}{1+y'^2} \right]^2 - \frac{1}{\alpha_{x'}^h} \left(\frac{\pi \mathrm{w}_{s,0}}{\lambda_p} \frac{x}{r} \right)^2 \left(1 + \frac{y_{r,s}}{r} \frac{y}{r} y' \right)^2
$$

$$
\frac{4\pi i}{\alpha_{x'}^h} \frac{\mathrm{w}_{s,0}}{\lambda_p} \frac{x}{r} \left(1 + y' \frac{y_{r,s}}{r} \frac{y}{r} \right) \left[\frac{x_0}{\mathrm{w}_{s,0}} \frac{\beta_k}{1+y'^2} + i\Gamma_k \pi \frac{y'}{1+y'^2} \frac{\mathrm{w}_{s,0} x_0}{y_{r,s}^2} \right]
$$

$$
\frac{1}{4\alpha_z^h} \left[\frac{-2}{\alpha_{x'}^h} \left(\pi \frac{x}{r} \frac{\mathrm{w}_{s,0}}{\lambda_p} \right)^2 \left(\frac{\mathrm{w}_{s,0}}{r} \frac{z}{r} + y' \frac{yz y_{r,s} \mathrm{w}_{s,0}}{r^4} \right) \right.
$$

$$
\frac{4\pi i}{\alpha_{x'}^h} \frac{\mathrm{w}_{s,0}}{\lambda_p} \frac{x}{r} \frac{z}{r} \frac{\mathrm{w}_{s,0}}{r} \left(\frac{x_0}{\mathrm{w}_{s,0}} \frac{\beta_k}{1+y'^2} + i\Gamma_k \pi \frac{\mathrm{w}_{s,0} x_0}{r^2} \frac{y'}{1+y'^2} \right)
$$

$$
+ 2\pi i \frac{\mathrm{w}_{s,0}}{\lambda_p} \frac{z}{r} \left(1 + \frac{y_{r,0}}{r} \frac{y}{r} y' \right) + 4\beta_k \frac{z_0}{\mathrm{w}_{s,0}} \frac{1}{1+y'^2}
$$

$$
\left. + 4i\Gamma_k \pi \frac{z_0 \mathrm{w}_{s,0}}{\lambda_s y_{r,s}} \frac{y'}{1+y'^2} \right]^2 - i\pi y'^2 \frac{y_{r,s}^2}{\lambda_p r} \left(1 - \left(\frac{y}{r} \right)^2 \right)
$$

$$
\left. - 2i\pi y' \frac{y_{r,s}}{\lambda_p} \left(1 - \frac{y}{r} \right) + i \tan^{-1}\left(\frac{y_{r,s}}{y_{r,p}} y' \right) - 2\frac{x_0^2 + z_0^2}{\mathrm{w}_{s,0}^2} \right\}, \tag{3.41}
$$

$$
\alpha_{x'}^h := i\pi \frac{\mathrm{w}_{s,0}^2}{r\lambda_p} \left[1 - \left(\frac{x}{r} \right)^2 \right] + \frac{2}{1+y'^2} + \left(\frac{\mathrm{w}_{s,0}}{\mathrm{w}_{p,0}} \right)^2 \frac{1}{1 + (\frac{y_{r,s}}{y_{r,p}} y')^2}
$$

$$
+ i\pi \frac{\mathrm{w}_{s,0}^2}{\lambda_p y_{r,p}} \frac{y_{r,s}}{y_{r,p}} \frac{y'}{1 + (\frac{y_{r,s}}{y_{r,p}} y')^2} \tag{3.42}
$$

$$
\alpha_{z'}^h := \frac{1}{\alpha_{x'}} \left(\pi \frac{\mathrm{w}_{s,0}}{\lambda_p} \frac{x}{r} \right)^2 \left(\frac{z \mathrm{w}_{s,0}}{r^2} \right)^2 + i\pi \frac{\mathrm{w}_{s,0}^2}{r\lambda_p} \left[1 - \left(\frac{z}{r} \right)^2 \right] + \frac{2}{1+y'^2}
$$

$$
+ \left(\frac{\mathrm{w}_{s,0}}{\mathrm{w}_{p,0}} \right)^2 \frac{1}{1 + (\frac{y_{r,s}}{y_{r,p}} y')^2} + i\pi \frac{\mathrm{w}_{s,0}^2}{\lambda_p y_{r,p}} \frac{y_{r,s}}{y_{r,p}} \frac{y'}{1 + (\frac{y_{r,s}}{y_{r,p}} y')^2} \tag{3.43}
$$

$$
\mathcal{V}_k^l = \int_{-\infty}^{\infty} dz' \; \frac{\pi \mathrm{w}_{s,0}^2 z_{r,s}}{\sqrt{\alpha_{x'}^l \alpha_{y'}^l}} \frac{1}{1+z'^2} \exp\left\{ \frac{\pi^2}{\alpha_{y'}^l} \left(\frac{\mathrm{w}_{s,0}}{\lambda_p} \right)^2 \left[i\frac{y}{r} \left(1 + z' \frac{z z_{r,s}}{r^2} \right) \right. \right.
$$

$$
\left. + i\frac{\pi}{\alpha_{x'}^l} \frac{xy}{r^2} \frac{\mathrm{w}_s^2}{r\lambda_p} \left(\frac{ix}{r} + z' \frac{ixz z_{r,s}}{r^3} - \frac{\beta_k}{\pi} \frac{x_0 \lambda_p}{\mathrm{w}_s^2} \right) - \frac{\beta_k}{\pi} \frac{y_0 \lambda_p}{\mathrm{w}_s^2} - i \right]^2
$$

$$
- z'^2 \frac{z_{r,s}^2}{\mathrm{w}_{p,0}^2} \left[\frac{i\pi \mathrm{w}_{p,0}^2}{\lambda_p r} \left(1 - \left(\frac{z}{r} \right)^2 \right) + 1 \right]
$$

$$
+ \frac{4\pi}{\alpha_{x'}^l} \left(\frac{\mathrm{w}_{s,0}}{\lambda_p} \right)^2 \left[i\frac{x}{r} \left(1 + z' \frac{z_{r,s} z}{r^2} \right) - \frac{\beta_k}{\pi} \frac{x_0 \lambda_p}{\mathrm{w}_s^2} \right]^2 +
$$

$$
2\pi i z' \frac{z}{r} \frac{z_{r,s}}{\lambda_p} + 4i\Gamma_k \pi z' \frac{z_{r,s}}{\lambda_s} \left[1 + \frac{x_0^2 + y_0^2}{z_{r,s}^2} \frac{1}{2(1+z'^2)} \right]
$$

$$
\left. - 2i\Gamma_k \tan^{-1}(z') - \frac{2(x_0^2 + y_0^2)}{\mathrm{w}_s^2} \right\}, \tag{3.44}
$$

where we have defined:

$$\alpha_{x'}^l := i\pi \frac{\mathrm{w}_{s,0}^2}{\lambda_p r}\left[1 - \left(\frac{x}{r}\right)^2\right] + \frac{2}{1 + z'^2} - 2i\Gamma_k \frac{z'}{1 + z'^2} + \left(\frac{\mathrm{w}_{s,0}}{\mathrm{w}_{p,0}}\right)^2, \qquad (3.45)$$

$$\alpha_{y'}^l := i\pi \frac{\mathrm{w}_{s,0}^2}{\lambda_p r}\left[1 - \left(\frac{y}{r}\right)^2\right] + \frac{2}{1 + z'^2} - 2i\Gamma_k \frac{z'}{1 + z'^2} + \frac{\pi^2}{\alpha_{x'}^l}\left(\frac{xy}{r^2}\frac{\mathrm{w}_s^2}{r\lambda_p}\right)^2. \qquad (3.46)$$

First, we note that probe-focusing terms are absent from the double-slit integral Eqs. (3.38) and (3.39). For X-rays, the Rayleigh length $y_{r,p} = \pi\mathrm{w}_{p,0}^2/\lambda_p \gg \mathrm{w}_{s,0}$ and so focusing terms can be removed from the integral, but will be kept when the probe field occurs alone. The integrals Eq. (3.33), Eq. (3.34) and Eq. (3.38), Eq. (3.39), we notice agreement in calculation of the vacuum-generated field $\mathbf{E}_d$ with vector diffraction theory, as expected. It can be viewed as the result of a Fresnel transform (the keeping the quadratic terms in $|\mathbf{r} - \mathbf{r}'|$, see e.g. [115]) of an aperture function transversed by the probe beam, which in our case, due to Babinet's principle and QED, takes the form of the strong-field spatial intensity distribution. We define useful diffraction parameters: $\nu_x^l = \mathrm{w}_{s,0}^2/\lambda_p r$, $\nu_z^l = \mathrm{w}_{p,0}^2/\lambda_p r$ and $\nu_{x,z}^h = \nu^h = \mathrm{w}_{s,0}^2/\lambda_p r$, which allow us under the condition $\nu \gg 1$ to keep Fresnel terms and consider ourselves in the near-field, *Fresnel* limit or alternatively under $\nu \ll 1$ to neglect Fresnel terms and consider ourselves in the far-field *Frauenhofer* limit.

The expressions for the diffracted field are unwieldy in the present form. As our analysis is accurate only to $\sim 1/\pi$, we can neglect many terms appearing in the above formulae. First of all, we study, for the typical situation in which, $\mathrm{w}_{s,0} + x_0 \ll \mathrm{w}_{p,0}$, the integrand with cosine term, $\mathcal{V}_3 + \mathcal{V}_4$. In the double-slit case, when $\left[\lambda_s/l_p, \lambda_s/\mathrm{w}_{p,0}\right] \ll \sqrt{1 + (y\lambda_p/\pi\mathrm{w}_{p,0}^2)^2}$, for $l_p \geq y_{r,p}$ the effective decay length of $1/\sqrt{1 + (y/y_{r,p})^2}$, the cosine oscillates rapidly enough to be safely neglected (c.f. Riemann-Lebesgue lemma), which can be seen to be fulfilled by X-rays. In the double-shaft case, the term can be neglected approximately when $\max[y_{r,s}/x_0, y_{r,s}/z_0] \ll 1$, which is fulfilled for the finite strong-beam separations we will be considering. Apart from in the special *refractive index* limit where $y \to 0$, this is satisfied for both optical and X-ray frequencies. In addition, as $x/r, z/r \ll 1$ we can neglect many terms in the polarisation which leaves us with two similar expressions:

$$\mathbf{E}_d^h(\mathbf{r}) \approx \frac{4\alpha}{45\lambda_p^2 r}\frac{I_0}{I_{\mathrm{cr}}}E_p(\mathcal{V}_1^h + \mathcal{V}_2^h)\left[\cos\theta, 0, \tfrac{7}{4}\sin\theta\right], \qquad (3.47)$$

$$\mathbf{E}_d^l(\mathbf{r}) \approx \frac{\alpha}{45\lambda_p^2 r}\frac{I_0}{I_{\mathrm{cr}}}E_p(\mathcal{V}_1^l + \mathcal{V}_2^l)\left[\cos\theta, 0, \tfrac{7}{4}\sin\theta\right]. \qquad (3.48)$$

In this often-encountered limit, the two geometries can be related to one another through the substitution $4\mathcal{V}^h \leftrightarrow \mathcal{V}^l$.

To conclude this section, we plot in Fig. 3.2, the result of numerical evaluation of the above integrals Eq. (3.41), Eq. (3.44) with $\theta = 0$, $\pi/4$ respectively and and typical experimental parameters mentioned in the introduction to this chapter to be expected from upcoming laser facilities. As is typical for diffraction patterns, we notice that the electric field vectors point in opposite directions in different fringes. We also note that the strongest part of the diffracted field in the central fringe points in the opposite direction to the probe, as expected from Le Chatelier's law, or like a
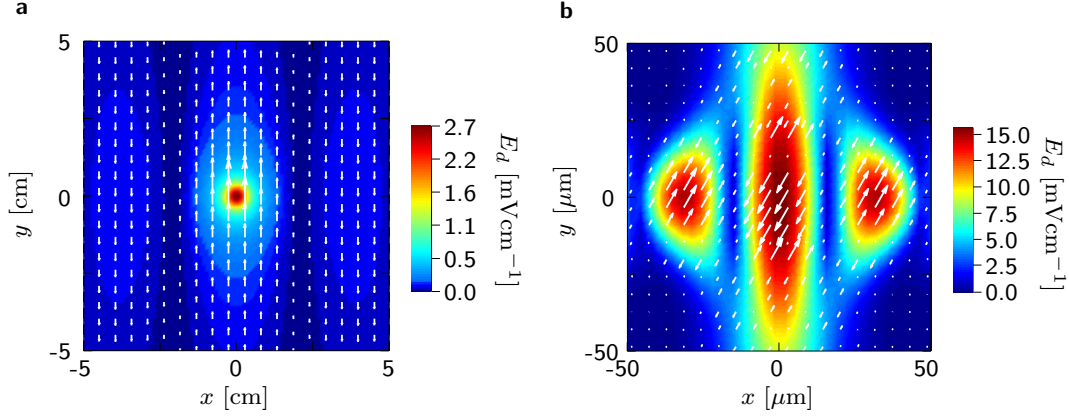
Figure 3.2: With the background colours representing the modulus electric field and the arrows indicating direction and amplitude, we plot the vacuum polarisation in **a** the double-shaft scenario for probe polarisation $\theta = 0$ and **b** the double-slit scenario for probe polarisation $\theta = \pi/4$.

Lenz's law for polarisable materials. That the field in the double-shaft case appears to disappear much quicker with x, z compared to the double-slit case is a consequence of its geometry. We comment more on the effects of beam shape in the following section, in which we discuss the directly measurable diffracted intensity.

3.2   Diffracted intensity

We calculate Poynting's vector through a surface in the detector plane, where we define the "detector plane" as shown in Fig. 3.1, $(x, z)|y, y \in \mathbb{R}^+$, with typically 10 cm $< y < 500$ cm. This is by definition far removed from the interaction centres and so $\mathbf{E} = \mathbf{E}_p + \mathbf{E}_d$ and we can use $\mathbf{S}(\mathbf{r}, \omega_p) = \mathbf{E}(\mathbf{r}, \omega_p) \wedge \mathbf{B}(\mathbf{r}, \omega_p)/4\pi$ or as $\mathbf{E} = \mathbf{B} \wedge \mathbf{k}$ in this vacuum region, $\mathbf{S}(\mathbf{r}, \omega_p) = |\mathbf{E}(\mathbf{r}, \omega_p)|^2 \hat{\mathbf{k}}/4\pi$ [10]. In the detector plane we have:

$$I_{\mathrm{t}} = \frac{\cos \vartheta}{4\pi} \langle |\mathbf{E}_p + \mathbf{E}_d|^2 \rangle, \tag{3.49}$$

where I_{t} is the total radiation intensity flowing through unit area in the detector plane and $\cos \vartheta = y/r$ (which will be set to one as x/r, $z/r \ll 1$. Writing the diffracted fields Eqs. (3.31) and (3.36) in the form $\mathbf{E}_d^{h,l} = -\alpha(I_0/I_{\mathrm{cr}})E_p \zeta_j^{h,l} \mathbf{v}_j^{h,l} \exp(i\eta)/2i + \mathrm{c.c.}$, $\eta = \omega_p r - \omega_p t - \psi_p$ and $\zeta_j^{h,l} \in \mathbb{C}$ and inserting it with the expression for the probe (Eq. (3.13) and Eq. (3.18)) into Eq. (3.49) yields:

$$I_{\mathrm{t}}(x, y, z) = I_p(x, y, z) + I_{pd}(x, y, z) + I_d(x, y, z), \tag{3.50}$$

---

[10]Since pair creation can be neglected, the average probe and strong field intensities will remain unchanged, so that we can use the vacuum version of Poynting's theorem.

where:

$$I_p(x, y, z) = \frac{1}{4\pi}\langle \mathbf{E}_p(\mathbf{r}) \cdot \mathbf{E}_p(\mathbf{r}) \rangle = I_p \frac{\exp\left[-2(x^2 + z^2)/(\mathrm{w}_p^2(y))\right]}{1 + (y/y_{r,p})^2}, \tag{3.51}$$

$$I_{pd}(x, y, z) = \frac{1}{2\pi}\langle \mathbf{E}_p(\mathbf{r}) \cdot \mathbf{E}_d(\mathbf{r}) \rangle = 2I_p\alpha\frac{I_0}{I_{\mathrm{cr}}} \frac{\exp\left[-(x^2 + z^2)/\mathrm{w}_p^2(y)\right]}{\sqrt{1 + (y/y_{r,p})^2}}$$

$$\times \left(\mathfrak{Re}\zeta_j \cos f_p - \mathfrak{Im}\zeta_j \sin f_p\right)\mathbf{v}_j \cdot \hat{\mathbf{E}}_p, \tag{3.52}$$

$$I_d(x, y, z) = \frac{1}{4\pi}\langle \mathbf{E}_d(\mathbf{r}) \cdot \mathbf{E}_d(\mathbf{r}) \rangle = I_p\left(\alpha\frac{I_0}{I_{\mathrm{cr}}}\right)^2 \mathbf{v}_j \cdot \mathbf{v}_k \,\mathfrak{Re}(\zeta_j\zeta_k^*). \tag{3.53}$$

and $\langle\rangle$ refers to time-averaging, $I_p = E_p^2/8\pi$ and f_p are the focusing terms Eq. (3.21) and we have assumed $x/r, z/r \ll 1$. Of most interest will be the change in intensity due to QED vacuum fluctuations $I_t - I_p$. We notice immediately, that the cross term, I_{pd} is a factor $I_{\mathrm{cr}}/\alpha I_0$ larger than the pure diffracted part, I_d. However we also see that due to the probe terms, I_{pd} is confined to the centre of the detector plane by a Gaussian, whereas I_d has no such strong decay[11]. It will first therefore, be most interesting to study I_d at larger transverse displacements x, z such that $I_d \gg I_{pd}, I_p$. Secondly, as I_{pd} decays at a rate $\sqrt{2}$ slower with detector co-ordinate x, z than I_p, there may be the possibility to study this vacuum signal in addition.

Using Eq. (3.47) and Eq. (3.48), we then have:

$$I_{pd}^h(x, y, z) = I_p\frac{4\alpha}{45\lambda_p^2 r}\frac{I_0}{I_{\mathrm{cr}}}\frac{\exp\left[-(x^2 + z^2)/\mathrm{w}_p^2\right]}{\sqrt{1 + (y/y_{r,p})^2}}[1 + \frac{3}{4}\sin^2\theta]$$

$$\left(\mathfrak{Re}(\mathcal{V}_3^h + \mathcal{V}_4^h)\cos f_p - \mathfrak{Im}(\mathcal{V}_3^h + \mathcal{V}_4^h)\sin f_p\right), \tag{3.54}$$

$$I_d^h(x, y, z) = I_p\left(\frac{4\alpha}{45\lambda_p^2 r}\frac{I_0}{I_{\mathrm{cr}}}\right)^2\left[1 + \frac{33}{16}\sin^2\theta\right]\left|\mathcal{V}_3^h + \mathcal{V}_4^h\right|^2. \tag{3.55}$$

As can be seen from Eqs. (3.54) and (3.55), the diffraction signal in both I_{pd} and I_d is maximised for $\theta = \pi/2$.

We imagine that in the double-shaft case, non-zero x_0, z_0, will generate a typical double-slit intensity pattern, with fringes along a direction perpendicular to the line joining the two strong-field centres, i.e. $x = zx_0/z_0 + c_1$, for an arbitrary constant c_1. We notice in the limit $x/r, z/r \ll 1$, the diffracted field polarisation vector Eq. (3.32), is to within $O\left((x/r)^2\right)$ independent of the x and z co-ordinates. In addition, with an optical laser $\nu = \mathrm{w}_{p,0}^2/\lambda_p r \ll 1$ and we will always be in the far field, so quadratic Fresnel terms in Eq. (3.33) can be neglected. It can be shown from Eq. (3.33) that under these conditions, there is in fact an SO(2) symmetry when the two vectors (x_0, z_0) and (x, z) are both subject to an orthogonal rotation, which confirms our physical intuition. Therefore, without loss of generality, we can set $z_0 = 0$. In the double-slit case, we might suspect that intensity results are completely independent of separation of the beams along probe-propagation axis y_0. This suspicion can be explained by considering the path difference between two diffracted waves emitted from the centres of the strong-fields centred at $\mathbf{r}_{1,2} = \pm(x_0, y_0)$. The total phase

---

[11]We also mention that the next order term in the weak field expansion of the Euler-Heisenberg Lagrangian Eq. (2.56) would give a term of the same order as I_d, but would be a cross term and again confined by the probe Gaussian.

difference will be due to the difference $\omega_p\big(|\mathbf{r}_1 - \mathbf{r}| - |\mathbf{r}_2 - \mathbf{r}|\big)$ as shown in Eq. (3.6) plus the difference due to probe phase, as each wave is generated in phase with the probe i.e. plus $2\omega_p y_0 y$. With again $x/r \ll 1$, one can show that the general condition for a minima at the detector is $2x_0 x/r + 2y_0(1 - y/r) = (2n+1)\pi/2$ for $n \in \mathbb{Z}$, and therefore since the separation y_0 is multiplied by essentially $(x/r)^2 \ll x/r \ll 1$, it should lead to no difference in the intensity pattern within the range of measurability. As this turns out to be the case, we set it equal to zero for the entire remaining intensity section, along with the phase difference between the two ultra-intense waves which is essentially the same effect.

3.2.1   Vacuum field I_d

Although much weaker in the centre of the detector plane, I_d is an attractive quantity to measure as decay with transverse co-ordinate is much slower than for I_p and I_{pd} and in some way, represents the pure vacuum contribution. In the following subsections, we investigate its form, and show how the shape of the patterns coincide with a solid-state perspective.

Field diffracted onto the x-axis

We first focus on the double-slit, X-ray probe configuration and study the diffraction pattern along the x-axis. Numerical evaluation of the leading-order QED contributions to the field diffracted onto the x-axis is shown in Fig. 3.3 **a**. With parameters given in Tab. 3.2, focusing the probe to $\mathrm{w}_{p,0} = 100~\mu$m, setting $\theta = \pi/2$ and separating the strong beams by $a/\mathrm{w}_{0,0} = 6$, we calculate I_d along the x-axis at $y = 1$ m, shown in Fig. 3.3 **a**. The figure clearly shows a familiar squared cosine with symmetric, decaying envelope function, similar to the square of the Fourier transform of a double-slit transmission aperture. This result is expected if one notes that with the above numerical parameters, the diffraction parameter ν_x along the x direction is much smaller than unity, which allows us to neglect Fresnel terms in the integral. By using Eq. (3.48), and integrating in just the x-direction we achieve:

$$I_d(x, y, z = 0, \omega_p) \propto I_{p,0} \exp\left[-\frac{(x/r)^2}{2\sigma_x^2}\right] \cos^2\left[\omega_p a(x/r)\right], \quad \sigma_x^2 := \frac{\lambda_p \sqrt{2}}{\pi \mathrm{w}_{s,0}}, \quad (3.56)$$

with $I_{p,0} = E_p^2/8\pi$, reproduces the position of the fringes, but with an envelope function that decays too quickly, exemplifying the need to consider the full three-dimensions. The cosine term originates from the interference between the vacuum current generated in the two slits, and is independent of the single-slit shapes of the strong beams. We compare this simplified Fourier pattern with the diffraction pattern generated by numerically evaluating the original three-dimensional integral in Fig. 3.3 **a**, and the deviation as x/r is increased shown. The overall agreement with the double-slit picture however, shows that when VPEs are elicited by a laser, one can successfully envisage the vacuum as a birefringent solid-state material. For a moment, we discuss I_d along the x-axis using the double-shaft set-up with X-ray wavelength. Using the same parameters as in the double-slit case, we plot the result in Fig. 3.4 **a**. In this way, we can make a direct comparison of the two geometries and notice a startling difference. The double-shaft fringes are in the same position as for the double-slit as one would expect, but in addition, the single-shaft, circular
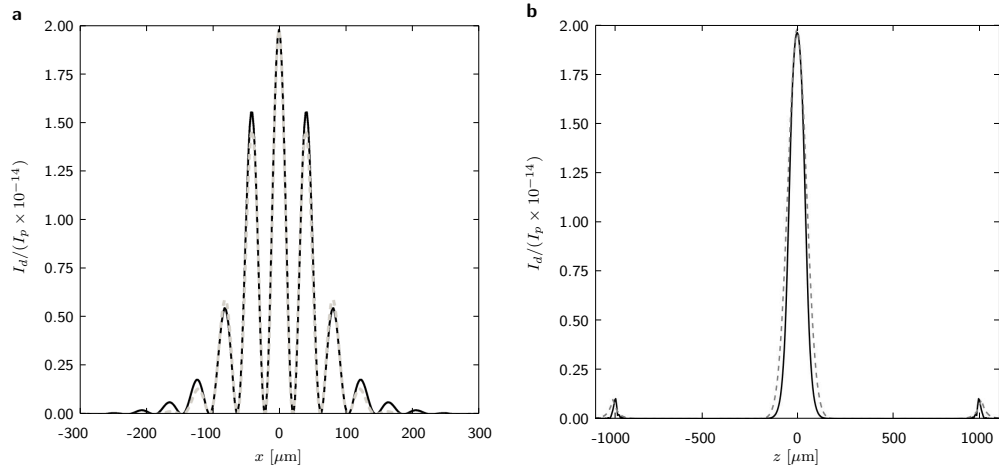
Figure 3.3: In **a**, the one-dimensional Euler-Heisenberg diffracted field along the x-axis for a strong-field separation $x_0/\mathrm{w}_{0,0} = 6$, $I_s = 10^{24}$ Wcm^{-2} and other parameters taken from Tab. 3.2, is plotted with a solid line. The dashed line indicates the result obtained by the simplified one-dimensional integral given by Eq. (3.56), with correct peak position but incorrect peak heights, particularly with increasing x-position. Similarly, in **b**, the one-dimensional field with $a/\mathrm{w}_{0,0} = 0$ is plotted along the z-axis, with the dotted line representing the simplified analytical approach keeping quadratic terms in the exponential, described in the text.

aperture diffraction pattern clearly appears. It follows that the envelope of the entire pattern therefore has a different shape to that in the double-slit case. By setting beam-separation to zero, we compare the envelopes in Fig. 3.4 **b**, from which we notice that although the double-shaft pattern appears to decay more quickly, it is actually the case that it is more peaked in the centre. This is a clear exemplification
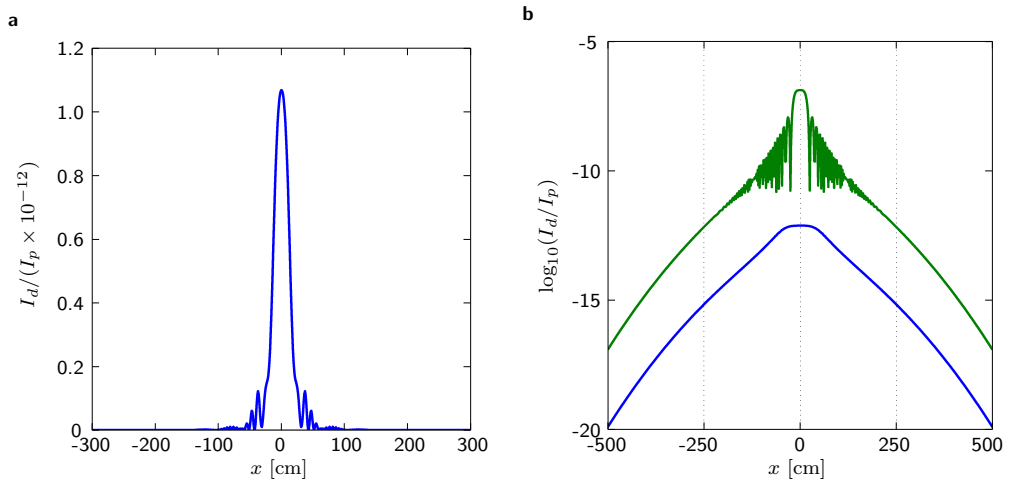

Figure 3.4: The effect of beam geometry. The double-shaft geometry with otherwise the same experimental parameters as in Fig. 3.3 **a** is depicted in **a** and the comparison of diffraction pattern envelopes (for zero beam-separation but otherwise the same parameters) is given in **b** with the double-shaft result larger than the double-slit one.

of the impact of beam geometry on diffraction pattern, as one might expect making the solid-state comparison.

Field diffracted onto the z-axis

Returning to the double-slit set-up, with the X-ray probe focused into a waist $\text{w}_{p,0} = 100$ μm, we consider the diffracted pattern in the z direction i.e. the axis of strong-field propagation. We set $x_0/\text{w}_{s,0} = 0$ and now $x = 0$ and $z \ll y$.

From Fig. 3.3 **b**, we see that the intensity pattern is formed by a central Gaussian, of width ≈ 50 μm, and two smaller exponential-shaped peaks some distance away. Concerning the central peak, when we consider that the amplitude of the strong field along the z-axis, and hence the "vacuum transmission aperture" is governed by the factor $1/(1 + (z'/z_{r,s})^2)$, we see very clearly that the diffracted electromagnetic field does not result from the aperture's Fourier transform, which would have been a decaying exponential, symmetric about the origin, i.e. the wrong shape and with a smaller width of about 10 μm. The presence of the two peaks can be described by the diffraction-grating-like sinusoid along the z'-axis. That the simple Fourier analysis applied in the previous case does not work here, is already clear from the diffraction parameter $\nu_z \sim 25$ not being smaller than unity. We wish to again explain our diffracted field qualitatively, but now how it, and so how Eq. (3.36), depends upon the z' co-ordinate in the detector plane, z. We can see from Eq. (3.44) how the decay of the integrand in the z'-direction is controlled by the softcore $1/(1+(z'/z_{r,s})^2)$ term. The importance and presence of this term in all co-ordinates prevents us separating out the z' from the x' and y' integration variables and hence the z from the x and y detector-plane co-ordinates in the integrands $\mathcal{V}_k$, as we managed to do in the previous case. However, if we consider that $x = 0$ and that $z \ll y$, we can again neglect in Eq. (3.9) the terms proportional to the vectors $\mathbf{u}_1$ and $\mathbf{u}_2$. Unlike the previous situation, in the present case one can recognise that the integrals $\mathcal{V}_3$ and $\mathcal{V}_4$ are not negligible. It can be shown by performing an analysis similar to that done in the previous case that the integrals $\mathcal{V}_1$ and $\mathcal{V}_2$ give rise to the central peak (with width $\text{w}_{p,0}/2 = 50$ μm) while the integrals $\mathcal{V}_3$ and $\mathcal{V}_4$ give rise to the secondary smaller peaks located at $z = \mp 2r\lambda_p/\lambda_0 = \mp 1000$ μm. As we have mentioned, these come about due to terms in the exponential, quadratic in the coordinates, which will have consequences for polarisation measurements. It should be noted that a finite strong-field pulse length, smaller than that of the probe, would show up as a single-slit envelope, whose form would depend on the temporal shape of the pulse and would probably suppress these smaller Fresnel peaks in experiment.

Field diffracted onto the x-z plane

Specialising now to the double-shaft set-up, we take strong-field laser parameters from Tab. 3.2. The effect of the double slits separated by $x_0/\text{w}_{0,0} = 40$ on a probe laser with waist $\text{w}_{p,0} = 290$ μm, is then shown in Fig. 3.5 on a 15 cm $\times$ 15 cm detector at a distance $y = 5$ m. Agreement with the classic double-slit formula can again be seen, indicated by crosses. Each maximum is slightly asymmetric with the peak shifted towards the centre of the pattern. In addition, the typical single-slit rings do not appear. These effects can be understood when studying the analytical expression of Eq. (3.55). The probe Rayleigh length $y_{r,p} \gg l_s$ and so probe defocusing occurs on
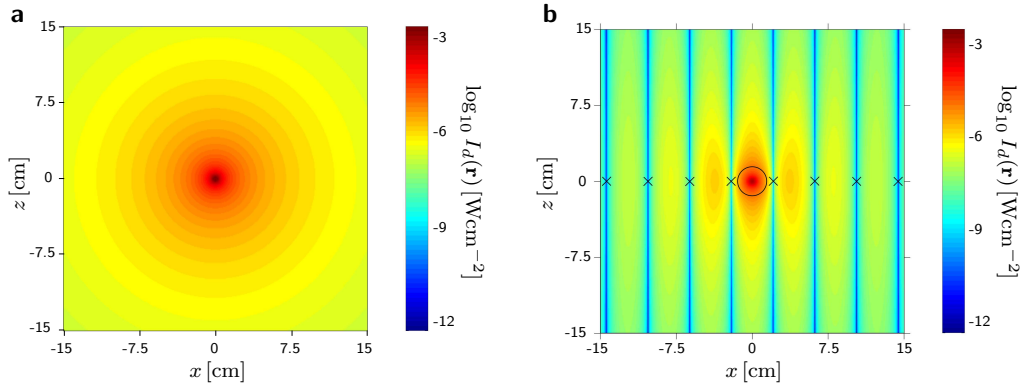
Figure 3.5: I_d, without and with strong laser separation ($x_0/\mathrm{w}_0 = 40$), for the parameters given in the text. The agreement of the well-known formula for diffraction minima: $n\lambda_p = d\sin\vartheta$ for $d = 2x_0$, $\lambda_p = 0.527$ μm, $n \in \mathbb{Z}$ is shown by crosses in **b**. The central circle demarcates the region in which $I_{pd} + I_p \geq 0.01 I_d$.

a length scale much larger than the typical decay length in the problem. In addition as the diffraction parameter $\nu = \mathrm{w}_{s,0}/\lambda_p r \sim 2 \times 10^{-7} \ll 1$, we can neglect all Fresnel terms in the integrand Eq. (3.33). We then arrive at an expression:

$$V_{1,2}^h = y_{r,s}\mathrm{w}_{s,0}^2 \int_{-\infty}^{\infty} d^3 r' \frac{\exp\left[-\mathscr{F}_{1,2}'^h\right]}{1 + y'^2}, \tag{3.57}$$

$$\mathscr{F}_{1,2}'^h = i\omega_p\left(y_{r,s}y' + \frac{\mathrm{w}_{s,0}xx' + y_{r,s}yy' + \mathrm{w}_{s,0}zz'}{r}\right)$$
$$+ \frac{2[(x - \beta_{1,2}x_0)^2 + (z - \beta_{1,2}z_0)^2]}{\mathrm{w}_{s,0}^2(1 + y'^2)} + \frac{x'^2 + z'^2}{\mathrm{w}_{p,0}^2}, \tag{3.58}$$

which we can approximately integrate, assuming $\lambda_p/\pi \mathrm{w}_{p,0} < x/r, z/r \ll 1$ and that the cosine integral can be neglected $y_{r,s}/x_0 \ll 1$. After insertion into I_d (Eq. (3.55)), we then have:

$$I_d \approx \frac{98\pi^3}{45^2} I_p\left(\frac{\mathrm{w}_{s,0}^2}{\lambda_p r}\right)^2\left(\alpha\frac{I_s}{I_{cr}}\right)^2 \cos^2\left[\omega_p\left(\frac{x}{r}x_0 + \frac{z}{r}z_0\right)\right] H\left(\frac{x^2 + z^2}{r^2}\right), \tag{3.59}$$

with H being the single-slit envelope function:

$$H\left(\frac{x^2 + z^2}{r^2}\right) = \frac{\exp\left[-\frac{\pi \mathrm{w}_{s,0}}{\lambda_p}(x^2 + z^2)/r^2\right]}{(x^2 + z^2)/r^2}. \tag{3.60}$$

In order to compare the accuracy of the envelope function, we set $x_0 = 0$ (which, as $\mathcal{V}_3, \mathcal{V}_4$ essentially become equal to $\mathcal{V}_1, \mathcal{V}_2$ corresponds to multiplying by a factor 4 the above expression for I_d) and the agreement with numerical results is then displayed in Fig. 3.6. Unlike the classic two-dimensional Fourier transformation of slit-like aperture functions, we have a fully three-dimensional integral and it is the final integration in the y' co-ordinate that gives the Coulomb-like dependence in detector-plane co-ordinates, x and z, which is softened further by an exponential at the origin (Eq. (3.60)). This smoothness of the three-dimensional aperture at once explains why no single-slit rings appear and also why the maxima, multiplied by this single-slit envelope, are "tilted" toward the centre of the pattern. With these

parameters, there is indeed an exponential decay but the decay length $\sim \lambda_p r / \pi \mathrm{w}_{s,0}$ is much larger than the region in which our calculations are valid, $x/r, z/r \ll 1$. As previously mentioned Coulomb-like dependence defines no decay length and within these values of x/r and z/r, changes very little on the detector plate compared to the probe Gaussian of width $\sim \mathrm{w}_{p,0} \ll x/r, z/r$, all of which supports the much greater width of I_d compared to I_{pd}. Turning to quantitative results, we envisage verifying
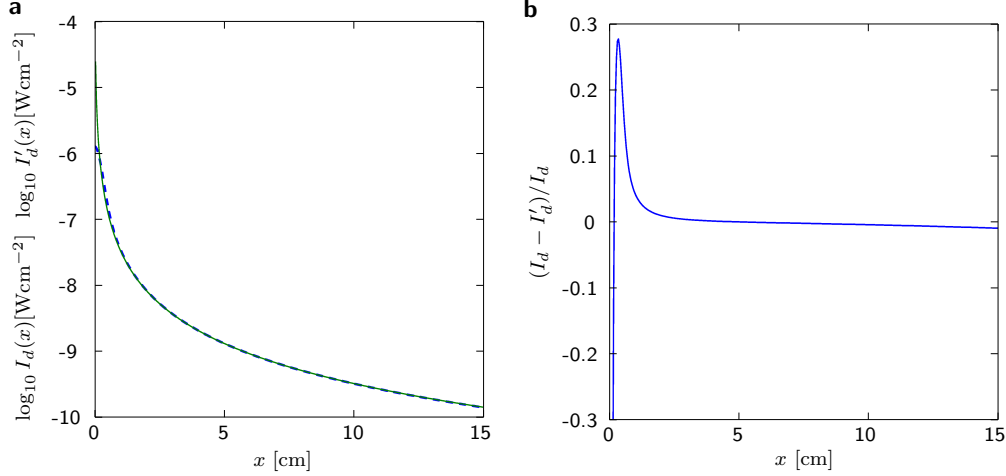

Figure 3.6: The agreement of the analytical approximation to the diffracted intensity $I'_d(x)$ for zero strong-beam separation. In **a**, we see how the envelope function $\sim 1/(x/r)^2$ attained after a full three-dimensional integral (dashed-line) agrees with the full numerical result, with **b** showing the normalised difference.

the phenomenon by either a full or partial resolution of the interference pattern, or else by simple counting of diffracted photons. By making the grid of points in Fig. 3.6 ever-finer, we can see how the integral and therefore the predicted number of photons per shot converges. Since the diffraction pattern must be smooth, this number should then yield a reliable value. At our probe's wavelength of 527 nm commercially available back-illuminated CCDs have an efficiency of 90% [143]. From numerical results for the aforementioned typical experimental parameters, on a region in which $I_d(\mathbf{r})$ is more than one-hundred times larger than $I_p(\mathbf{r})$ and $I_{pd}(\mathbf{r})$, taking into account CCD efficiency, we expect per shot of the strong field, 4 photons from the vacuum signal. This point is further expounded in Sec. 3.2.3.

3.2.2   Probe-vacuum cross-term I_{pd}

Evaluation of the I_{pd} term Eq. (3.54) in the double-slit arrangement, for a strong-beam separation of $x_0/\mathrm{w}_{s,0} = 12$, $\theta = \pi/2$ and the remaining parameters those in Tab. 3.2, is shown in Fig. 3.7 **a**. The position of the double-slit fringes is still clearly noticeable and agrees with the classic formula but there is also some new structure in the z-direction. Since the I_{pd} term spreads out in the x-z plane with a width $\sqrt{2}$ larger than that of the probe, there exist regions in which the ratio of diffracted to probe signal is favourable (see the log plot of the signal-to-noise ratio Fig. 3.7 **b**). In order to maximise this advantage, we choose parameters such that the spread of the probe is smallest on the detector, which given a probe width of $\mathrm{w}_{p,0}\sqrt{1 + (y\lambda_p/\pi \mathrm{w}_{p,0})^2}$,
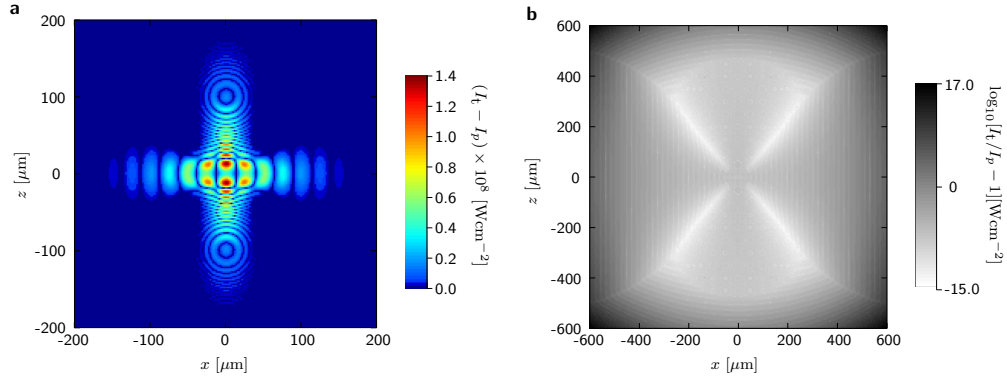
Figure 3.7: Plot **a** is of the double-slit I_{pd} vacuum signal intensity, with the same experimental parameters as Fig. 3.3. In plot **b**, we show the logarithm to the base 10 of the relative difference in intensity due to the vacuum signal in **a**, I_{pd}/I_p, the signal-to-noise ratio.

is minimised for $w_{p,0} = \sqrt{y\lambda_p/\pi}$, giving a width of $\sqrt{2y\lambda_p/\pi}$. At the same time, moving too far from the centre of the pattern will reduce the intensity to the point where nothing can be detected. If we consider drilling a hole of radius ρ into the centre of the detector and taking the decay of the $\mathbf{E}_d$ term in I_{pd} to be comparatively flat as an approximation we obtain limits on ρ:

$$\left[\ln N_{pd}\right]^{1/2} \gtrsim \frac{\rho}{w_p(y)} \gtrsim \left[\ln \frac{N_p}{N_{pd}}\right]^{1/2}, \tag{3.61}$$

for total incident probe and cross-term diffracted photons N_p, N_{pd}. This agrees with the intuitive notion that to stand any chance of measurement, the total signal must be larger than statistical noise, which if modelled with Poisson statistics implies $N_{pd} > \sqrt{N_p}$ [12]. Now, we can either fulfil this condition that the vacuum signal is larger than the minimum background noise over the entire plate, or we can consider measuring counts only in regions where $N_{pd}(\rho) \gtrsim N_p(\rho)$. In both cases, the number of diffracted photons will simply increase with probe intensity, whereas as N_p depends only on laser energy and wavelength λ_p and so for larger probe intensity, we can easier fulfil both bounds on ρ in Eq. (3.61). First setting $y = 50$ cm and the still at ELI comfortably attainable $I_0 = 5 \times 10^{24}$ Wcm^{-2}, for a probe focal width of 8 μm, we achieve $N_{pd} = 7.5 \times 10^7$ from $N_p = 8.0 \times 10^{12}$ probe photons per shot. Secondly, we can plot how $N_{pd}(\rho)$ varies with hole radius, and for a tighter probe beam focal width of $w_{p,0} = 3.6$ μm, which, in the light of recent results of focusing hard 20keV photons to a width of $7nm$[131], we expect to be attainable in the near future, we achieve the dependency shown in Fig. 3.2.2. In the region $N_{pd}(\rho) \gtrsim N_p(\rho)$, taking into account the efficiency of commercially-available CCDs for $\lambda_p = 0.4$ nm or 3.2 keV photons($\gtrsim 90\%$ [8]), we expect approximately two diffracted photons to be measurable per shot of the probe beam. This can then be compared with the results of the previous section for I_d which, by not being subject to the probe Gaussian envelope, has a much wider spread, and is possibly easier to measure as reported in

---

[12]When the statistical error on the number of photons is modelled by a Poisson distribution, the relative error in the mean photons measured per shot, μ, given by $1/\sqrt{n\mu}$ for n shots. As long as lower intensity lasers still satisfy the condition $N_{pd} > \sqrt{N_p}$, they can indeed be used, it is just a question of how long the experiment can be run to make $n\mu$ large enough to effectively eliminate statistical errors.

[102], with the caveat that an optical probe was used with an energy 2.5×10^3 larger than in the present X-ray case.
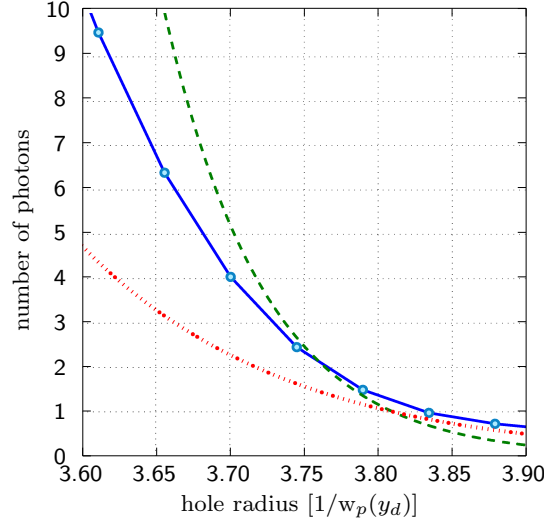

Figure 3.8: For a probe beam focused to $w_{p,0} = 3.6$ μm, $w_{p,0} = 5.0$ μm and a large enough detector hole radius ρ, the photon count from the vacuum-probe cross term $N_{pd}(\rho)$ (solid-line) becomes comparable to that from the probe $N_p(\rho) = N_p(0) \exp(-2(\rho/w_p)^2)$ (dashed-line) (here around 2 diffracted photons) and greater than statistical noise from the probe $\sqrt{N_p(\rho)}$ (dotted-line).

3.2.3   Photon counting

One can pose the question: how many photons do we require in order that we can say, to some confidence level, that we indeed have the anticipated double-slit pattern? Such a question is likely to be theoretical unless experimentalists can align the strong and probe beams with sufficient precision. Nonetheless, one can calculate the *visibility*, V of any interference pattern by splitting the detector into strips aligned parallel to the pattern and with equal widths ideally capturing alternate regions of maxima and minima. The total intensity falling on regions containing "maxima" is then assigned I_{max} and that falling on minima I_{min}. In an experiment, as the number of photons N that have been registered by the detector, increases, the visibility:

$$V(N) = \frac{I_{max}(N) - I_{min}(N)}{I_{max}(N) + I_{min}(N)} \qquad V \in \mathbb{R}, \;\; 0 < V < 1, \qquad (3.62)$$

should tend towards the population visibility $V_\infty = \lim_{N \to \infty} V(N)$. As $V(N)$ is a stochastic variable, we can imagine how it will fluctuate around this population value. Defining the sample size with a maximum number of photons per experiment N_0, we can conduct many "photon counting" trials to observe how the relative error $(V(N) - V_\infty)/V_\infty$ drops below a given error value after a certain number of photons have arrived. Focusing on the most attractive results: I_d for the double-shaft, shown in Fig. 3.5, we performed $10,000$ such numerical experiments, in each of which, are registered $N_0 = 10,000$ photons.

By "drilling" a hole in the centre of the I_d distribution, we can consider regions in which $I_d \geq 100(I_{pd} + I_p) \gg I_{pd} + I_p$. Using the symmetry in the total diffraction pattern, we can sum grid squares along the direction of the fringes and after normalising to unit area, reduce the two-dimensional to a one-dimensional PDF (probability density function), which in our case, had 256 points. Since, when forming the visibility, we are only interested in the counts in the I_{max} and I_{min} bins, we split the 256 points into 16 bins of alternating maxima-minima stripes and average the contents. We now have a 16-point PDF and assign, based upon the shape of the pattern the eight "maxima" and eight "minima". From this we can already calculate the population visibility, because $N \to \infty$ photons would distribute themselves exactly in the proportions given by the PDF. This yields in our case, $V_\infty = 47.6\%$. We then randomly generate detected photon positions based upon this PDF, forming a list with 10,000 entries. The visibility $V(N)$ is then calculated for the first N points and the relative error calculated as a function of N. An example of some stochastic "trails" the visibility followed, are registered in Fig. 3.9 **b**. This is then repeated 10,000 times and the 10,000 trails are then analysed to find the maximum N_x at which an error was greater than a given value x. These N_xs are then averaged over and the results plotted in Fig. 3.9 **a**. With our aforementioned experimental parameters for measur-
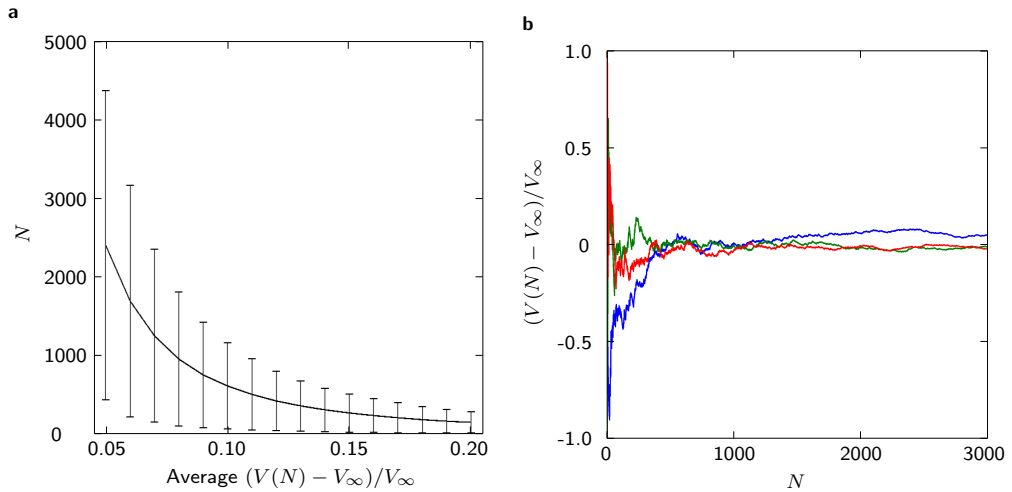
Figure 3.9: In **a**, with 10,000 photons per 10,000 trials, the expected number of photons N required to reduce the error in the visibility below the values on the horizontal axis is plotted, along with error bars given by the standard deviation of N over the trials. Three typical stochastic "trails" of how the visibility $V(N)$ with number of registered photons N oscillates around the population visibility V_∞ is depicted in **b**.

ing I_d in the double-shaft set-up, we deduce from Fig. 3.9 **a**, that $\sim 1,000$ photons are required before the error in the visibility will typically fall below 10%, although the standard deviation remains fairly large. With ELI, this corresponds to an operating time of approximately four hours. This process could then be repeated for e.g. I_{pd}.

3.3   Induced ellipticity and polarisation rotation

The goal of this section is to calculate the rotation of the polarisation ψ and induced ellipticity ε of the probe electromagnetic wave when the vacuum contribution is added, $\mathbf{E}_{\mathrm{t}} = \mathbf{E}_p + \mathbf{E}_d$. We will show how the geometry of the pulses plays again an important role. Focusing our analysis on the polarisation of the diffracted probe on a small region around the origin in the detector plane allows us to deal with collimated waves for which polarisation quantities are well-defined. Moreover in this region, we can also compare results to previous calculations [142, 82]. We then set $x, z \to 0$ in Eq. (3.47) and notice that in the double-shaft case, for a finite strong-field separation, we have a mirror symmetry in both x, x_0 and z, z_0 co-ordinates. Therefore, the same diffracted field impinges on $(x, z) = (0, 0)$ if we perform a reflection on one beam in the x_0 and z_0 co-ordinates, i.e. simply place the one beam on top of the another and form a "single-shaft" geometry of a single, displaced strong laser beam. In the double-slit geometry, although this symmetry is present in the x and x_0 co-ordinates, as both strong beams together generate a standing wave, we cannot replace the two with a single beam set-up. However, it has already been argued that the wave oscillations contribute only a negligible amount to the diffracted field Eq. (3.48) and so, when $y_0 \ll y_{r,p}$, y_0 is an inconsequential parameter in polarisation measurements in the double-slit case (which we demonstrate later), so in principle a displaced single-slit geometry would give very similar results to the double-slit case.

Once derived, our results will be an enhancement of the single-slit, on-axis ($x_0 = y_0 = 0$) geometry of [142], which also lacked probe defocusing terms and suffered therefore from the unphysical result that all vacuum polarisation effects on the probe polarisation tended to zero with increasing observation distance. These results therefore form a useful comparison to discuss the effects of these changes in the experimental set-up.

Derivation of expressions

We begin by deriving expressions for the ellipticity and polarisation direction in the most straightforward way. These two quantities are independent of time and this detail must also appear in the derivation. This can be achieved by utilising the fact that the probe field and vacuum contribution are in phase. We will concentrate on the electric field part of the wave as by Faraday's equation the magnetic part will have the same behaviour, and imagine the field vector tracing out an ellipse: where $\mathbf{E}_{\mathrm{t}}(\mathbf{r}, t) = \mathbf{E}_p(\mathbf{r}, t) + \mathbf{E}_d(\mathbf{r}, t)$, as shown in Fig. 3.10. With $\eta = \psi_p + \omega_p t - k_p y$, by splitting up the sinusoidal time dependence into spatial and temporal parts, we can rewrite Eqs. (3.47) and (3.48) using the time-dependence of the strong field defined in Eq. (3.29) as well as the probe field in the following way:

$$\mathbf{E}_d^h(\mathbf{r}, t) = \frac{I_0}{I_{cr}} \frac{8\alpha E_p}{45\lambda_p^2 r} \left(\mathfrak{Re}\mathcal{V}_2^h \sin\eta - \mathfrak{Im}\mathcal{V}_2^h \cos\eta \right) \left[\cos\theta, 0, \tfrac{7}{4}\sin\theta \right], \qquad (3.63)$$

$$\mathbf{E}_d^l(\mathbf{r}, t) = \frac{I_0}{I_{cr}} \frac{\alpha E_p}{45\lambda_p^2 r} \sum_{n=1}^{2} \left(\mathfrak{Re}\mathcal{V}_n^l \sin\eta - \mathfrak{Im}\mathcal{V}_n^l \cos\eta \right) \left[\cos\theta, 0, \tfrac{7}{4}\sin\theta \right], \qquad (3.64)$$

$$\mathbf{E}_p(\mathbf{r}, t) = \left(\mathrm{E}_p^{(1)} \sin\eta - \mathrm{E}_p^{(2)} \cos\eta \right) \left[\cos\theta, 0, \sin\theta \right], \qquad (3.65)$$
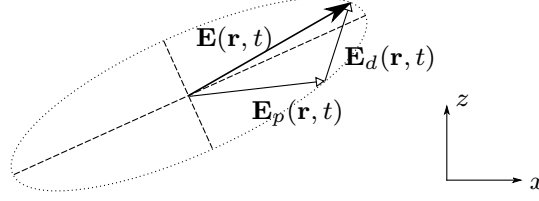
Figure 3.10: The total emergent field $\mathbf{E}_{\mathrm{t}} = \mathbf{E}_p + \mathbf{E}_d$, which for an angle of probe polarisation $\theta \neq 0$, has components both parallel to the polarised vacuum in the x-direction as well as perpendicular in the z-direction. The phase difference acquired from the differing refractive indices these components feel, induces an ellipticity in the emergent field (birefringence). The probe vector is rotated when the diffracted component, which is in phase, is added (dichroism).

where we have defined:

$$
\mathrm{E}_p^{(1)} := \mathrm{E}_p \frac{\exp[-\frac{x^2+z^2}{\mathrm{w}_p}]}{1 + (y/y_{r,p})^2} \qquad \mathrm{E}_p^{(2)} := \mathrm{E}_p \frac{\exp[-\frac{x^2+z^2}{\mathrm{w}_p}]}{1 + (y/y_{r,p})^2} \frac{y}{y_{r,p}}. \tag{3.66}
$$

For either geometry we can form the following matrix equation:

$$
\begin{pmatrix} \mathbf{E}_{\mathrm{t}}^{h,l} \cdot \hat{\mathbf{x}} \\ \mathbf{E}_{\mathrm{t}}^{h,l} \cdot \hat{\mathbf{z}} \end{pmatrix} = \begin{pmatrix} (4\mathfrak{Re}\mathcal{X}^{h,l} + E_p^{(1)})\cos\theta & (-4\mathfrak{Im}\mathcal{X}^{h,l} + E_p^{(2)})\cos\theta \\ (7\mathfrak{Re}\mathcal{X}^{h,l} + E_p^{(1)})\sin\theta & (-7\mathfrak{Im}\mathcal{X}^{h,l} + E_p^{(2)})\sin\theta \end{pmatrix} \begin{pmatrix} \sin\eta \\ \cos\eta \end{pmatrix}, \tag{3.67}
$$

with:

$$
\mathcal{X}^h = \frac{2\alpha}{45\lambda_p^2 r} \frac{I_0}{I_{\mathrm{cr}}} E_p \mathcal{V}_2^l, \tag{3.68}
$$

$$
\mathcal{X}^l = \frac{\alpha}{180\lambda_p^2 r} \frac{I_0}{I_{\mathrm{cr}}} E_p \sum_{n=1}^{2} \mathcal{V}_n^l. \tag{3.69}
$$

Eq. (3.67) can be inverted and squared to eliminate the time-dependent terms and give the desired equation of an ellipse, $A^{h,l}x^2, +B^{h,l}xz + C^{h,l}z^2 = r^2$, where the x and z co-ordinates are given by the corresponding components of the total electric field and:

$$
\begin{aligned}
A^{h,l} &= \left[(E_p^{(1)})^2 + (E_p^{(2)})^2 + 14(\tilde{\mathcal{V}}_r^{h,l} E_p^{(1)} + \tilde{\mathcal{V}}_i^{h,l} E_p^{(2)}) \right. \\
&\quad \left. + 49((\tilde{\mathcal{V}}_r^{h,l})^2 + (\tilde{\mathcal{V}}_i^{h,l})^2) \right] \sin^2\theta, \\
B^{h,l} &= -\left[(E_p^{(1)})^2 + (E_p^{(2)})^2 + 11(\tilde{\mathcal{V}}_r^{h,l} E_p^{(1)} + \tilde{\mathcal{V}}_i^{h,l} E_p^{(2)}) \right. \\
&\quad \left. + 28((\tilde{\mathcal{V}}_r^{h,l})^2 + (\tilde{\mathcal{V}}_i^{h,l})^2) \right] \sin 2\theta, \\
C^{h,l} &= \left[(E_p^{(1)})^2 + (E_p^{(2)})^2 + 8(\tilde{\mathcal{V}}_r^{h,l} E_p^{(1)} + \tilde{\mathcal{V}}_i^{h,l} E_p^{(2)}) \right. \\
&\quad \left. + 16((\tilde{\mathcal{V}}_r^{h,l})^2 + (\tilde{\mathcal{V}}_i^{h,l})^2) \right] \cos^2\theta, \tag{3.70}
\end{aligned}
$$

where $\tilde{\mathcal{V}}_r^{h,l} = \mathfrak{Re}\tilde{\mathcal{V}}^{h,l}$, $\tilde{\mathcal{V}}_i^{h,l} = \mathfrak{Im}\tilde{\mathcal{V}}^{h,l}$ with $\tilde{\mathcal{V}}^h = 2\mathcal{V}_1^h$ and $\tilde{\mathcal{V}}^l = \mathcal{V}_1^l + \mathcal{V}_2^l$. The situation is simplified by first performing an orthogonal rotation of the co-ordinates $\mathbf{M}(\phi_0) \in$ SO(2) by an angle ϕ_0 which removes the xz term and thus aligns the major and minor axes of the ellipse with the x and z the co-ordinates. Once this rotation angle

ϕ_0, equal to the total polarisation angle, is found, the formula for the ellipticity is then simply the ratio of the minor to the major axis lengths i.e. the new coefficients A', C' of x^2 and z^2, giving the following:

$$\tan 2(\theta + \psi) \;=\; \frac{-B}{C - A}, \tag{3.71}$$

$$(\tan \varepsilon)^2 \;=\; \frac{(A + C)\sqrt{(A - C)^2 + B^2} - (A - C)^2 - B^2}{(A + C)\sqrt{(A - C)^2 + B^2} + (A - C)^2 + B^2}, \tag{3.72}$$

where $\theta + \psi = \phi_0$ is the new polarisation for the total field, probe plus vacuum. By expanding these expressions Eq. (3.71) to first order in all small variables: $\tilde{\mathcal{V}}_{r,i}^{h,l}/E_p$, ψ and ε, one finally achieves the desired quantities:

$$\psi^h \;=\; \frac{\alpha \sin 2\theta}{15\lambda_p^2} \frac{I_0}{I_{cr}} \Big(\frac{\mathfrak{Re}\mathcal{V}_1^h}{y} + \frac{\mathfrak{Im}\mathcal{V}_1^h}{y_{r,p}} \Big), \tag{3.73}$$

$$\varepsilon^h \;=\; \frac{\alpha \sin 2\theta}{15\lambda_p^2} \frac{I_0}{I_{cr}} \Big(\frac{\mathfrak{Re}\mathcal{V}_1^h}{y_{r,p}} - \frac{\mathfrak{Im}\mathcal{V}_1^h}{y} \Big), \tag{3.74}$$

$$\psi^l \;=\; \frac{\alpha \sin 2\theta}{120\lambda_p^2} \frac{I_0}{I_{cr}} \sum_{k=1}^{2} \Big(\frac{\mathfrak{Re}\mathcal{V}_k^l}{y_{r,p}} + \frac{\mathfrak{Im}\mathcal{V}_k^l}{y} \Big), \tag{3.75}$$

$$\varepsilon^l \;=\; \frac{\alpha \sin 2\theta}{120\lambda_p^2} \frac{I_0}{I_{cr}} \sum_{k=1}^{2} \Big(\frac{\mathfrak{Im}\mathcal{V}_k^l}{y_{r,p}} - \frac{\mathfrak{Re}\mathcal{V}_k^l}{y} \Big). \tag{3.76}$$

Analysis and results

We notice that unlike the previous case, these vector vacuum polarisation effects are maximised for $\theta = \pi/4$. In addition, since diffraction doesn't play a role and ψ and ε increase with frequency (even after the integrations are performed), we would profit from switching to an X-ray probe laser such as the XFEL at DESY whose parameters were mentioned in Tab. 3.1.

As an initial check of our results, taking the limit of $x_0, y_0, \to 0$; $y_{r,p} \to \infty$ in ψ^l, ε^l, we recover the expression in [142]. We also note that the introduction of more experimentally relevant defocusing terms in the probe, produces the more realistic and expected result that $\lim_{y \to \infty}\{\psi, \varepsilon\} = \{\psi_\infty, \varepsilon_\infty\} \neq \{0, 0\}$.

As a further confirmation of validity, we can compare these expressions to existing calculations arrived at by Heinzl et al. [82] when we take $x_0 = z_0 = 0$ and the two limits: the *refractive-index* and the *crossed-field* limit. The first is obtained when we take $y \to 0$ (near region), in a regime where ψ becomes linear with y and disappears, and ε converges to a constant. The crossed-field limit corresponds to a constant strong field, i.e. $k_0 \to 0$, which we can achieve when we let the counter-propagating pulse be e.g. of the form of a cosine. This ensures that neither the strong electric nor magnetic field disappears in this limit, so that we can keep the normalisation used in Eqs. (3.73) and (3.74). To be consistent, the time-averaging procedure which was equivalent to neglecting evanescent waves must be repeated with the precondition that $k_0 = 0$ as $\langle \cos^2(\omega_p t) \rangle = 1/2 \neq \langle \lim_{\omega_p t \to 0} \cos^2(\omega_p t) \rangle = 1$, for a $\langle \rangle$ a time-average over integer number of periods. Then Eq. (3.74) tends to the result in [82]:

$$\varepsilon = \frac{2\alpha\pi}{15} \frac{I_0}{I_{cr}} \frac{l}{\lambda_p} \sin 2\theta; \qquad l = \frac{y_{r,p} y_{r,0}}{y_{r,p} + y_{r,0}}. \tag{3.77}$$

The only difference to the formula in [82] is that we have incorporated the focusing of the strong- and probe- fields, which automatically generates the effective interaction length l of the beams. Focusing on our results, first in the double-slit geometry, we
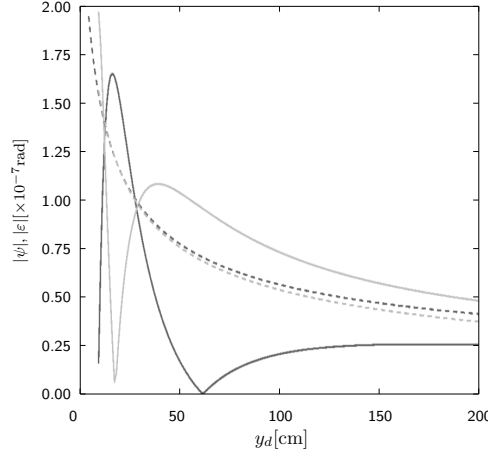

Figure 3.11: With parameters from Tab. 3.2, dark lines represent absolute polarisation rotation and light ones absolute induced ellipticity, the dashed lines are values for $x_0 = 0$ without probe defocusing terms given in [142], and the solid lines represent the new values with strong-field beams separated by $x_0/\mathrm{w}_{s,0} = 10$.

vary y and set $\theta = \pi/4$ to maximise the effect of the polarised vacuum and show a demonstrative plot in Fig. 3.11, for how ψ^l and ε^l vary for a fixed strong-field beam separation, $x_0/\mathrm{w}_{s,0} = 10$, $y_0 = 0$, with the other parameters taken from Tab. 3.2. The first difference we note is that in comparison with results from [142], for $y \ll y_{r,p}$, polarisation and ellipticity oscillate rapidly and there are sizeable ranges where both are larger than that for previously derived results. For the choice of parameters in the plot, $y_{r,p} \approx 80$ m, and so if we keep within this range, i.e. disregard the effect of defocusing terms, we can clearly ascertain the improvement brought by separating the strong-field beams. This perhaps counterintuitive result is an exemplification of VPEs' sensitive dependence on beam geometry and can be shown to be consistent by following through the conditions on the detector-plane co-ordinates and studying the form of the integrals $\mathcal{V}_{1,2}$ (Eqs. (3.33) and (3.38)) which appear in our expressions for ψ and ε (we can once more disregard the contribution of $\mathcal{V}_{3,4}$):

$$\mathcal{V}_{1,2} = \int dy'\, dz' \frac{1}{1 + (z'/z_{r,s})^2} \exp\left[-i\omega_p \frac{z'^2}{2y} - \frac{z'^2}{\mathrm{w}_{p,0}^2}\right] \mathcal{I}_{y',\pm}\, \mathcal{J}_{x',\pm}, \qquad (3.78)$$

$$\mathcal{I}_{y',\pm} = \int dy' \exp\left[\frac{-2(y' - y_0)^2}{\mathrm{w}_0^2}\right], \qquad (3.79)$$

$$\mathcal{J}_{x',\pm} = \int dx' \exp\left[-i\omega_p \frac{x'^2}{2y}\right] \exp\left[-\frac{x'^2}{\mathrm{w}_{p,0}^2}\right] \exp\left[\frac{-2\left(x' \mp x_0\right)^2}{\mathrm{w}_0^2}\right], . \qquad (3.80)$$

From Eq. (3.79) we can see more clearly, that under these conditions (most notably that $y_0 \ll y_{r,p}$), since there is no other structure in the y-direction, y_0 becomes an inconsequential parameter when measuring polarisation and ellipticity in the double-slit case and is set to zero. By separating strong-field beams in the x-direction, we see that we only produce an effect on the x'-integrals, $\mathcal{J}_{x',\pm}$. When considering the contribution from the first complex exponential factor in Eq. (3.80), for a fixed x_0, in

varying y, we vary the overlap this factor's real cosine and imaginary sine functions with the other two Gaussian integrand factors, which have maxima at $x' = 0$ and $x' = \mp a$ respectively. Hence some values of y form local maxima in ψ and ε, and due to the trigonometric nature of the varying function, we have the oscillating shape in Fig. 3.11. However, in the limit $y \to 0$, both of these values tend to constants:

$$\psi = 0; \quad \varepsilon = \frac{\alpha\sqrt{\pi}}{30\sqrt{2}} \frac{I_s}{I_{\text{cr}}} \frac{\text{w}_{s,0}}{\lambda_p} \exp\left[-\frac{2x_0^2}{\text{w}_{s,0}^2}\right] \sin 2\theta \tag{3.81}$$

We also show how ψ and ε depend upon beam-separation x_0 in Fig. 3.12, which
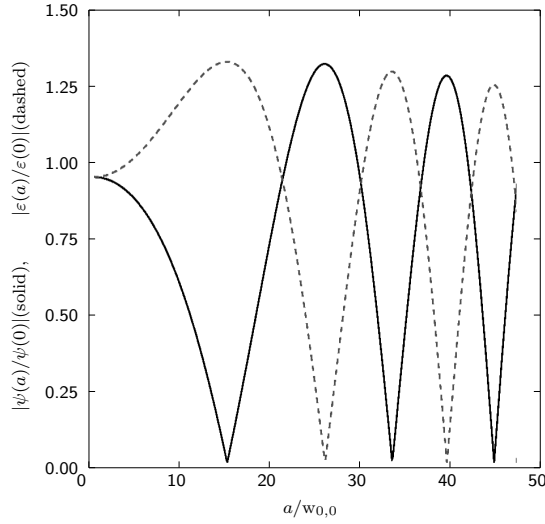

Figure 3.12: The ratios of $|\psi(x_0)/\psi(0)|$ (continuous line) and $|\varepsilon(x_0)/\varepsilon(0)|$ (dashed line) in the double-slit set-up for the same parameters as in Fig. 3.3 but with $\text{w}_{p,0} = 200\ \mu\text{m}$. The ratio $|\psi(x_0)/\psi(0)|$ was chosen in preference to the ratio of $|\psi(x_0)|$ with that in the original paper [142] as introduction of focusing terms doesn't make the latter a viable comparison.

also shows oscillatory behaviour, with the consistency of the results being explained with similar arguments to those above for the dependence on y. In varying x_0, the first two factors in Eq. (3.80) act as fixed peaks, whereas the final Gaussian term is moved to place its peak $x = \mp x_0$, at such a position which could be used to maximise the integral. We recall from Eq. (3.73)-Eq. (3.76) that ψ and ε have predominantly real and imaginary parts respectively. When considering the contribution from the imaginary part of the integrand, we see that the maximum of the first complex exponential factor, i.e. of the sinusoidal, will not occur at the origin, unlike that of the second Gaussian factor, and hence in order to maximise this integral comprising three functions we should place the peak of the third function somewhere between the peaks of the first two, which corresponds to a value $x_0 \neq 0$. Moreover, as the first sinusoidal factor is periodic, and has a wavelength much smaller than the width $\text{w}_{p,0}$, of the Gaussian which multiplies it, we should have a series of maxima in both $\psi(x_0)$ and $\varepsilon(x_0)$ which decay slowly with x_0 (see Fig. 3.12). For the case $y \ll y_{r,p}$, our explanation would on the one hand predict that the value of $\varepsilon(x_0)$ would initially rise as x_0 increases, and on the other hand justify the maximum of $\psi(x_0)$ being very close to the origin, and hence that $\psi(x_0)$ would decrease as x_0 initially increases from 0. These results can be further confirmed via differentiation under the integral in

Eq. (3.78), and are exactly what we observe in the numerical evaluation depicted in Fig. 3.12. This increase therefore physically exemplifies the role played by Fresnel terms and non-trivial beam geometry. From numerical analysis, the polarisation and ellipticity were found to increase by a factor of 1.4 over $x_0 = 0$ values. It should be noted that neither through varying y nor y_0 directly, did we observe any notable dependence of the results on y_0, corroborates our earlier argument for setting $y_0 = 0$.

In the single-shaft set-up, this time using X-rays, we also see a similar increase in the ellipticity and polarisation rotation.(see Fig. 3.13). For the same experimental parameters as in Fig. 3.3 but with $y = 50$ cm and $a/\mathrm{w}_{s,0} = 10$, we achieve a modest increase in the ellipticity of 1.3 over $x_0 = 0$ values. A double-shaft geometry was tested as to leading to exactly the same relative increase as for the off-axis single-shaft one, which as previously explained, can be understood as a consequence of the symmetry of the set-up. This increase drops off quickly with a, which is a consequence of the shaft geometry, just as seen for the rapid drop-off of I_d with respect to the double-slit set-up.
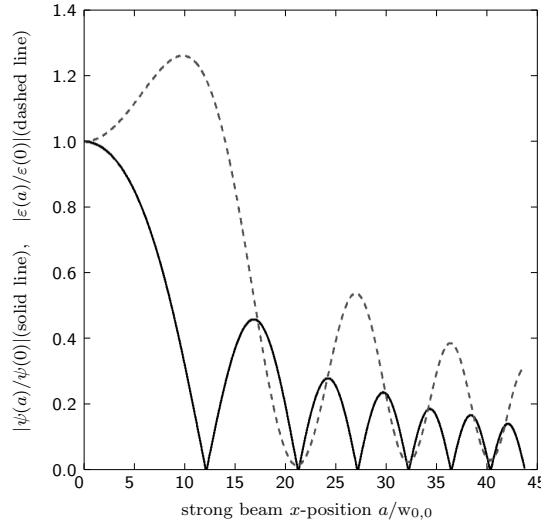

Figure 3.13: The ratios of $|\psi(x_0)/\psi(0)|$ (continuous line) and $|\varepsilon(x_0)/\varepsilon(0)|$ (dashed line) in the single-shaft set-up for the same experimental parameters as in Fig. 3.12 but with $y = 50$ cm.

3.4   Discussion

The prospect of observing the polarised quantum vacuum using lasers is certainly enticing. There are many predictions, from the theory that explains the side of nature we believe we understand best, waiting to be tested in as yet unexplored parameter regimes. With upcoming laser facilities such as ELI [60] and HiPER [86], the technology will soon be ripe to exploit, with also the possibility of discovering new physics [80, 4, 3, 75, 170]. In this arena, on the one hand, we have envisaged a further realisation in the many generations of the double-slit experiment in which we remove all material constituents and investigate light-by-light diffraction. On the other, we have shown how polarisation results can be increased by using such a

double-slit configuration. Often, beam shape and the effects of non-trivial Fresnel diffraction have played a role. From a realistic perspective, in order to observe such effects, many shots of an ultra-intense laser are required. Due to the incredible intensities involved, the accuracy in the positioning of the strong lasers will, aside from issues concerning beam profile, pulse shape, triggering and focal points, prove a great experimental challenge. Nevertheless, a detection of any diffracted photons, in whatever fashion, would be a breakthrough. We now comment on some of the idealisations of our calculations.

Gaussian beam

Throughout our analysis, what we have named a "Gaussian beam" was only the leading-order solution of Maxwell's equation for a wave-like vector potential [154]. The expansion is in the diffraction parameter $\varepsilon = w_{s,0}/y_{r,s}$, with $y_{r,s}$ being the relevant Rayleigh length and since for $\varepsilon \ll 1$, this is approximately an angle with the propagation axis, the solution is also known as the "paraxial beam". This lead to us assigning a provisional accuracy of $\approx \varepsilon = 1/\pi$ to our calculation. We briefly study the effect of higher orders of the general Gaussian beam given in [155], by writing down a general integrand for all possible corrections. The simplified expressions for the diffracted field in the double-shaft case Eq. (3.47) can act as a starting point, showing, that we need only focus on $\mathcal{V}_{1,2}$ for finite beam separation. Ignoring prefactors and choosing a wide probe-beam $w_{p,0} \gg w_{s,0}$, at an observation point $r = y$, we can write:

$$
\delta E_d \quad \sim \quad \int d^3 r' \left(\frac{z}{w_{s,0}} \right)^l \left(\frac{x}{w_{s,0}} \right)^{2m'} \left(\frac{w_s(y)}{w_{s,0}} \right)^{k+1} \left(\frac{x^2 + z^2}{w_s^2(y)} \right)^{t'}
$$
$$
\exp \left[-i\omega_p \left(\frac{x'^2 + z'^2}{2r} \right) - \frac{2}{w_s^2(y)} (x'^2 + z'^2 + x_0^2) - \frac{4\beta_k}{w_s^2(y)} (x' x_0) \right]
$$

where $\sim$ shows the illustrative nature of our arguments, $l = 0$ or 1, $m' = 0$ or 1, $k, n, t' \in \mathbb{N}_0$, and all are equal to zero in the leading-order case we considered. We have also neglected the effect of a phase difference between the probe and strong-field, as this simply amounts to a spatial shift in the longitudinal direction of the time-averaged strong-field, which as already argued, in neither geometry, makes a measurable difference to the diffracted field. By integration it can be shown that all higher order contributions are approximately less than or equal in magnitude to $\epsilon^2 = 1/\pi^2$ times our leading-order solution. In addition, we also note the result from [155] that the first correction to the total intensity of the full Gaussian beam is $\varepsilon^2/4 \sim 0.03$, which motivates us taking only the leading-order term in our calculations as our results are proportional to the strong-field intensity or its value squared. It is possible however, that higher-order corrections may slightly reduce the visibility of the pattern.

Beam shape

One assumption that we have made in considering our set-up "realistic" is that the ultra-intense laser beams that will be produced at forthcoming laser facilities can be faithfully described by the Gaussian beam solution. However, from a detailed study of a $7\,\mu$m-diameter focal spot generated at the Vulcan laser ($\lambda = 1054\,$nm), it was

found that a q-Gaussian of the form $q(\rho) = [1 + (\rho/4.4539)^2]^{-1.4748}$, for ρ equal to the transverse radial co-ordinate, produced the best fit [139, 134]. Although the beam profile $q(\rho)$ is not a solution to Maxwell's equation, the claim that only a distinct separation of beams is required to generate an interference pattern, irregardless of beam shape, can in some way be tested. For our strong beam focal spot of dimension $\mathrm{w}_{s,0} = 0.8$ μm, we instead choose to study $q_1(\rho) = [1 + (\rho/2\mathrm{w}_{s,0})^2]^{-3/2}$, which can be partially analytically tackled. Although it is not possible to calculate a corresponding number of photons, it *is* possible to calculate the visibility. In the double-shaft set-up, using the standard set of parameters given in Tab. 3.2, and a longitudinal beam shape given by the same factor as for the Gaussian beam, the visibility was found to remain approximately the same.

Pulse duration

In using Gaussian beams to represent our lasers, we are, as discussed in the introduction to this chapter, taking the leading order solution to the Helmholtz and simple harmonic oscillator equations. In order to characterise ultra-short laser pulses, it is necessary to include details of the pulse envelope. Suppose we consider the pulse envelope to be Gaussian, then what we are really doing is placing a condition on the spectrum of the radiation[13]. Therefore a general solution to Maxwell's equation can be written as an integral of the product of a solution to the Helmholtz equation, the simple harmonic oscillator equation and a spectral function giving the amplitude of each term, or:

$$f(x, y, z, t, \omega_0, t_0, \mathrm{w}_0) = \int d\omega \; \widetilde{A}(t_0, \omega_0, \omega) g(x, y, z, \omega, \mathrm{w}_0) \exp\left[i\omega(t - z/c)\right], \quad (3.82)$$

with $g(x, y, z, \omega, \mathrm{w}_0)$ being a solution to the Helmholtz equation and t_0 eventually a pulse length and w_0 a pulse width. To obtain a Gaussian pulse, we require the spectral function to equal its Fourier transform, also a Gaussian and can set $\widetilde{A}(t_0, \omega_0, \omega) = (t_0/\sqrt{2\pi}) \exp(-[(\omega - \omega_0)t_0^2]/2)$. It turns out (see e.g. [90]), that by expanding the Helmholtz part of the integral $g(x, y, z, \omega, \mathrm{w}_0)$ as a Taylor series around $\omega = \omega_0$, the nth order of the solution scales as $s \approx [1/(\omega_0 t_0)]^n$. For an electric field polarised along the x-axis and travelling in the z-direction, we have:

$$E_x^{(0)}(t - \frac{z}{c}) = E_0 \exp\left[-\frac{(t - \frac{z}{c})^2}{2t_0^2}\right]$$

$$E_x^{(1)}(t - \frac{z}{c}) = \left\{1 + \frac{2s}{i + \frac{2z}{k_0\mathrm{w}_0^2}}\frac{t - \frac{z}{c}}{t_0}\left[-\frac{iz}{k_0\mathrm{w}_0^2} + \frac{x^2 + y^2}{\mathrm{w}_0^2}\left(1 - \frac{1}{2 + \frac{ik_0\mathrm{w}_0^2}{z}}\right)\right]\right\}$$
$$\times E_x^{(0)}(t - \frac{z}{c}), \quad (3.83)$$

with $E_x^{(n)}$ the nth-order temporal correction to the electric field in the x-direction [90]. Therefore, asserting monochromaticity $\omega_0 t_0 \gg 1$ is equivalent to taking the zeroth-order temporal correction $E_x^{(0)}$. For all other corrections, there is a coupling between temporal and spatial beam corrections which become important in femtosecond pulses [186] and sufficiently increases calculational complexity. In our

---

[13]A temporal Gaussian itself is not a solution to the simple harmonic oscillator equation, but a superposition of plane waves solutions can give a function which has a Gaussian envelope in time.

calculations, we have effectively used a square-wave temporal pulse form. We can see from the zeroth-order, purely temporal correction in Eq. (3.83), that if the pulse is longer than our typical interaction length l, $\sqrt{2}ct_0 > l$, we can consistently approximate the Gaussian with a square wave within the interaction volume. In the *double-shaft* geometry, as our strong-field beams have a longitudinal decay of the form $1/(1 + (z/z_{r,s})^2)$, we define $l = 2z_{r,s}$. As $ct_0 = (0.3 \times t_0 \text{ [fs]}) \ \mu\text{m}$, and $2z_{r,s} \approx 5 \ \mu\text{m}$, we have picked $t_0 = 30$ fs in our numerical examples and scaled the intensity accordingly, such that we are comfortably within the total power given in Tab. 3.1. In the *double-slit* case, although the interaction length along the axis of probe propagation is $w_{s,0}$, along the axis of strong-field propagation it is again $2z_{r,s}$, because of the more difficult geometry and triggering that would be required, we set the duration of the strong field equal to that of the probe, $t_0 = 100$ fs.

Beam geometry

Whilst initially appearing to be different experiments, the double-slit and double-shaft scenarios are two idealisations of the general case of one wide laser beam probing two other, sharply-focused beams. We can relate the two set-ups to one another by beginning with the double-shaft instance and considering an anti-clockwise rotation in the $y - z$ plane, ϕ of one of the beams, $E_{s,1}$ say, and a rotation by the same amount in an opposite fashion $-\phi$ of the other beam, in this case $E_{s,2}$, as in Fig. 3.14. This allows us to consider two important points: i) the effect of not having entirely parallel strong-field beams which, due to the finite size of the apparatus, will occur when focusing the beams; ii) how the double-shaft and double-slit geometries are related to one another. Denoting rotated quantities by primes and suppressing (x, y, z, t)
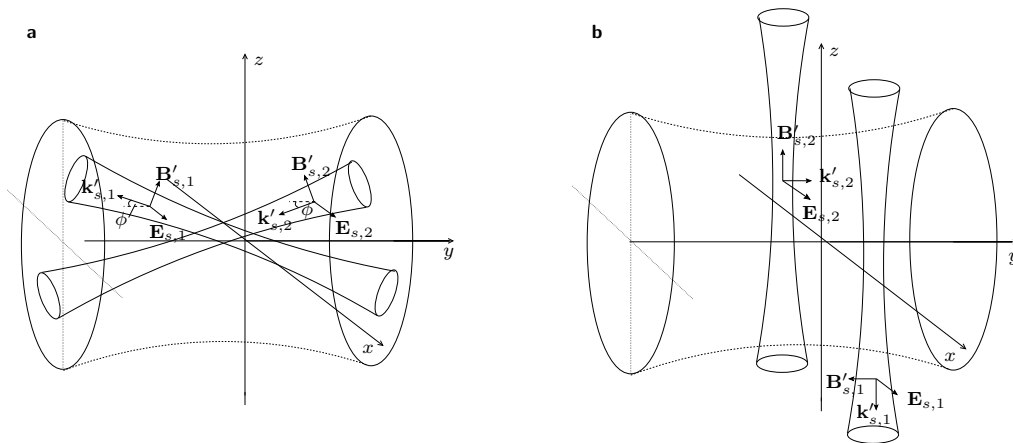

Figure 3.14: The two strong laser beams in the double-shaft set-up are rotated opposite directions in the $y - z$ plane by an angle ϕ as indicated in **a**. For $\phi = 3\pi/2$, we should have the double-slit set-up **b**.

co-ordinates on fields so that $\mathbf{E}_{s,1} := \mathbf{E}_{s,1}(x,y,z,t)$, we then have:

$$\mathbf{k}'_{s,1} = k_{s,1}\big(\cos\phi\,\hat{\mathbf{k}}_{s,1} + \sin\phi\,\hat{\mathbf{z}}\big), \tag{3.84}$$

$$\mathbf{k}'_{s,2} = k_{s,2}\big(\cos\phi\,\hat{\mathbf{k}}_{s,2} - \sin\phi\,\hat{\mathbf{z}}\big), \tag{3.85}$$

$$\mathbf{E}'_{s,1} = \mathbf{E}_{s,1}, \tag{3.86}$$

$$\mathbf{E}'_{s,2} = \mathbf{E}_{s,2}, \tag{3.87}$$

$$\mathbf{B}'_{s,1} = \mathbf{B}_{s,1}\cos\phi + \mathbf{E}_{s,1}\cdot\hat{\mathbf{x}}\,\sin\phi\hat{\mathbf{y}}, \tag{3.88}$$

$$\mathbf{B}'_{s,2} = \mathbf{B}_{s,2}\cos\phi - \mathbf{E}_{s,2}\cdot\hat{\mathbf{x}}\,\sin\phi\hat{\mathbf{y}}. \tag{3.89}$$

Substituting these fields into the applicable polarisation and magnetisation expressions Eqs. (3.25) and (3.26) respectively, we achieve the more general:

$$\mathbf{P}'(\phi) = \frac{16\pi\alpha^2}{45m^4}\Big[4E_{s,1}E_{s,2}(1-\cos 2\phi)\mathbf{E}_p + 4\Big(\mathbf{E}_s\cdot\mathbf{E}_p - \mathbf{B}_s\cdot\mathbf{B}_p\cos\phi\Big)\mathbf{E}_s$$
$$+7\Big(\mathbf{E}_s\cdot\mathbf{B}_p + \mathbf{B}_s\cdot\mathbf{E}_p\cos\theta\Big)\Big(\mathbf{B}_s\cos\phi + (\mathbf{E}_{s,1} - \mathbf{E}_{s,2})\cdot\hat{\mathbf{x}}\sin\theta\hat{\mathbf{y}}\Big)\Big], \tag{3.90}$$

$$\mathbf{M}'(\phi) = -\frac{16\pi\alpha^2}{45m^4}\Big[4E_{s,1}E_{s,2}(1-\cos 2\phi)\mathbf{B}_p + 4\Big(\mathbf{E}_s\cdot\mathbf{E}_p - \mathbf{B}_s\cdot\mathbf{B}_p\cos\phi\Big)$$
$$\times\Big(\mathbf{B}_s\cos\theta + \sin\theta\hat{\mathbf{y}}(\mathbf{E}_{s,1} - \mathbf{E}_{s,2})\cdot\hat{\mathbf{x}}\Big) - 7\Big(\mathbf{E}_s\cdot\mathbf{B}_p + \mathbf{B}_s\cdot\mathbf{E}_p\cos\theta\Big)\mathbf{E}_s\Big], \tag{3.91}$$

which fulfill the necessary requirements: $P'(0) = P^h, M'(0) = M^h$ and $P'(3\pi/2) = P^l, M'(3\pi/2) = M^l$. In making a small angle approximation in ϕ we can observe the deviation from the idealised case:

$$\mathbf{P}'(\delta\phi) = \frac{16\pi\alpha^2}{45m^4}E_p\sin\eta\Big\{2J_1\Big[4\cos\theta\hat{\mathbf{x}} + 7\sin\theta\hat{\mathbf{z}}\Big] + 14\delta\phi J_2\sin\theta\hat{\mathbf{y}}$$
$$+\frac{(\delta\phi)^2}{2}\Big[(16J_3 - 4J_1)\cos\theta\hat{\mathbf{x}} + (16J_3 - 21J_1)\sin\theta\hat{\mathbf{z}}\Big]\Big\}, \tag{3.92}$$

$$\mathbf{M}'(\delta\phi) = \frac{16\pi\alpha^2}{45m^4}E_p\sin\eta\Big\{2J_1\Big[7\sin\theta\hat{\mathbf{x}} - 4\cos\theta\hat{\mathbf{z}}\Big] - 8\delta\phi J_2\cos\theta\hat{\mathbf{y}}$$
$$+\frac{(\delta\phi)^2}{2}\Big[(16J_3 + 7J_1)\sin\theta\hat{\mathbf{x}} - (16J_3 + 12J_1)\cos\theta\hat{\mathbf{z}}\Big]\Big\} \tag{3.93}$$

where J_i is independent of time, having already been averaged over:

$$J_1 = \frac{1}{2}\Big[E_{s,1}^2 + E_{s,2}^2 + E_{s,1}E_{s,2}\cos\Big(\frac{2k_s y}{y^2 + 2_{r,s}^2}xx_0 + \delta\psi_s\Big)\Big], \tag{3.94}$$

$$J_2 = \frac{1}{2}(E_{s,1}^2 - E_{s,2}^2), \tag{3.95}$$

$$J_3 = E_{s,1}E_{s,2}\cos\Big(\frac{2k_s y}{y^2 + 2_{r,s}^2}xx_0 + \delta\psi_s\Big). \tag{3.96}$$

We can ask the question, in our experimental scenario, how large do we expect $\delta\phi$ to be? We envisage the vacuum chamber planned to be used for ELI to be $10\text{m} \times 4\pi\text{m}^2$, with two mirrors of 1 m diameter, focusing two laser beams down to the experiment interaction centre, located a distance of 5 m along the optical axis,

giving a $\delta\phi \sim 0.1$. With a correction of such a size, we should also consider the detector position in calculating the total diffracted intensity, I_d, (see e.g. Fig. 3.5) of $x_d/r_d, z_d/r_d \sim 0.03$. Using Eqs. (3.92) and (3.93) to calculate J_{vac}, it turns out that all corrections proportional to $\delta\phi$ vanish and leave us with:

$$J'_{\mathrm{vac}}(\delta\phi) = \mathbf{P}'(\delta\phi) + \mathbf{M}'(\delta\phi) \wedge \hat{\mathbf{r}} - \left(\mathbf{P}'(\delta\phi){\cdot}\hat{\mathbf{r}}\right)\hat{\mathbf{r}}, \tag{3.97}$$

$$= \frac{4\alpha^2 E_p}{45m^4}\sin\eta\left\{2J_1\begin{pmatrix}8\cos\theta\\0\\14\sin\theta\end{pmatrix} - 4J_1\begin{pmatrix}0\\7\frac{z}{r}\sin\theta + 4\frac{x}{r}\cos\theta\\0\end{pmatrix}\right\} \tag{3.98}$$

neglecting terms $O\left((x/r)^2, \delta\phi(x/r), (\delta\phi)^2\right)$. We mention that the calculation for the double-slit scenario reaches the same conclusion (as it must) and we can therefore justify our results that, within overall calculational accuracy $\sim 1/\pi$, we can regard the strong beams as propagating anti-parallel to the probe.

In order to describe arbitrarily aligned strong beams, we could make use of Euler angles to relate them to our double-shaft set-up. Any geometry can be arrived at by the algorithm: i)rotation clockwise about the z-axis by an angle ϕ; ii) rotation clockwise about the new x-axis by an angle θ; iii) rotation clockwise about the new z-axis by an angle ψ. x_0 and z_0 would then be made independent for both beam, and a y_0 would be introduced into the strong-beam expressions.

As many shots of the laser are required to build up a diffraction pattern, an important criterion is that of reproducibility. If the separation of the strong laser beams changes from one shot to the next by a factor of more than $1/(2m+1)$, where m is the maximum order of minima or maxima anticipated on the detector, then, starting from the outer edges of the pattern, the characteristic shape will be washed out. From the double-shaft example in Fig. 3.5, this corresponds to being able to position the strong beams with an accuracy of $1/7$ or 9.1 μm.

Residual gas

The focusing of ultra-intense laser beams such as those to be employed at ELI, must take place in a synthetic vacuum. The large apparatus required places restrictions on the minimum size of the vacuum chamber and hence the quality of the vacuum. Residual gas particles may also radiate and contribute a background to the double-slit pattern. As the main component of residual case is by far and away hydrogen [10], we can imagine that one shot of an X-ray probe laser, and due to the high intensity, through multiphoton processes, one shot of an optical probe laser will ionise all particles giving a dilute plasma. In the same way that vacuum, being polarised by the ultra-intense laser, exhibits a modified refractive index n_v, so too will a dilute plasma $n_{pl} = 1 + \delta n_{pl}$, where $\delta n_{pl} = (\omega_{pl}/\omega_p)^2/2$, with $\omega_{pl}^2 = e^2\rho/m$ being the square of the plasma frequency and ω_p the probe angular frequency (note that the analogous contribution to the plasma frequency of heavier particles like protons can be neglected due to their much larger mass). Beginning with the expressions of the vacuum polarisation and magnetisation Eq. (3.25)-Eq. (3.28), one can calculate the correction $\delta n_v = a(\alpha/45\pi)(I_{s,0}/I_{cr})$ [173], where a is a numerical factor $a \sim O(1)$ that we set to 1. The condition $\delta n_{pl} \ll \delta n_v$ is fulfilled, for the laser intensity employed in our numerical examples $I_{s,0} \sim 10^{24}$ Wcm^{-2} by a plasma density $\rho \ll 10^{13}$ cm^{-3}. When regarded as an ideal gas, i.e. obeying $P = k_B\rho T$ at temperature T, at standard

temperature and pressure (293 K, 1 atm), we obtain $P \lesssim 10^{-6}\text{-}10^{-5}$ Torr. If we compare this to the case of ELI which should have a similar sized vacuum chamber, for which it is planned to produce a vacuum of the order $\sim 10^{-12}$ torr, the limits mentioned seem easily attainable.

Any decoherence of the double-slit pattern will reduce its visibility $V(P)$, from the ideal vacuum value V_0 by $V = V_0 \exp(-P/P_d)$, where $P_d = k_B T / 2y\sigma_{\text{coll}}$ is the so-called degeneracy pressure with y being the observation distance and σ_{coll} an effective collision cross section between the diffracted photons and the residual gas (see [89] for a derivation). For photon energies of the order of eV and keV, the cross section is of the order of that for Thomson scattering [133], $\sigma_T = 6.7 \times 10^{-25}$ cm^2 [93], which gives us for an ideal gas a ratio $P/P_d = 2y\rho\sigma_T$, which for an observation distance $y = 500$ cm, unless the density of residual gas is much larger than already calculated, will not have an appreciable effect. Therefore we can conclude that a synthetic vacuum of pressure $P \lesssim 10^{-6}\text{-}10^{-5}$ Torr is sufficient to safely neglect degeneracy pressure.

Finite temperature

We can pose a further question of our proposed experiment: to what extent will a thermal background prove a source of decoherence? We can imagine cryogenically cooling the CCD apparatus to minimise thermal effects within the detection equipment so that the main source would come from thermal photons, in equilibrium with the sides of the vacuum chamber. If the CCD has a spectral resolution of $\delta\omega$, then the background to our double-slit pattern will come from black-body photons indiscriminately landing on the detection plate (we can ignore further interaction between probe photons and black body photons as the intensities are far too low for this to contribute to our results). For a total energy $\mathcal{E}$ per unit volume V our black-body spectrum gives:

$$\frac{\mathcal{E}}{V} = \frac{8\pi(k_B T)^4}{c^3 h^3} \int_{\hbar(\omega-\delta\omega)/k_B T}^{\hbar(\omega+\delta\omega)/k_B T} dx \frac{x^3}{e^x - 1} \approx \frac{\hbar\omega^3 \delta\omega}{\pi^2 c^3} \frac{1}{e^{\hbar\omega/k_B T} - 1}. \qquad (3.99)$$

Now we can imagine all possible thermal photons incident on the detector during the interval τ to have come from an "effective volume" given in a conservative estimate (as only a small fraction of photons in this volume will be headed for the detector) by a hemisphere of radius $c\tau$ around the detector's centre. Setting $V = 2\pi(c\tau)^3/3$, we can reformulate the expression in terms of the number of incident thermal photons $N(T)$ with wavelength $\lambda_0 \pm \delta\lambda$:

$$N(T) = \frac{16\pi^2}{3} \left(\frac{c\tau}{\lambda_0}\right)^3 \frac{\delta\lambda}{\lambda_0} \frac{1}{e^{hc/k_B T\lambda_0} - 1}, \qquad (3.100)$$

giving a temperature in terms of the number of photons N:

$$T(N) = \frac{hc}{k_B \lambda_0} \left[\ln\left(1 + \frac{16\pi^2}{3}\left(\frac{c\tau}{\lambda_0}\right)^3 \frac{\delta\lambda}{\lambda_0}\frac{1}{N}\right) \right]^{-1}. \qquad (3.101)$$

If one could trigger the opening and closing of shutters in front of the CCD with the passage of the laser beams, we could take the corresponding shutter speed to be the

same order as for commercial cameras $\tau \sim 100\mu s$[14]. With a filter able to separate frequencies within $\delta\lambda/\lambda_0 \sim 0.1$[15] for our optical photons $\lambda_0 = 0.527$ μm, in order that we have less than one thermal photon (compared with a signal of four) per shot of the strong laser in the effective volume, we require a temperature $T \lesssim 360K$. For a conservative estimate, this is still above room temperature and pressure, and we take the effect of a finite-temperature background to be negligible.

Conclusion

The vacuum polarisation effects described in this chapter have yet to be confirmed. We have put forward two geometries that utilise diffraction effects to spatially separate the vacuum signal from the background and we calculate a few photons per shot of the lasers will be, in principle, measurable for the two different types of vacuum field intensity - the pure term I_d and the cross-term I_{pd}. In addition, we have shown how a double-slit like set-up can actually be used to increase vacuum birefringence and dichroism. This originates from the important Fresnel terms as part of the process of diffraction of probe photons. Fresnel terms were also seen to play a role in the shape of the diffraction pattern envelopes, especially when the diffraction parameter $\nu > 1$ as was the case in the double-slit case in a direction parallel to the strong beams. In addition to diffraction, beam shape was seen to play an important role. First the very different fall-off of patterns in the double-shaft case with respect to the double-slit one and second, with the standing wave of the double-slit set-up being responsible for the extra secondary peaks far from the centre of the pattern parallel to these waves. In the current section, we have argued that the role of many typical hindrances such as an imperfect vacuum, finite temperature, temporal effects, an imperfect beam geometry will have negligible effect on our results. As many shots of the lasers are required, our main obstacle in addition to the yet to be attained strong-field intensities is that of reproducibility. That all three beams can be combined in the envisaged fashion on such a short time scale of 100 fs, not to mention that the strong-field beams can be consistently aligned to within tens of micrometres represent considerable experimental challenges. However, even if the double-slit pattern would prove difficult to reproduce, the principle of diffraction is a robust one, and is a useful addition to the array of possible experimental scenarios to test QED in this relatively unexplored regime.

---

[14]Using electronic shutter technology designed for back-illuminated CCDs, in [125] a 25 cm^2 CCD with recording frequency even in the MHz range was fabricated.

[15]For example, the *v18t* filter in [25] has a full-width at half maximum $\delta\lambda/\lambda_0 \approx 0.05$ around $\lambda_0 = 527$ nm.

Chapter 4

Scattering of a photon in an electromagnetic wave

Complementary to our approach in the previous chapters which was based upon effective field theory and the vacuum average of the current operator, we now focus on the full quantum calculation of the relativistic photon-photon scattering amplitude. In particular, we derive formulae describing how a photon is scattered by an electromagnetic wave, which will then be specialised to a constant crossed field. With a view to applying the solution in the setting of a thermal photon gas, our aim for this chapter will be to calculate the first-order vacuum polarisation correction to the photon's refractive index.

Calculation of the polarisation tensor in an external field has a long history. Properties of the tensor in a constant magnetic field have been studied by many authors [132, 172, 160], but only very few solutions of the Dirac equation in non-trivial external fields have been found. Exceptions include Schwinger's result for an arbitrary constant EM field [158], Volkov's in a plane wave background [177], in the Redmond configuration [148] – a combination of constant magnetic field and plane wave – as well as in a Coulomb field [42, 78], with arbitrary EM fields lying beyond current calculational methods. The polarisation tensor has been calculated in a general constant, homogeneous electromagnetic field in [15], using Schwinger's exact solution for the Green's function. In a non-crossed ($\mathscr{F}\mathscr{G} \neq 0$), constant EM background, the tensor was also derived in [49], in which the solution for parallel electric and magnetic fields [175] was Lorentz transformed to a more general configuration. In addition the "string-theory inspired" *world-line* formalism, in which a one-dimensional path integral is evaluated to yield quantum vacuum amplitudes has also been employed to calculate the tensor in a constant external EM field [51]. Of particular relevance to us will eventually be the *crossed-field* configuration, defined constant electric and magnetic field vectors, equal in magnitude and mutually orthogonal, which was investigated in [136] and reviewed in [150].

We will apply the *operator diagram technique* developed in the 1970s by Baier, Katkov, Milstein and Strakhovenko [17, 18] and applied in [19, 16] to plane waves (i.e. the vector potential is transverse and a function of $\varphi = kx$), which suits our

primary interest in describing processes in lasers. We will follow the last two references to arrive at the general expression for the coefficients of the expansion of the polarisation operator in terms of a basis relevant to the problem at hand. This technique involves evaluating operator traces making the usual external field substitution $\hat{p} \rightarrow \hat{P} = \hat{p} + eA\mathbb{1}$ and has the advantage of leading to relatively simple analytic expressions. Using the full quantum theory allows a broader application of the solution than in the effective field theory, being not restricted to the assumption $\omega \ll m$, which could become important in the broadband thermal ensemble.

4.1 Calculation of the polarisation operator in an external electromagnetic wave

Maxwell's classical solution for the propagation of a photon finds its lowest-order quantum correction in the polarisation operator. This inherently describes the polarisation of virtual electron-positron pairs in the vacuum, which generate a *vacuum current* as expounded in Ch. 2 and Ch. 3. For the free Dirac field, these terms are normally neglected as the vacuum current should vanish due to isotropy, but in an external field, these inner fermionic loops can be polarised and contribute to the dynamics of the Dirac field. The question is how to incorporate the external field. Processes that are higher order in the external field coupling must contain an extra term of the order $\sim eA/m$ which is nothing more than the invariant parameter $\xi = (m/\omega)(E/E_{\mathrm{cr}})$. When this is of the order of unity, which is the case for our domain of enquiry (for the upcoming ELI and HiPER lasers $\xi \approx 690$), the external field can no longer be included perturbatively. Moreover, although the convergence of perturbation approaches to quantum field theory is far from proven[1], also in the external field of e.g. a heavy nucleus, the expansion parameter $Z\alpha$ can be large. An alternative approach for strong external fields would be to then move the dependence of the external field into the "free", unperturbed solution for the wavefunction and view just the internal QED interactions as the perturbative. This puts us in the *Furry* picture [70] in which, in our case, the Dirac equation must be solved in an external plane wave, yielding propagators which are then exact in the external-field. The process can be summarised in Fig. 4.1 which we reproduce from Ch. 2, in which we note, via charge conjugation symmetry, the exchange of an odd number of photons in the transition amplitude is prohibited. This is also known as *Furry's theorem* (see App. A.1.3). We also mention, that it has been shown, at least for the first two orders, that when the external field is strong, the coupling with photons scales as $\alpha\varkappa^{2/3}$, which for us as $\alpha\varkappa^{2/3} \ll 1$, justifies us taking the leading order diagram. We begin by first referring list of conventions given in the introduction Sec. 1.1 used in the following calculations. We define the *scattering matrix*, S_{fi} as the operator relating an initial quantum state $|i\rangle$ to a final quantum state $\langle f|$ in some scattering process, via $|f\rangle = S_{fi}|i\rangle$. An additional matrix, T_{fi} encodes all non-trivial processes

---

[1]This was shown most clearly by Dyson [56] who lucidly argued that if the series expansion converges in $\alpha \sim e^2$, it must also converge for $e^2 \rightarrow -e^2$, but this would imply the reversal of electrostatic laws with like charges attracting and unlike ones repelling. Then one can imagine how the virtual e^+-e^- pairs of the vacuum would not recombine but instead would be spontaneously created so that at any point in time, a finite probability would exist that a pathological state would be achieved in which large numbers of such pairs would be created and the vacuum would disintegrate. This is one of the motivations behind more mathematically rigorous and abstract formulations of relativistic quantum mechanics such as algebraic quantum field theory [69].
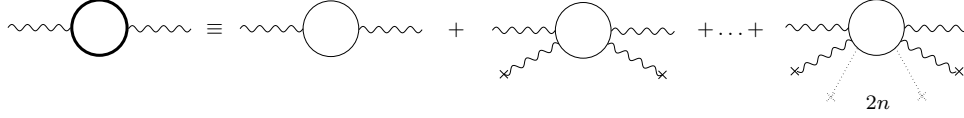
Figure 4.1: The polarisation operator in an external field (left-hand side) with fermion propagators exact in the external field (bold curved lines) can regarded as a sum of free-field polarisation processes in which all possible topologically unique even exchanges of photons with the external field (marked with an ×) occur.

through $S_{fi} = \delta_{fi} + i(2\pi)^4 \delta^{(4)}(P_f - P_i)T_{fi}$, where a four-dimensional delta function has been included to encapsulate momentum conservation between total initial and final momenta, P_i, P_f. We are specifically interested in the process of a photon with initial momentum k_1 being scattered into a momentum state k_2. Using the generalisation of the scattering matrix to continuum states, this amplitude corresponds to $\langle k_2|S(k_2, k_1)|k_1\rangle$, which we label $T(k_2, k_1)$. Then from the Dyson expansion of the S-matrix for the QED coupling in co-ordinate space [120] (spacetime and spinor indices suppressed) $ie\bar{\psi}(x)\gamma A(x)\psi(x)$, we have:

$$S(k_2, k_1) = -e^2 \int d^4x_1 d^4x_2 \gamma A(x_1) iG_F(x_2, x_1)\gamma A(x_2)\big(-iG_F(x_1, x_2)\big), \qquad (4.1)$$

where the normal-ordering has already been carried out; represented by the fermionic Green's function $G_F(x_2, x_1) := -i\langle \hat{T}\psi(x_2)\bar{\psi}(x_1)\rangle$ for a time-ordering operator $\hat{T}$. We mention that for QED, the Green's function is built so as to satisfy the inhomogeneous Dirac equation in an external EM field $(i\gamma D - m)G(x_2, x_1) = -i\delta^{(4)}(x_2 - x_1)$ with the usual $iD = i(\partial - ieA)$ external field replacement[2]. We also note, that there is only one topologically unique diagram in the one-loop calculation.

Expanding the photon field in terms of annihilation and creation operators, we can rewrite $T(k_2, k_1)$ as:

$$T(k_2, k_1) \quad = \quad \frac{1}{2V\sqrt{\omega_{k_2}\omega_{k_1}}}\varepsilon_\mu(k_1)\varepsilon_\nu(k_2)T^{\mu\nu}, \qquad (4.2)$$

with

$$T^{\mu\nu} = -\frac{e^2}{(2\pi)^4}\int d^4x_1 d^4x_2 \, \gamma^\nu G_F(x_2, x_1)\mathrm{e}^{ik_2 x}\gamma^\mu G_F(x_1, x_2)\mathrm{e}^{-ik_1 x} \qquad (4.3)$$

$$T^{\mu\nu} = -\frac{e^2}{(2\pi)^4}\int d^4x_1 d^4x_2 \, \gamma^\nu \langle x_2|G_F(\hat{p})\mathrm{e}^{ik_2\hat{x}}|x_1\rangle\gamma^\mu\langle x_1|G_F(\hat{p})\mathrm{e}^{-ik_1\hat{x}}|x_2\rangle \qquad (4.4)$$

$$T^{\mu\nu} = -\frac{e^2}{(2\pi)^4}\int d^4x \, \mathbf{Tr} \, \langle x|G_F(\hat{p})\mathrm{e}^{-ik_1\hat{x}}\gamma^\mu G_F(\hat{p})\mathrm{e}^{ik_2\hat{x}}\gamma^\nu|x\rangle, \qquad (4.5)$$

where in the second line we have used the operator representation of the Green's function $G_F(x_2, x_1) = \langle x_2|G_F(\hat{p})|x_1\rangle$, $G_F(\hat{p}) = 1/(\gamma\hat{P} - m)$, $\hat{P} := \hat{p} + eA\hat{\mathbb{1}}$, and in the final line we have used the cyclicity of the trace. In this section, we will outline the steps required to evaluate Eq. (4.5), which begin with the definition of a suitable basis for the problem.

---

[2] That the replacement $p \to p + eA/c$ in the Lagrangian is a valid relativistic generalisation of the zero-field expression can be shown as it reproduces the Lorentz-force equation. It can be derived considering a Lorentz invariant, co-ordinate independent action which must also lead to the zero-field expression, see e.g. [93]

Polarisation tensor and vector basis

We define our plane wave via the vector potential:

$$A^\mu(\varphi) = a_1^\mu \psi_1(\varphi) + a_2^\mu \psi_2(\varphi), \tag{4.6}$$

where functions $\psi_{1,2}(\varphi)$ solve Maxwell's wave equation with $\varphi := \varkappa x = \varkappa^0 x^0 - \boldsymbol{\varkappa} \cdot \mathbf{x}$, all amplitude coefficients are contained within the vectors $a_{1,2}^\mu$, and the wave is transverse through $a_1 a_2 = \varkappa a = 0$ and in vacuum $\varkappa^2 = 0$. The invariant intensity defined in Ch. 1 is then $\xi^2 = e^2 |a^2|/m^2$.

The polarisation tensor relates initial to final polarisations and therefore initial to final vector potentials and so occurs in the corresponding wave equation. Using Dyson's equation:

$$D(k) = \frac{D^{(0)}(k)}{1 - D^{(0)}(k)\Pi(k)}, \tag{4.7}$$

for the exact photon propagator $D(k)$ and zeroth-order photon propagator $D^{(0)}(k) = 1/k^2$, inverting both sides gives $k'^2 = k^2 - \Pi(k)$, for an exact photon momentum k'. Our first-order approximation to $\Pi(k)$ will therefore appear in the dispersion relation as:

$$\left[k^2 g^{\mu\nu} + k^\mu k^\nu - \Pi^{\mu\nu}(k)\right] e_\nu(k) = 0, \tag{4.8}$$

$$\Pi^{\mu\nu}(k) e_\nu(k) = \frac{1}{i(2\pi)^4} \int d^4 k' \, T^{\mu\nu}(k, k') e_\nu(k'). \tag{4.9}$$

Being a tensor, $T^{\mu\nu}$ can be decomposed into a linear superposition of products of four-vectors. It is logical to define two orthonormal bases relevant to the physics before and after the scattering event, and we follow [19] by first defining:

$$\Lambda_1^\mu = \frac{(kf_1)^\mu}{\varkappa k \sqrt{-a_1^2}}, \qquad \Lambda_2^\mu = \frac{(kf_2)^\mu}{\varkappa k \sqrt{-a_2^2}}, \tag{4.10}$$

$$\Lambda_3^\mu = \frac{\varkappa^\mu k_1^2 - k_1^\mu \varkappa k}{\varkappa k \sqrt{-k_1^2}}, \qquad \Lambda_4^\mu = \frac{\varkappa^\mu k_2^2 - k_2^\mu \varkappa k}{\varkappa k \sqrt{-k_2^2}}, \tag{4.11}$$

where

$$f_{1,2}^{\mu\nu} = \varkappa^\mu a_{1,2}^\nu - a_{1,2}^\mu \varkappa^\nu, \quad (kf_{1,2})^\nu = k_\mu f_{1,2}^{\mu\nu}, \tag{4.12}$$

so that we have:

$$\Lambda_1^2 = \Lambda_2^2 = \Lambda_3^2 = \Lambda_4^2 = -1, \tag{4.13}$$

$$\Lambda_i^\mu \Lambda_{j,\mu} = 0 \quad \text{for} \quad i, j \in \{1, 2, 3\} \text{ or } \{1, 2, 4\}, \tag{4.14}$$

where we note $F^{\mu\nu} = \sum_{j=1,2} f_j^{\mu\nu} \psi_j'(\varphi)$. Being superpositions of four-vectors, the Λ vectors are themselves Lorentz covariant and have been so constructed that they can be combined with the photon wave-vector to form two orthonormal sets for k_1 and k_2:

$$\left\{ k_1/\sqrt{k_1^2}, \Lambda_1, \Lambda_2, \Lambda_3 \right\} \quad \& \quad \left\{ k_2/\sqrt{k_2^2}, \Lambda_1, \Lambda_2, \Lambda_4 \right\}. \tag{4.15}$$

Using one set for each spacetime component of $T^{\mu\nu}$, we can span the tensor's 16 component produce vector space $V \otimes V$. However, from Eq. (4.8), we can see that the polarisation tensor is symmetric, which reduces the space to 10 components. In addition, the polarisation operator $\Pi^{\mu\nu}(k_1, k_2)$ is transverse $k_{1\mu}\Pi^{\mu\nu}(k_1, k_2) = \Pi^{\mu\nu}(k_1, k_2)k_{2\nu} = 0$, which removes four further components from T. Finally, we recall that all processes involving odd numbers of external photons are forbidden by Furry's theorem, as described in App. A.1.3. The effect of this restriction can be seen by studying possible combinations of the above bases. It can be shown by direct calculation [19] that the combinations:

$$
\begin{aligned}
\Lambda_{1,2}^{\mu} \Lambda_3^{\nu} &= \left[(\varkappa k)^2 \sqrt{-a_1^2 k_1^2} \right]^{-1} \left\{ \left(k_\rho \varkappa^\rho a_{1,2}^{\mu} - k_\rho a_{1,2}^\rho \varkappa^\mu \right) \left(\varkappa^\nu k_1^2 - k_1^\nu (\varkappa k) \right) \right\} \\
&= \left[(\varkappa k)^2 \sqrt{-a_1^2 k_1^2} \right]^{-1} \left\{ (k\varkappa) k_1^2 a_{1,2}^{\mu} \varkappa^\nu - (k a_{1,2}) k_1^2 \varkappa^\mu \varkappa^\nu \right. \\
&\qquad \left. - (k\varkappa)^2 a_{1,2}^{\mu} k_1^\nu + (k a_{1,2})(\varkappa k) \varkappa^\mu k_1^\nu \right\},
\end{aligned}
\tag{4.16}
$$

and likewise $\Lambda_{1,2}^{\mu} \Lambda_4^{\nu}$, do not contribute. We are then left with five possible combinations and can expand $T^{\mu\nu}$ fully as:

$$
T^{\mu\nu} = c_1 \Lambda_1^{\mu} \Lambda_2^{\nu} + c_2 \Lambda_2^{\mu} \Lambda_1^{\nu} + c_3 \Lambda_1^{\mu} \Lambda_1^{\nu} + c_4 \Lambda_2^{\mu} \Lambda_2^{\nu} + c_5 \Lambda_3^{\mu} \Lambda_4^{\nu}.
\tag{4.17}
$$

We may refer to $c_{1,\ldots,5}$ as *form-factors*, being complicated functions of laser intensity and laser and photon momenta. However it is clear that they must be Lorentz and gauge-invariant scalars. Since the only objects to hand that could form such scalars are $F_{\mu\nu}$, $F_{\mu\nu}^*$, k_μ and recognising from dimensional analysis that F, F^* must be accompanied by e/m^2, the only three possible scalars are:

$$
\chi = \frac{e\sqrt{|(F_{\mu\nu}k^\mu)^2|}}{m^3}, \qquad f = \frac{e^2 \mathscr{F}}{m^4}, \qquad g = \frac{e^2 \mathscr{G}}{m^4}.
\tag{4.18}
$$

Now that the stage has been set, we see that the calculation of the polarisation operator can be reduced to determining the coefficients $c_1 \to c_5$. In the following section, we briefly recapitulate the main steps taken in [19].

Derivation of polarisation operator form factors

Our general strategy will be to remove operator hats so that we can end up with an integral for the polarisation coefficients. We first rewrite Eq. (4.5) for clarity:

$$
T^{\mu\nu} = -\frac{e^2}{(2\pi)^4} \int d^4x \, \mathbf{Tr} \, \langle x | S_F(\hat{p}) \mathrm{e}^{-i k_1 \hat{x}} \gamma^\mu S_F(\hat{p}) \mathrm{e}^{i k_2 \hat{x}} \gamma^\nu | x \rangle,
$$

and begin by removing the exponential terms. Recognising the position operator in momentum space as $\hat{x}_p^\mu = -i\eta_\sigma^\mu \partial/\partial p_\sigma$, one can show, using an infinitesimal expansion, that $\exp(ik\hat{x})$ is the generator of momentum translations, namely that $\exp(i\delta\hat{x})|k\rangle = |k + \delta\rangle$ and $\exp(i\delta\hat{x})f(p)\exp(-i\delta\hat{x}) = f(p + \delta)$. Therefore $\langle x|f(p)\exp(-ik\hat{x}) = \exp(-ikx)\langle x|f(p + k)$. Applying these results, multiplying propagators by the identity $(\gamma\hat{P} + m)/(\gamma\hat{P} + m)$ and utilising trace cyclicity, we achieve:

$$
\begin{aligned}
T^{\mu\nu} = -\frac{e^2}{(2\pi)^4} \int d^4x \exp\left[i(k_2 - k_1)x \right] \mathbf{Tr} \, \Big\langle x \Big| \frac{1}{(\gamma\hat{P} + k_1)^2 - m^2} \gamma^\mu \\
\frac{1}{(\gamma\hat{P})^2 - m^2} (\gamma\hat{P} + m) \Big[2\hat{P}^\nu + \gamma^\nu \slashed{k}_2 + (m - \gamma\hat{P})\gamma^\nu \Big] \Big| x \Big\rangle.
\end{aligned}
\tag{4.19}
$$

Using $\langle x|f\big[\gamma(P+k_1)\big]|x\rangle = \langle x|\exp(-ik_1\hat{x})f\big[\gamma(P+k_1)\big]\exp(ik_1\hat{x})|x\rangle = \langle x|f\big[\gamma P\big]|x\rangle$, the final term in square brackets in Eq. (4.19) can be brought into the form:

$$T'^{\mu\nu} = \frac{e^2}{(2\pi)^4}\int d^4x \exp\Big[i(k_2-k_1)x\Big]\mathbf{Tr}\left[\Big\langle x\Big|\frac{1}{(\gamma\hat{P})^2-m^2}\Big|x\Big\rangle\gamma^\mu\gamma^\nu\right], \qquad (4.20)$$

which can be shown to be independent of the external field and so disappears on renormalisation. Exponentiating propagators we then achieve:

$$T^{\mu\nu} = -\frac{e^2}{(2\pi)^4}\int_0^\infty dt\int_0^\infty ds \exp[-im^2(s+t)]\widetilde{T}^{\mu\nu}, \qquad (4.21)$$

$$\widetilde{T}^{\mu\nu} = \int d^4x \exp[i(k_2-k_1)x]\mathbf{Tr}\Big[\langle x|\exp\big\{it(\hat{P}+k)^2\big\}\gamma^\mu$$
$$\exp\big\{is\hat{P}^2\big\}\big(\gamma\hat{P}+m\big)\big(\gamma^\nu k\!\!\!/_2 + 2\hat{P}^\nu\big)|x\rangle\Big]. \qquad (4.22)$$

Now we would like to disentangle the exponentials in Eq. (4.22) which are functions of non-commuting operators. To do this, we can use results from the operator method developed by Baier, Katkov, Milstein and Strakhovenko, which we explain in App. A.2. Also in App. A.2, are the steps required to reach the next part of the derivation:

$$\widetilde{T}^{\mu\nu} = \int d^4x \exp[i(k_2-k_1)x]\langle x|\exp\big[it(P+k_1)^2\big]\exp\big[isP^2\big]B^{\mu\nu}|x\rangle,$$

$$B^{\mu\nu} = \mathbf{Tr}\left[\gamma^\mu\Big(1-\frac{er^+(s)}{2(\varkappa P)}k\!\!\!/f\!\!\!/\Big)\big(\gamma P+m\big)\big(\gamma^\nu k\!\!\!/_2 + 2P^\nu\big)\right.$$
$$\left.\times\Big(1+\frac{er^-(t)}{2\varkappa(P+k)}k\!\!\!/f\!\!\!/\Big)\right], \qquad (4.23)$$

where:

$$r^+(s) = \psi(\varphi+2(\varkappa P)s)-\psi(\varphi), \quad r^-(t) = \psi(\varphi-2\varkappa(P+k)t)-\psi(\varphi). \qquad (4.24)$$

Now, as we will eventually contract $B^{\mu\nu}$ with our orthogonal basis, due to the transversality of the polarisation operator, all terms including $f^{\mu\nu}$ or $\varkappa^\mu$ can be automatically discarded. Using the trace formulae Eqs. (A.10-A.15) given in App. A.1.2, we then have:

$$B^{\mu\nu} = 4\big\{2\hat{P}^\mu\hat{P}^\nu + P^\mu k_2^\nu - g^{\mu\nu}(k_2P) - \big(e^+(s)+e^-(t)\big)\big[g^{\mu\nu}(Pfk)$$
$$-k_2^\mu(Pf)^\nu + P^\mu(kf)^\nu\big] + \big(e^+(s)-e^-(t)\big)\big[(Pf)^\mu(2P^\nu+k_2^\nu)$$
$$+(kf^\mu)P^\nu\big]\big\}, \qquad (4.25)$$

where

$$e^+(s) = \frac{er^+(s)}{2(\varkappa P)}, \qquad e^-(t) = -\frac{er^-(t)}{2\varkappa(P+k)}, \qquad (4.26)$$

with all combinations $e^\pm f$ summed over the suppressed subscripts $1,2$. Having dealt with the fermionic trace, we consider the remaining operators. It turns out, that the single operator term that can be formed on contraction with the $T^{\mu\nu}$ basis Eq. (4.15) is (k_2P), which doesn't commute with all other terms. By considering this term alone in the integral and rewriting k_2P in the form $\{(P+k_2)^2-m^2-[(P^2-m^2)+k_2^2]\}$ and again using $\exp(ik\hat{x})f(p)\exp(-ik\hat{x}) = f(p+k)$, it can be shown, that the k_2P term

is equivalent to one in which $(k_2 P) \to -k_2^2/2$. This allows all operators occurring in the numerator to be regarded as c-numbers.

Now we can consider the rest of $\widetilde{T}^{\mu\nu}$, utilising the disentangling method for to write exponentiated operators in terms of integrals, Eq. (A.51), to give:

$$
\begin{aligned}
\widetilde{I}^{\mu\nu} &= \langle x| \exp\left[it(\hat{P}+k_1)^2\right] \exp\left[is\hat{P}^2\right] B^{\mu\nu}|x\rangle \\
&= \langle x| \exp\left\{ it \int_0^1 \frac{dy}{a^2}[a(P+k)+ea^2 r^-(ty)]^2 \right\} \exp\left\{ it(P+k_1)_\perp^2 \right\} \\
&\quad \exp\left\{ itP_\perp^2 \right\} \exp\left\{ is \int_0^1 \frac{dy}{a^2}[aP+ea^2 r^+(sy)]^2 \right\} B^{\mu\nu}|x\rangle.
\end{aligned}
\tag{4.27}
$$

Now comes the important step of specifying a basis. We choose the plane wave to be directed along the 3-axis, i.e. $\varkappa^0 = \varkappa^3$, and $\mathbf{a}_1, \mathbf{a}_2$ lie in the 1-2 plane. In this plane wave, the conserved quantities are known to be $p^0 - p^3, p^1, p^2$, which can be shown by their operators commuting with the Hamiltonian [23] and so we make the co-ordinate transformation:

$$
|x\rangle = |x^0, x^1, x^2, x^3\rangle \to |k'\rangle = |\theta, \nu, a_1 x, a_2 x\rangle,
\tag{4.28}
$$

$$
\theta = (x^0 - x^3)/\sqrt{2}, \quad \nu = (x^0 + x^3)/\sqrt{2}, \quad p_\theta = i\frac{\partial}{\partial \theta}, \quad p_\nu = i\frac{\partial}{\partial \nu},
\tag{4.29}
$$

giving:

$$
\varphi = \sqrt{2}\varkappa^0 \theta, \qquad
\begin{aligned}
P^0 &= p^0 = (p_\theta + p_\nu)/\sqrt{2}, \\
P^2 &= p^3 = (p_\theta - p_\nu)/\sqrt{2},
\end{aligned}
\qquad
\begin{aligned}
(\varkappa P) &= \sqrt{2}\varkappa^0 p_\nu \\
P_0^3 - P_3^2 &= 2p_\theta p_\nu.
\end{aligned}
$$

Now, we can rewrite the amplitude $\widetilde{I}$ as an integral using

$$
\langle x|G(\hat{p})|x\rangle = \int d^4 p' \langle x|G(\hat{p})|p'\rangle \langle p'|x\rangle = \int d^4 p' G(p').
\tag{4.30}
$$

If we first consider the simpler problem of $B^{\mu\nu} = g^{\mu\nu}$, we can then integrate over each transformed variable, the results being:

$$
\langle \theta| e^{it(P+k_1)^2} e^{isP^2} |\theta\rangle = \frac{\pi}{s+t} e^{2itk_{1\theta}(p_\nu + k_{1\nu})} \delta\left(p_\nu + \frac{rk_1\nu}{s+t} \right),
\tag{4.31}
$$

$$
\langle \nu| \frac{\pi}{s+t} e^{2itk_{1\theta}(p_\nu + k_{1\nu})} \delta\left(p_\nu + \frac{rk_1\nu}{s+t} \right)|\nu\rangle = \frac{\pi}{s+t} e^{2itk_{1\theta} k_{2\nu} \frac{s}{s+t}},
\tag{4.32}
$$

$$
\begin{aligned}
&\langle xa_1, xa_2| \exp\left\{ 2it \int_0^1 dy \, e\Delta_j(\mu y)\left(a_j(P+k)\right) + ite^2 a_j^2 \int_0^1 dy \, \Delta_j^2(\mu y) \right. \\
&\quad -it\left[(P^1 + k^1)^2 + (P^2 + k^2)^2 \right] + 2is \int_0^1 dy \, e\Delta_j(\mu y) a_j P \\
&\quad \left. + ise^2 a_j^2 \int_0^1 dy \, \Delta_j^2(\mu y) - is(P^{1\,2} + P^{2\,2}) \right\} |xa_1, xa_2\rangle = \\
&\qquad\qquad\qquad \frac{-i\pi}{s+t} e^{i(s+t)e^2 a_j^2 \left[\left(\int_0^1 dy \, \Delta_j(\mu y) \right)^2 - \int_0^1 dy \, \Delta_j^2(\mu y) \right] - \frac{ist}{s+t} k_1^2},
\end{aligned}
\tag{4.33}
$$

with sums over $j \in \{1, 2\}$ and:

$$\Delta_{1,2}(\mu y) = \psi_{1,2}(\varphi - 2(\varkappa k)\mu y) - \psi_{1,2}(\varphi), \tag{4.34}$$

to give for $I = \widetilde{I}_{\mu\nu}(B_{\mu\nu} = g_{\mu\nu})g^{\mu\nu}/4$:

$$I = \frac{-i\pi^2}{s+t}e^{i\mu k_1^2 + i(s+t)\beta}, \tag{4.35}$$

where:

$$\beta_{1,2} = -e^2|a_{1,2}^2|\left[\int_0^1 dy\, \Delta_{1,2}^2(\mu y) - \left(\int_0^1 dy\Delta_{1,2}(\mu y)\right)^2\right], \qquad \mu = \frac{st}{s+t}. \tag{4.36}$$

Following this, we can consider the individual terms of $B^{\mu\nu}$ appearing in $\widetilde{I}^{\mu\nu}$. Since this is an integral over d^4P and we have at most terms of order $P^\mu P^\nu$, we can integrate by parts and use our result for I Eq. (4.35). We can show that the full integral $\widetilde{I}^{\mu\nu}(B^{\mu\nu})$ is equal to the result Eq. (4.35) after making the following replacements in $B^{\mu\nu}$:

$$P^\mu \quad \rightarrow \quad R^\mu = -k_1^\mu \frac{t}{s+t} - ea_1^\mu \int_0^1 dy\Delta_1(\mu y) - ea_2^\mu \int_0^1 dy\Delta_2(\mu y), \tag{4.37}$$

$$P^\mu P^\nu \quad \rightarrow \quad R^\mu R^\nu + \frac{i}{2(s+t)}\left(\frac{a_1^\mu a_1^\nu}{a_1^2} + \frac{a_2^\mu a_2^\nu}{a_2^2}\right). \tag{4.38}$$

With the $\langle x|x\rangle$ operation performed, all that is left is to contract $\widetilde{T}^{\mu\nu}$ with our basis Eq. (4.15). We then renormalise the polarisation operator in the typical way for an external field (see App. A.1.3), by subtracting off $\widetilde{T}^{\mu\nu}_{F=0}$ terms. After much algebra, bearing in mind symmetry of integrals and gauge invariance of T, we achieve the final integral expressions for $c_1 \rightarrow c_5$:

$$c_n = -\frac{i\alpha}{2\pi}\int_{-1}^1 dv \int_0^\infty \frac{d\tau}{\tau}\int d^4x\, e^{i(k_2-k_1)x}e^{-im^2\tau\left(1-\frac{k_1^2(1-v^2)}{4m^2}\right)}b_n, \tag{4.39}$$

where we have gone over to new integration variables:

$$s + t = \tau, \; v = (s-t)/(s+t), \; \mu = \tau(1-v^2)/4, \qquad \&$$

$$D_{1,2} = \int_0^1 dy\Delta_{1,2}(\mu y) + \frac{v^2}{1-v^2}\Delta_{1,2}(\mu), \tag{4.40}$$

$$b_1 = 2\xi_1\xi_2 m^2\left[D_1\int_0^1 dy\Delta_2(\mu y) - \frac{\Delta_2(\mu)}{1-v^2}\int_0^1 dy\Delta_1(\mu y)\right]e^{i\tau\beta}, \tag{4.41}$$

$$b_2 = 2\xi_1\xi_2 m^2\left[D_2\int_0^1 dy\Delta_1(\mu y) - \frac{\Delta_1(\mu)}{1-v^2}\int_0^1 dy\Delta_2(\mu y)\right]e^{i\tau\beta}, \tag{4.42}$$

$$b_3 = 2m^2\left[\xi_1^2 D_1\int_0^1 dy\Delta_1(\mu y) + \frac{\xi_2^2\Delta_2(\mu)}{1-v^2}\int_0^1 dy\Delta_2(\mu y)\right]e^{i\tau\beta}$$
$$\quad - \left(\frac{i}{\tau} + \frac{k_2^2}{2}\right)(e^{i\tau\beta} - 1), \tag{4.43}$$

$$b_4 = 2m^2\left[\xi_2^2 D_2\int_0^1 dy\Delta_2(\mu y) + \frac{\xi_1^2\Delta_1(\mu)}{1-v^2}\int_0^1 dy\Delta_1(\mu y)\right]e^{i\tau\beta}$$
$$\quad - \left(\frac{i}{\tau} + \frac{k_2^2}{2}\right)(e^{i\tau\beta} - 1), \tag{4.44}$$

$$b_5 = -\frac{1}{2}\sqrt{k_1^2 k_2^2}(1-v^2)(e^{i\tau\beta} - 1), \tag{4.45}$$

and $\beta = \beta_1 + \beta_2$. The coefficient formulae Eqs. (4.39-4.45), are suitable for any form of transverse plane wave. We mention in addition, our remark that the polarisation tensor can only depend on the gauge and Lorentz-invariant scalars χ, $\mathscr{F}$ and $\mathscr{G}$ is also seen to be justified, considering the coefficients c_n (ξ is related to $\mathscr{F}$ and $\mathscr{G}$) and the vector bases $\{k_{1,2}, \Lambda_1, \Lambda_2, \Lambda_{3,4}\}$, when $k_1^2 \to 0$ as will be imposed later on. In order to progress further, we need to specify the vector potential.

4.2   Constant crossed field

We wish to take the formulae of the preceding section and specialise them to the case of a constant crossed EM field. This is effectively the same as taking the zero-frequency limit of a plane wave, with the $\mathbf{E}$ and $\mathbf{B}$ vectors perpendicular to one another. In this limit, $\mathscr{F} = \mathscr{G} = 0$ and χ is the only Lorentz-invariant scalar. Following [151], considering the probability for processes as a function of these three parameters $W(\chi, \mathscr{F}, \mathscr{G})$, in general, considering $\mathscr{F}$ and $\mathscr{G}$ as small and imagining Taylor-expanding the probability in these parameters, one can see that the case of a constant crossed-field $W(\chi, 0, 0)$ is a valid approximation to probability in an arbitrary field when:

$$\mathscr{F}, \mathscr{G} \ll 1, \qquad \mathscr{F}, \mathscr{G} \ll \chi. \tag{4.46}$$

In addition to the expansion argument, we can also understand physically why results from the constant crossed field can even be applied to oscillating fields. We can make the analogy of ionisation of atoms in the gas phase with pair production in vacuum (i.e. "ionisation" of the vacuum), which is understood in the non-linear regime by the value of the *Keldysh adiabacity parameter* $\gamma = \sqrt{2mI_p}\omega/eE$, which for an ionisation potential $I_p = 2m$ becomes $\gamma = 2/\xi$. Therefore, when the work done by the field over the Compton wavelength is much larger than the energy of a field quantum ($\xi \gg 1$), the vacuum polarisation processes said to be in the *tunnelling regime* ($\gamma \ll 1$) and so do not see the oscillation of the field.

Recalling our vector potential:

$$A^\mu(\varphi) = a_1^\mu \psi_1(\varphi) + a_2^\mu \psi_2(\varphi),$$

we can take the zero-frequency limit, without loss of generality on a linearly-polarised wave and so take immediately $\psi_2(\varphi) = 0$. Since a constant field implies a linear vector potential, we set $f_1 = \varphi = \varkappa_0(x^0 - x^3)$ ($\varkappa^2 = 0$ implying $\varkappa^0 = \pm\varkappa^3$ and we chose the positive root in the previous section). In order to be dimensionally correct, we choose $\mathbf{a}_1 = \mathbf{E}_0/\varkappa^0$ for a constant vector $\mathbf{E}_0$. A^μ is then independent of the external field plane wave frequency, and the constant electric field strength enters as $\mathbf{E} = -\mathbf{E}_0$, allowing us to take the limit $\varkappa^\mu \to 0$ without obstruction. We first note

the important components of the integral:

$$\Delta_2(\mu y) = 0, \tag{4.47}$$

$$\Delta_1(\mu y) = = -\frac{1}{2}(\varkappa k)\tau(1-v^2)y, \tag{4.48}$$

$$\int_0^1 dy \Delta_1(\mu y) = -\frac{1}{4}(\varkappa k)\tau(1-v^2), \tag{4.49}$$

$$D_1 = -\frac{1}{4}(\varkappa k)\tau(1+v^2), \tag{4.50}$$

$$\beta = -\beta_1 = -\frac{1}{3}\frac{1}{16}e^2|a^2|\tau^2(\varkappa k)^2(1-v^2)^2, \tag{4.51}$$

are all, like all other integration terms, independent of spatial co-ordinates, as might be expected in a homogeneous external field. Therefore we can perform the integral in d^4x and immediately recover four-momentum conservation in a constant crossed field:

$$c_n = -i\alpha(2\pi)^3 \int_{-1}^1 dv \int_0^\infty \frac{d\tau}{\tau} \exp\left[-im^2\tau\left(1 - \frac{k_1^2(1-v^2)}{4m^2}\right)\right] b_n \delta^{(4)}(k_2 - k_1), \tag{4.52}$$

$$b_1 = b_2 = 0, \tag{4.53}$$

$$b_3 = \frac{1}{8}m^2\xi^2(\varkappa k)^2(1+v^2)(1-v^2)\tau^2 e^{-i\beta\tau^3} - \left(\frac{i}{\tau} + \frac{k_2^2}{2}\right)\left(e^{-i\beta\tau^3} - 1\right), \tag{4.54}$$

$$b_4 = \frac{1}{4}m^2\xi^2\mu^2(\varkappa k)^2(1-v^2)\tau^2 e^{-i\beta\tau^3} - \left(\frac{i}{\tau} + \frac{k_2^2}{2}\right)\left(e^{-i\beta\tau^3} - 1\right), \tag{4.55}$$

$$b_5 = -\frac{1}{2}\sqrt{k_1^2 k_2^2}(1-v^2)\left(e^{-i\beta\tau^3} - 1\right). \tag{4.56}$$

There comes an important point of consistency. Since we are interested in the one loop correction to photon propagation, we must assume that we are calculating the effect on a vacuum photon, i.e. that $k_1^2 = 0$. In actual fact, we will show, with this very calculation, that taking into account the quantum corrections due to the polarised vacuum, $k_1^2 \neq 0$! This kind of circularity of argument can, in a standard way, be avoided by calculating loops to all orders using Dyson's series to obtain the exact self-energy $\Pi(k)$, which can then be used in the Dyson equation to give the exact photon propagator in an external field (see e.g. [119]) Eq. (4.7). When we make the assumption $\alpha\varkappa^{2/3} \ll 1$, the exact polarisation operator $\Pi(k)$ is well approximated by the one-loop calculation with $k^2 = 0$.

In calculating the c_n's, we encounter two main types of integrals:

$$I_1 = \int_0^\infty d\tau \tau e^{-im^2\tau} e^{-i\beta\tau^3}, \tag{4.57}$$

$$I_2 = \int_0^\infty \frac{d\tau}{\tau^2} \int_{-1}^1 dv e^{-im^2\tau}\left(e^{-it\frac{\tau^3}{3}(1-v^2)^2} - 1\right), \tag{4.58}$$

$t = e^2|a^2|(\varkappa k)^2/16$. We can integrate these analytically in one variable and choose τ. I_1 can then be rewritten in a more familiar form:

$$I_1 = i\beta^{-1/3}\frac{d}{dm^2}\int_0^\infty d\tau \exp\left(-\frac{im^2\tau}{\beta^{1/3}} - \frac{i\tau^3}{3}\right), \tag{4.59}$$

$$I_1 = \beta^{-2/3}f'\left[\frac{m^2}{\beta^{1/3}}\right], \tag{4.60}$$

$$f\left[\frac{m^2}{\beta^{1/3}}\right] = \left[i\text{Ai}\left(\frac{m^2}{\beta^{1/3}}\right) + \text{Gi}\left(\frac{m^2}{\beta^{1/3}}\right)\right] \tag{4.61}$$

where Ai and Gi are the Airy and Scorer's functions, corresponding to the real and minus the imaginary part of the integral respectively, whose properties are briefly recapitulated in App. B. I_2, it turns out, is simpler to tackle as a double-integral. Using the substitution $v' = 1 - v^2$ and after integrating by parts and making the further substitution $v'' = 4/v'$, we can rewrite Eq. (4.58) as:

$$I_2 = \frac{4}{3}t^{2/3}\int_0^1 dv'\, v'^{1/3}\sqrt{1-v'}\frac{d}{dm^2}\int_0^\infty d\tau \exp\left[\frac{-im^2}{(tv^2)^{1/3}}\tau - i\frac{\tau^3}{3}\right], \quad (4.62)$$

$$I_2 = \frac{4}{3}\int_4^\infty dv''\left(\frac{4\sqrt{t}}{v''}\right)^{2/3}\frac{\sqrt{v''-4}}{v''\sqrt{v''}}f'\left[\left(\frac{mv''}{4\sqrt{t}}\right)^2\right]. \quad (4.63)$$

Now since the polarisation operator represents quantum corrections to the lightcone condition Eq. (4.8), we separate out the delta-function and polarisation basis and define new coefficients $\alpha_{3,4}$ which appear directly in the dispersion relation for the photon:

$$\frac{1}{i(2\pi)^4}T_{\text{ren}}^{\mu\nu}(k_1,k_2) = \left[\alpha_3\Lambda_1^\mu\Lambda_1^\nu + \alpha_4\Lambda_2^\mu\Lambda_2^\nu\right]\delta^{(4)}(k_2-k_1), \quad (4.64)$$

$$\left\{k_1^2 g^{\mu\nu} - \frac{1}{(\varkappa k)^2}\left[\alpha_3\frac{(kf_1)^\mu(kf_1)^\nu}{-a_1^2} + \alpha_4\frac{(kf_2)^\mu(kf_2)^\nu}{-a_2^2}\right]\right\}e_\nu(k_1) = 0, \quad (4.65)$$

$$\alpha_3 = \frac{-\alpha}{2\pi}\left\{\int_{-1}^1 dv\left[\frac{1}{8}m^2\xi^2(\varkappa k)^2(1+v^2)(1-v^2)I_1\right] - iI_2\right\}, \quad (4.66)$$

$$\alpha_4 = \frac{-\alpha}{2\pi}\left\{\int_{-1}^1 dv\left[\frac{1}{4}m^2\xi^2(\varkappa k)^2(1-v^2)I_1\right] - iI_2\right\}. \quad (4.67)$$

After substituting Eqs. (4.60) and (4.63) into the above expressions, we achieve:

$$\alpha_3 = \alpha_3(\kappa) = \frac{-2\alpha m^2}{3\pi}\int_4^\infty \frac{2v-2}{v\sqrt{v(v-4)}}\left(\frac{\kappa}{v}\right)^{2/3}f'\left(\left[\frac{v}{\kappa}\right]^{2/3}\right), \quad (4.68)$$

$$\alpha_4 = \alpha_4(\kappa) = \frac{-2\alpha m^2}{3\pi}\int_4^\infty \frac{2v+4}{v\sqrt{v(v-4)}}\left(\frac{\kappa}{v}\right)^{2/3}f'\left(\left[\frac{v}{\kappa}\right]^{2/3}\right), \quad (4.69)$$

where we have introduced a dimensionless scattering parameter which will dictate the size of the quantum effect:

$$\kappa = \frac{(\varkappa k)\xi}{m^2} = \frac{E_0}{E_{\text{cr}}}\frac{k^0-k^3}{m} = \kappa_0\frac{k^0-k^3}{m}, \quad (4.70)$$

for $\kappa_0 = E_0/E_{\text{cr}}$ and $E_0^2 = \mathbf{E}\cdot\mathbf{E}$ and $f'(z)$ is given by Eq. (B.10) in App. B. The parameter κ is simply χ for photons, and clearly encodes the two paths to vacuum polarisation effects: either by increasing the intensity or by increasing photon energies. It also only depends on photon momentum in the direction of the field wavevector, with a maximum for photons counterpropagating antiparallel to the (DC) field. The numerical evaluation of these integrands is then discussed in App. B. We can check our results by comparison with Ritus' [150] for constant crossed fields, noting the change of metric, that $L_\mu = F_{\mu\nu}k_{1\nu}$, $L_\mu^* = F_{\mu\nu}^*k_{1\nu}$ and using the formulae in App. A.1.1, we can show:

$$\Lambda_1^\mu\Lambda_1^\mu = \frac{L^\mu L^\nu}{L^2}\bigg|_{(\eta\to-\eta)}, \qquad \Lambda_2^\mu\Lambda_2^\mu = \frac{L^{*\mu}L^{*\nu}}{L^2}\bigg|_{(\eta\to-\eta)}, \quad (4.71)$$

and also that our expressions for Eqs. (4.68) and (4.69) are equivalent, and therefore that our dispersion relation Eq. (4.65) agrees.

The lightcone condition depends upon the polarisation of the photon in a constant external field, which we can best observe using the initial photon's basis $\{k_1, \Lambda_1, \Lambda_2, \Lambda_3\}$. Specialising to the Lorentz gauge $\partial A = 0$ implies removal of the $k^\mu k^\nu$ terms in Eq. (4.65), which then gives:

$$
\begin{aligned}
k^2 &= 0 & \text{for} \quad & \mathrm{e}_\nu^{(l)}(k) = f_1(k)\, k_\nu\, \delta(k^2), \\
k^2 &= 0 & \text{for} \quad & \mathrm{e}_\nu^{\prime(l)}(k) = f_2(k)\, \Lambda_{3\,\nu}\, \delta(k^2), \\
k^2 &= -\alpha_3 & \text{for} \quad & \mathrm{e}_\nu^{(1)}(k) = f_3(k)\, \Lambda_{1\,\nu}\, \delta(k^2 + \alpha_3), \\
k^2 &= -\alpha_4 & \text{for} \quad & \mathrm{e}_\nu^{(2)}(k) = f_4(k)\, \Lambda_{2\,\nu}\, \delta(k^2 + \alpha_4),
\end{aligned}
\tag{4.72}
$$

where $\mathrm{e}^{(l)}, \mathrm{e}^{\prime(l)}$ are scalar and longitudinal polarisations, and $\mathrm{e}_\nu^{(1)}, \mathrm{e}_\nu^{(2)}$ transverse with f_i, $i \in \{1, 2, 3, 4\}$ being arbitrary functions, which we will set to one. As might have been expected, only the directions originally transverse to the external polarising EM field define a non-trivial dispersion for other photons. What about longitudinal and scalar polarisations? Do they represent propagating photon modes? Although in the absence of charges scalar and longitudinal photons do not constitute observable degrees of freedom, having zero norm, and although the relative proportion of each can be altered by choosing different Lorentz gauges, their presence is not entirely ruled out [92]. Moreover, they play an important role in Coulomb fields as well as the Casimir effect. The question in the setting of vacuum polarisation is further discussed in [40, 160, 174].

4.3   Modified refractive index

Following [19], we define the refractive index $n(k)$ through:

$$
n^2(k) = 1 - k^{\,2}/(k^0)^2,
\tag{4.73}
$$

which is simply a rewriting of $c \to c/n = k^0/|\mathbf{k}|$. The polarisation operator has defined two distinct axes, perpendicular to the external field momentum. A general photon will have a polarisation e that is linear combination of these eigenpolarisations, with each component being dispersed differently, leading to birefringent and dichroic effects. As can be seen from Eq. (4.65), the dispersion is related to the projection of the polarisation on one of the eigenvalues, squared with e.g. dispersion along Λ_1 given by:

$$
k^{\,2} = -\alpha_3 (\Lambda_1 \mathrm{e})^2.
\tag{4.74}
$$

We can define a change in refractive index, δn, via:

$$
\delta n := n - 1 = \frac{1}{2(k^0)^2}\left[\alpha_3(\Lambda_1 \mathrm{e})^2 + \alpha_4(\Lambda_2 \mathrm{e})^2\right] + O\left[(\alpha_{3,4}/k^0)^2\right].
\tag{4.75}
$$

Before plotting $\delta n(\kappa)$ for general values of κ, we can first test that we recover the correct weak-field $\kappa \ll 1$ and strong-field $\kappa \gg 1$ asymptotic limits in both the analytics and numerics. Defining $n_{1,2}$ and $\omega_{1,2}(\mathbf{k})$ as the refractive indices and frequencies

of a wave with polarisation satisfying $(\Lambda_{1,2}\,\mathrm{e})^2 = -1$, $\omega_0^2 = \mathbf{k}\cdot\mathbf{k}$, we can rearrange Eq. (4.73) into:

$$\omega_{1,2} \;\; = \;\; \omega_0 + \alpha_{3,4}/2\omega_0. \tag{4.76}$$

Using the asymptotic limits derived for $\alpha_{3,4}(\kappa)$ Eqs. (B.20) and (B.21) in App. B one can then show:

$$\lim_{\kappa \ll 1}\omega_{1,2}(\mathbf{k},\kappa) \;\; = \;\; \omega_0 - \frac{11 \mp 3}{180}\frac{\alpha m^2}{\pi \omega_0}\kappa^2 - i\alpha m^2 \sqrt{\frac{3}{2}}\frac{3 \mp 1}{32}\frac{\kappa}{\omega_0}\exp\left[-\frac{8}{3\kappa}\right], \tag{4.77}$$

$$\lim_{\kappa \gg 1}\omega_{1,2}(\mathbf{k},\kappa) \;\; = \;\; \omega_0 + \frac{(5 \mp 1)\sqrt{3}}{56}\bigl(1 - i\sqrt{3}\bigr)\Gamma^4(2/3)\frac{\alpha m^2}{\pi^2 \omega_0}\bigl(3\kappa\bigr)^{2/3}, \tag{4.78}$$

which agree with [136] and [49]. First, we see we have recovered the famous $\sim \kappa^2$ correction from weak fields and $\sim \kappa^{2/3}$ from strong fields. Secondly, we note that the weak field limit has the same ratio of coefficients as the Euler-Heisenberg Lagrange expressions in Ch. 3. Moreover, using the definition $D^i = \varepsilon^{ij}E^j = P^i + E^i$ for an electric displacement D^i, relative permittivity ε^{ij}, polarisation P^i and electric field E^i and $n = \sqrt{\varepsilon}$ (with the $\sqrt{}$ understood as referring to eigenvalues ε^i of a diagonalised system $D'^i = [\varepsilon^1 E'^1, \varepsilon^2 E'^2, \varepsilon^3 E'^3]$ neglecting the relative permeability μ^{ij} without loss of generality), one can show that the weak field limit of δn in Eq. (4.77) is consistent with the expressions from effective field theory we used for vacuum polarisation Eq. (3.3) in Ch. 3.

For general parameters of κ, the correction $\delta n_{1,2}$ corresponding to $(\Lambda_{3,4}\mathrm{e}) = 1$ respectively is plotted in Fig. 4.3.
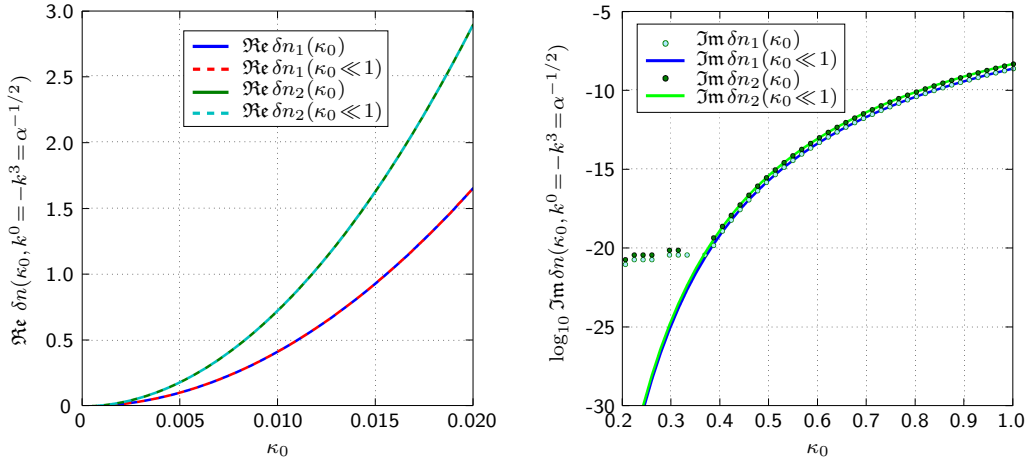
Figure 4.2: Correction to the refractive index $\delta n(\kappa_0)$ in a constant crossed field.

For the real part of the refractive index, we have taken the limit of $\kappa_0 \sim 0.02$ corresponding to upcoming laser facilities ELI and HiPER [60, 86] with the plot showing excellent agreement with the asymptotic weak-field expression. For the imaginary part of the refractive index, we have chosen larger values of κ_0 in order that the results are at all observable. Again, the asymptotic expression shows excellent agreement, up to the point where the maximum numerical accuracy has been reached, clearly seen by deviation of the numerical points from the theoretical curve.

Having the solution of scattering in a constant crossed field for a single photon, we can sum over a thermal ensemble of photons and investigate how the properties of

the thermal vacuum are modified when polarised by an external field. We investigate this question in detail in the following chapter.

Chapter 5

Polarisation of the thermal vacuum in a constant crossed field

In this chapter, we focus on photon-photon scattering in a constant EM field at finite temperature with particular interest in ultra-intense lasers. Our approach is complementary to other analyses using effective field theory generalised to finite temperature, which were limited to the domain of $\omega \ll m$. We demonstrate how macroscopic thermodynamical observables are altered as a result of scattering in a thermal photon gas and comment on the question of a thermal correction to pair creation rates.

As we continue onward on the quest for new physics, we look for unprobed parameter regimes in which to test our current understanding of the universe. In the last decades interest in finite temperature field theory has soared, fuelled by both outstanding questions in QCD related to the QGP phase diagram and astrophysics, being used to describe cosmological electron-positron-photon plasmas and active galactic nuclei [7, 179]. There remains multiple formalisms which compete to develop quantum statistical mechanics in a field-theoretic setting. To complement the current section, we provide in App. C a brief introduction to the main contenders[1] the Matsubara and Keldysh formalisms and summarise their range of applicability. For the case of strong external EM fields at finite temperature, there are currently few definitive results. In fact, for a few years in the 90s, there was even discord about whether the effective field theory one-loop contribution to pair-production in a constant EM field was altered by the generalisation to finite temperature or not. Authors using a real-time formalism [41], the thermofield dynamics formalism [117] as well as the Matsubara formalism [71] first claimed the affirmative but since convincing results of the real-time formalism [57] showed how the imaginary part of the

---

[1]A third formalism, *thermofield dynamics*, conceived by Takahashi and Umezawa in 1975 [163, 164] also makes use of a real-time variable, appealing directly to the average over the thermal ensemble rather instead of an integration contour in complex time to accommodate temperature. Although it can be used to describe nonequilibrium physics, it has found most application in spacetimes other than the four-dimensional Minkowskian, which is of primary interest to us.

one-loop effective Lagrangian was exactly zero (see also [49])[2], there have been no further counter-assertions. This demonstrates the trickiness of thermal field theory in Evans' remark "a quantum plasma [is] not a quantum vacuum"[61] and criticism of thermofield dynamics [113]. In actual fact, real-time results show that a thermal contribution does indeed occur, but that it is the two-loop contribution that is most significant for both the refractive effects and pair-creation rates in effective field theory when generalised to finite temperature in the limit $T \ll m$ [74]. The explanation given is that the internal photons in the two-loop polarisation operator, being massless, are much more susceptible to thermal effects than the leading-order fermionic loop, which is suppressed by a factor $\exp(-m/T)$ at low temperatures [58]. The one loop QED effective Lagrangian for slowly-varying electromagnetic fields generalised to finite temperature [57] was also used to calculate thermally-induced photon splitting [58], for which it was shown only for high temperatures and constant magnetic fields ($T/m, B/B_{\mathrm{cr}} \sim 0.2$) that the effect was appreciable. The effects of a thermal background on photon-photon scattering using effective field theory have also been investigated [168], with particular emphasis on the dispersion relation of photons in the CMB (Cosmic Microwave Background).

A main hindrance of applying finite-temperature field theory to problems involving strong external fields, is that many interesting processes such as photon-splitting and pair-creation will ultimately alter the occupation distribution in a non-trivial way such that the ensemble cannot be regarded as thermal anymore i.e. as having a well-defined temperature. The non-linearity of strong field phenomena twinned with non-equilibrium dynamics is a theoretically demanding area. Even in purely photon-photon interactions, for sufficiently intense fields, there is a wealth of collective non-linear phenomena to consider (for a review, see e.g. [123]).

The need to restrict temperature ranges is due in part to gauge-dependent results (see references [3] in [29]) and infra-red divergences that appear in perturbation theory when $T \gg m$. This occurs when calculating loop diagrams such as the polarisation operator. These ultra-relativistic temperatures give a non-zero polarisation operator and thus a "thermal mass" of the photon $e^2 T^2/3$ [162, 73]. When the external photon energy is of the order of this thermal mass $\sim \sqrt{\alpha}T$, so-called "soft momenta", the perturbation approach breaks down when using the assumption of massless photons $k^2 = 0$. This can be remedied with *hard-thermal loop resummation* summarised in App. C.4.

Theoretical method

In the current chapter, we model the polarised thermal vacuum as a photon gas which scatters in an external constant crossed EM field. The amplitude for scattering processes is then calculated by taking the single photon-scattering amplitude and summing over the thermal boson distribution. There are two assumptions that are inherent to this approach which we justify in the following, using a system of units $\hbar = c = 4\pi\epsilon_0 = k_{\mathrm{B}} = 1$.

   i. Thermal photons are included perturbatively. Considering how a general external-field amplitude would be altered by the next-order contribution from a photon

---

[2]It has also interestingly been recently shown in thermofield dynamics that in 1+1 massless QED, both the real and imaginary parts of the one-loop retarded photon self-energy vanish [44].

vertex, we see that the expansion parameter for such higher-order processes is of the order $\sim eA/m = eE/m\omega = \xi$. Now considering thermal photons to have a frequency $\omega \sim T$ and the electric field to be of the order of the square root of the energy density, using the result for a photon gas [149] that $U/V = \pi^2 T^4/15$ for energy U and volume V, one can show that the condition that thermal photons can be included perturbatively is equivalent to $T \ll m/\sqrt{\alpha}$.

ii. The effects of a thermal electron and photon mass are neglected. In our calculation of the polarisation operator, we make the assumption that the one-loop diagram is a valid approximation, and use on-shell electron and photon masses ($k^2 = 0$) accordingly. However, as the temperature increases, so do the electron and photon *thermal mass* corrections which come from evaluating the mass and polarisation operators respectively in a thermal environment. The thermal photon mass has already been calculated by considering the interaction between photons in the gas [168], in which it was found that the resulting correction to the refractive index is $(44\pi^2/2025)\alpha^2(T/m)^4$. We can compare this correction with the change induced by the external field, derived in Eq. (4.75) to be at least $(8/180)(\alpha/\pi)(E/E_{\mathrm{cr}})^2$. In order to neglect this inter-photon interaction, we must satisfy the condition $T \ll m\left[(45/22\pi^3\alpha)I/I_{\mathrm{cr}}\right]^{1/4}$, which for intensities I of the order of those in upcoming laser facilities ELI and HiPER, corresponds to $T \ll 0.3m$. The electron thermal mass has also been calculated. It has been shown that in the limit $T \ll m$, the thermal correction to the electron mass is $(2/3)\alpha\pi T^2$, implying that the assumption $T \ll m$ is a suitable limit to neglect these effects. As this condition is less restrictive than that for the photon mass, we are left with the condition $T \ll 0.3m$ for our considered values of external field intensity.

Signatures of the polarised vacuum

The external field introduces an anisotropy to the system, which as we have seen, leads to an anisotropy in the refractive index i.e. a vacuum birefringence that could be measured. In addition, the change in refractive index, causing a shift in the photon gas energy levels, should lead to a change in measurable thermodynamic variables such as the pressure. Moreover, although our results assume thermal equilibrium, for sufficiently high values of $\kappa_0 T$, pair creation would take place and although numbers of pairs cannot be consistently calculated, the parameters at which pair creation will begin to become a factor, can be ascertained. In the current chapter, we present calculations for the change in thermodynamical quantities and discuss the question of pair-production, bearing in mind the restriction $T \ll 0.3m$.

5.1   Thermodynamics of a polarised thermal vacuum

We begin by calculating the free energy or *Helmholtz function* Ω of the system. From this single function, one can derive all other interesting thermodynamical quantities (see e.g. Eq. (C.3)). In a vanishing external field, our results must tend to those of a photon gas.

5.1.1   Free energy of a free photon gas

We consider a system of dimension L^3 filled with a thermal gas of photons. The Helmholtz function can be arrived at through the grand partition function, Z:

$$Z = \mathbf{Tr}\, e^{-\beta \hat{H}}, \tag{5.1}$$

where we have already inserted the condition that the chemical potential is zero for photons and the trace is a sum over all possible ensembles. For our system, $\hat{H}$ can be written as $\sum_{\mathbf{k}} \omega(\mathbf{k}) \hat{N}(\mathbf{k})$[3]. Quantising along the axes of the box defined using the orthonormal set $\{\hat{\mathbf{x}}, \hat{\mathbf{y}}, \hat{\mathbf{z}}\}$ gives us the condition $\mathbf{k} = (\pi/L)[m_x \hat{\mathbf{x}}, m_y \hat{\mathbf{y}}, m_z \hat{\mathbf{z}}]$ for the three quantum numbers $\mathbf{m} = \{m_x, m_y, m_z\} \in \mathbb{Z}^3$. In addition to a product of sums over configurations, one also has a sum over occupancies $l \in \mathbb{N}_0$:

$$Z = \mathbf{Tr}\, e^{-\beta \hat{H}} \quad = \quad \prod_{m_x, m_y, m_z} \sum_{l=0}^{\infty} e^{-\beta l \omega(\mathbf{m})} \tag{5.2}$$

$$= \quad \prod_{m_x, m_y, m_z} \left(1 - e^{-\beta \omega(\mathbf{m})} \right)^{-1}. \tag{5.3}$$

The free energy is then given by:

$$\Omega = -\frac{1}{\beta} \ln Z = \frac{1}{\beta} \sum_{m_x=-\infty}^{\infty} \sum_{m_y=-\infty}^{\infty} \sum_{m_z=-\infty}^{\infty} \ln \left[1 - e^{-\beta \omega(\mathbf{m})} \right]. \tag{5.4}$$

We wish to turn these sums into an integral. First of all, we rewrite the sum over configurations $\mathbf{m}$ as a sum over components of $\mathbf{k}$ and then note that the density of states in d^3k-space is $(L/2\pi)^3$. In addition, as the polarisation also defines an eigenstate of the Hamiltonian and as the energy is independent of polarisation, we have a factor 2 due to degeneracy[4]. All this gives us:

$$\Omega = \frac{V}{4\pi^3 \beta} \int d^3k \ln \left[1 - e^{-\beta \omega} \right], \tag{5.5}$$

where the volume $V = L^3$ and $d^3k = \omega^2 d\omega d\cos\theta_k d\phi$. Noting that $P = -(\partial\Omega/\partial V)_T$, taking the limit $L \to \infty$ and integrating once by parts, we achieve the famous result:

$$P = \frac{1}{3\pi^2 \beta^4} \int_0^{\infty} dx \frac{x^3}{e^x - 1} = \frac{1}{3}\sigma T^4, \tag{5.6}$$

where σ is the Stefan-Boltzmann constant, $\sigma = \pi^2 k_B^4 / 15(c\hbar)^3$.

5.1.2   Free energy of a photon gas in a constant crossed field

The derivation in an external field proceeds in much the same way as for the free field case. The main difference can be seen from the dispersion relation Eq. (4.8), which in the Lorentz gauge becomes:

$$\omega^2 g^{\mu\nu} |\mathbf{k}, e_\nu(\mathbf{k})\rangle = \left[(\mathbf{k} \cdot \mathbf{k}) g^{\mu\nu} + \Pi^{\mu\nu} \right] |\mathbf{k}, e_\nu(\mathbf{k})\rangle, \tag{5.7}$$

---

[3] We have already performed the standard removal of the $\hbar\omega/2$ zero-point modes [66].

[4] We could instead include a final sum $\sum_{r=1,2}$ for polarisation states r in the trace and label $|n_{x,y,z}\rangle$ as $|n_{x,y,z}^r\rangle$, but this would just be equivalent to gaining a factor 2.

implying that the "new" photon energies are functions of both wavevector and polarisation. Our analysis in Ch. 4 consisted of diagonalising $\Pi^{\mu\nu}$ or equivalently, in specifying the eigenbasis Eq. (4.72), comprising the normalised four-vectors $\{e^{(l)}, e'^{(l)}, e^{(1)}, e^{(2)}\}$, with the first two corresponding to scalar and longitudinal polarisations respectively. This implies that the photon energies of each momentum mode should carry a polarisation index: $\omega = \omega_r(\mathbf{k})$, $r \in \{0, 1, 2, 3\}$. Therefore when performing the trace, an additional sum over the four polarisations is required. As noted at the end of Sec. 4.2, the existence of scalar or longitudinal photons is still an unresolved issue and we too, will observe that they play no role in our calculations. Beginning from the expression for the free energy of a photon gas Eq. (5.5), with an additional sum over polarisations and a factor $1/4$ in comparison to the free-field case due to the fixing of the polarisation[5], we have:

$$\Omega = -\frac{1}{\beta} \ln Z = \frac{V}{16\pi^3 \beta} \sum_{r=0}^{3} \int d^3k \ln\left[1 - e^{-\beta\omega_r}\right]. \tag{5.8}$$

Now $\omega_r = \omega/n_r$ for refractive index $n_r = 1 + \delta n_r$, with $\delta n_0 = \delta n_3 = 0$ and δn_1, δn_2 corresponding to the results derived in Eq. (4.75) with $(\Lambda_{3,4}e) = 1$ respectively. Using again the relation $P = -(\partial\Omega/\partial V)_T$, we can expand the logarithm in a Taylor series around $n_r = 1$ to give:

$$P = -\frac{1}{16\pi^3 \beta} \sum_{r=0}^{3} \int d^3k \left\{ \ln\left[1 - e^{-\beta\omega}\right] - \frac{\beta\omega}{e^{\beta\omega} - 1}\delta n_r + O\left[(\delta n_r)^2\right]\right\} \tag{5.9}$$

$$= P_0 + \delta P. \tag{5.10}$$

One can then verify that evaluating P_0 leads to the expression Eq. (5.6) for a free photon gas. In order to calculate δP, we recall that $\delta n_{1,2} = \alpha_{3,4}(\kappa)/2\omega^2$, with $\kappa = \kappa^0 \omega(1 - \cos\theta_k)$, slightly rewriting Eq. (4.70), with θ_k being the angle between $\mathbf{k}$ and the external field momentum $\boldsymbol{\varkappa}$. We then have:

$$\delta P = \delta P_1 + \delta P_2, \tag{5.11}$$

$$\delta P_{1,2} = \frac{1}{8\pi^2 \beta^4} \int_0^\infty dx \int_0^2 dy \frac{x^3}{e^x - 1} \frac{\beta^2 \alpha_{3,4}(\kappa^0 xy/\beta m)}{2x^2}, \tag{5.12}$$

where we have performed the trivial integral in ϕ_k and gone over to new integration variables $y = 1 - \cos\theta_k$ and $x = \beta\omega$. We mention that although x runs to ∞ corresponding to a momentum much larger than the pair-creation threshold, as $T \ll 0.3m$, the high-momentum tail will be exponentially damped. In addition, although the integral can be performed analytically in y, the complicated expression that ensues does not aid numerical evaluation.

Bearing in mind these restrictions which amount to $\kappa^0 Txy/m \ll 0.3\kappa^0$, with κ^0 being of the order ~ 0.02 for the upcoming ELI and HiPER laser facilities [60, 86] and considering the excellent approximation of the weak-field limit of the refractive index to the values plotted in Fig. 4.3, it suffices to use the weak-field expansion of δn_r in $\delta P_{1,2}$.

---

[5]This is performed in analogy to an electron gas in a constant, homogeneous, magnetic field, in which the Hamiltonian includes a term proportional to the spin's projection onto the field $\sim \pm(1/2)\mu \cdot \mathbf{B}$, for electron magnetic moment μ [110].

Weak-field expansion of pressure difference in a photon gas in a constant crossed field

In the weak-field limit, the shifts in the refractive index become:

$$\lim_{(\kappa^0 Txy/m)\to 0} \delta n_{1,2}\big(\kappa^0 Txy/m\big) = \frac{\beta^2 \alpha_{3,4}(\kappa^0 Txy/m)}{2x^2} = \frac{11 \mp 3}{180}\frac{\alpha}{\pi}(\kappa_0 y)^2. \qquad (5.13)$$

On insertion into Eq. (5.12), after some trivial integration, one acquires:

$$\lim_{(\kappa^0 T/m)\to 0} \delta P(\kappa^0 T, T^2) = \frac{11\pi\alpha}{4050}\left(\frac{\kappa_0}{\beta^2}\right)^2, \qquad (5.14)$$

$$\lim_{(\kappa^0 T/m)\to 0} \frac{\delta P}{P_0} = \frac{11\alpha\kappa_0^2}{90\pi}, \qquad (5.15)$$

or in SI units:

$$\lim_{(\kappa^0 k_{\mathrm{B}} T/mc^2)\to 0} \delta P(\kappa^0 T, T^2) = \frac{11\pi\alpha\kappa_0^2}{4050}\frac{(k_{\mathrm{B}} T)^4}{(c\hbar)^3}. \qquad (5.16)$$

That the change in pressure is positive can be explained using physical intuition. The thermal ensemble is a trace over the Boltzmann factor which is a function of the photon energies. For a fixed energy ω, the momenta of the photons in an external field $k = \sqrt{\mathbf{k}\cdot\mathbf{k}} = n\omega$ will increase with refractive index, n. In the weak-field limit, $\delta n > 0$, so the thermal photon momenta increase and correspondingly so too does the pressure. From Eq. (5.15) we note that the relative change in pressure is independent of temperature. This implies that even for low temperatures, where our assumption of thermal equilibrium should comfortably hold to a sufficient level of accuracy, as pair-creation rates tend to zero, the polarised vacuum has an effect. Although it is unlikely that this pressure change can be measured directly (as the detection apparatus would have to be actually in the strong field), it poses the question, whether vacuum polarisation effects can be observed in macroscopic measurements.

5.2   Discussion and Outlook

Although a goal is to devise a realistic experimental scenario in which one could measure the effects of the polarised vacuum through the change in thermodynamic variables, there remain substantial theoretical issues to be addressed. We can identify the three most immediate points to be tackled, involving taking a step towards more realistic inclusion of field, temperature and effects:

i. Evaluation of the thermal pair-production rate: completion of this task would not only allow us to corroborate our assumption of thermal equilibrium for our calculation of thermodynamic effects, but it would also provide parameters at which the potentially easier to measure process of pair production would become probable. Moreover, if the result turns out to be non-zero, one could specialise the solution in a general EM wave Eq. (4.39) to the case of a constant electric field, which could then be used to ascertain the thermal correction to Schwinger's pair-production formula, and to the value E_{cr} regarded as an indicator of the pair-production threshold in the absence of temperature. This

would then provide a direct link with existing results in the literature, which for the case of a constant electric field using Matsubara, Keldysh and thermofield formalisms, seem to now all agree that there is no thermal correction to the pair-creation threshold to one-loop order effective field theory [73, 57, 43]. In the following we present preliminary considerations as to how we could formulate an expression for the thermal pair-production rate:

We derive in App. A.1.3, the relationship between the polarisation operator and the rate of pair creation R, (Eq. (A.23)):

$$R(\omega, \kappa, e) = \mathfrak{Im} \frac{e_\mu e_\nu \Pi_e^{\mu\nu}(\kappa)}{k^0}. \tag{5.17}$$

In order to average this rate over the thermal ensemble, we can appeal to classical statistics and use the average of the number operator $N(\omega, \beta) = \langle \hat{N}(\omega) \rangle_\beta$:

$$
\begin{aligned}
\langle R(\omega, \kappa, e) \rangle &= V \int \frac{d^3 k}{(2\pi)^3} R(\omega, \kappa, e) P(\omega, e, \beta) \\
&= \frac{V}{16\pi^3 N(\beta)} \sum_{r=1,2} \int d^3 k R(\omega, \kappa, e_r) N(\omega, \beta),
\end{aligned} \tag{5.18}
$$

where $\langle \rangle$ refers to averaging over the thermal ensemble, $P(\omega, e, \beta)$ is the thermal photon probability density, $N(\beta)$ is equal to the average total number of photons and:

$$N(\omega, \beta) := \frac{1}{e^{\beta\omega} - 1}. \tag{5.19}$$

The expression Eq. (5.18) can then be shown to reproduce the correct limits when the rate is replaced by unity (giving $\langle 1 \rangle = 1$) and when the external field tends to zero (giving zero rate). Bearing in mind that we will again be considering values of $\kappa \ll 1$ and are constrained by $T/m \ll 1$, since the weak-field limit of $\alpha_{3,4}$ agrees excellently with the numerical solution in this range (see Fig. 4.3 **b**), we are justified in using the corresponding expression here in the rate. The weak-field rate:

$$\lim_{\kappa \to 0} R(\omega, \kappa, e_r) = \frac{3 - \delta_{r1} + \delta_{r2}}{16} \sqrt{\frac{3}{2}} \frac{\alpha m^2 \kappa}{\omega} e^{-\frac{8}{3\kappa}}, \tag{5.20}$$

can be inserted in Eq. (5.18) and if we again switch to integration variables $x = \beta\omega$ and $y = 1 - \cos\theta$, we achieve:

$$\langle R(\omega, \kappa, e) \rangle = \frac{3\sqrt{3}}{64\sqrt{2}\pi} \frac{\alpha \kappa_0 m}{\zeta(3)} \int_0^\infty dx \int_0^2 dy \, x^2 y \frac{e^{-8\beta m/3\kappa_0 yx}}{e^x - 1}, \tag{5.21}$$

where β is dimensionless, with temperature measured in units of the electron mass and where we have used the result:

$$N(\beta) = V \int \frac{d^3 k}{(2\pi)^3} \frac{1}{e^{\beta\omega} - 1} = \frac{\zeta(3)V}{\pi\beta^3},$$

where ζ is the Riemann zeta function and $\zeta(3) \approx 1.20$. The final expression for the rate Eq. (5.21) can be again seen to reproduce correct limits for $\kappa_0, T \to 0$. Although in principle possible to numerically evaluate, a next step could be to evaluate the rate for the typical situation of $\beta m/\kappa_0 \gg 1$.

ii. Displacement of system from equilibrium: only in a very few, special and most probably unrealistic cases, can the effect of a strong external field be regarded as preserving equilibrium. Therefore any first steps towards an experimentally-realistic scenario must involve some understanding of systems displaced from equilibrium. One possible example that could be studied is the case of a photon gas in the field of a circularly-polarised wave. From [19], for scattering of a photon with initial momentum k_1 to k_2, in an external field of photon momentum $\varkappa$, the T-matrix can be written in terms of a sum of polarisation operators:

$$T(k_1, k_2) = \Pi_{(0)}\delta(k_1 - k_2) + \Pi_{(-)}\delta(k_1 - k_2 - 2\varkappa) + \Pi_{(+)}\delta(k_1 - k_2 + 2\varkappa).$$

This scenario offers on the one hand a system weakly displaced from equilibrium with energy levels being mixed by the external field frequency, and on the other a system of equations that is only slightly less tractable than for the constant field case. As we could no longer assume thermal equilibrium, we would have to calculate the polarisation operator in the context of e.g. the Keldysh formalism. Using real-time non-equilibrium methods would also provide the possibility of investigating the $T \sim m$ limit, taking into account the fermion field and being able to calculate pair-creation rates. In addition, one could then calculate the effect the presence of generated pairs have on assumptions of thermal equilibrium.

iii. Field inhomogeneity: any realistic scenario must involve detection equipment placed away from the incredible intensities required before vacuum polarisation effects become measurable. With the exception of pair creation and perhaps some bulk thermodynamic quantities such as the specific heat, this would necessitate some form of inhomogeneity in the fields. However, any form of field inhomogeneity at finite temperature would seem to displace the system from equilibrium and so this line of enquiry could only be taken up after including non-equilibrium effects.

To conclude, many questions still remain open about the nature of the polarised vacuum when subject to heat. However, our technique is original and complements methods already applied to similar external field backgrounds. Moreover, the power of our approach is that any wave background can in principle be calculated, and the link to vacuum polarisation effects is direct.

Chapter 6

Summary and outlook

6.1 General summary

Vacuum polarisation effects in intense lasers was the title chosen to best summarise the aims of the work. Our goal was to devise a realistic scenario involving intense lasers, in which the effect of the polarised vacuum could be measured. By utilising interference effects, we showed how elastic real photon-photon scattering could in principle be measured with the next generation of laser facilities. In addition, we also considered what role finite temperature plays in vacuum polarisation effects. The thesis was balanced fairly equally in terms of applied and theoretical aspects. For the case of vacuum diffraction, we were also able to place special emphasis on experimental aspects, whereas the finite temperature discussion remained predominantly theoretical.

Opening with a brief history of key experimental and theoretical results related to the polarised vacuum and motivating the present need for a continued study of the myriad hitherto unobserved vacuum polarisation effects, we began in **chapter 2** with a discussion of effective field theory. Not only have the majority of papers on QED vacuum polarisation been partially or fully based on the corresponding Euler-Heisenberg Lagrangian, but generalisations to finite temperature at least in 3+1 dimensions have almost exclusively relied upon its predictive power. Considering the applicability to low frequency photons $\omega \ll m$, this theoretical approach is particularly suited to describing vacuum polarisation phenomena in lasers and is therefore an essential component in any substantial work on the polarised vacuum. After deriving the main object of calculational interest – the functional determinant – in a scalar field theory and discussing the generalisation to QED, we included details of a suitable method to evaluate such determinants, applying it to the pedagogical example of a constant magnetic field. Citing approaches that solve for the general case of a constant EM field, we expanded the resulting Euler-Heisenberg Lagrangian in the weak-field limit, which formed the basis for calculations in **chapter 3**.

Chapter 3 saw the application of the Euler-Heisenberg Lagrangian to a realistic experimental scenario. Inspired by probe + strong laser calculations such as [142], we took the novel approach of introducing a second strong laser and explicitly studied the interference effects that were generated as a result. We showed how, using ultra-intense lasers, it is in principle possible to fabricate a double-slit consisting entirely of

light [102]. Not only is this an important further generation of the classic experiment displaying the inherent wave-particle duality so central to the interpretation of quantum mechanics, it also represents a realistic scenario in which one could measure, for the very first time, elusive elastic real photon-photon scattering. Moreover, by using the interference between scattered probe photons in the centre of each strong laser, one is in principle able to spatially separate this vacuum signal from the otherwise overwhelming probe background. By calculating the intensity pattern in Sec. 3.2, we were able to relate the number of expected photons per shot and the total number of required photons for a pattern, to parameters of the laser, in regions of high signal-to-noise ratio. In doing so, we introduced *photon diffraction* as a key signature of the polarised vacuum in collisions of laser beams. Throughout **chapter 3** we demonstrated the sensitivity of the single-slit diffraction pattern to the shape of the strong-field laser beam whilst also showing how robust the phenomenon of diffraction was, with a distinct spatial separation of the beams being the main prerequisite to obtaining an interference pattern. In addition, these effects were demonstrated in two different beam geometries, which can be related to one another via a continuous transformation, and it was shown how sensitive the diffracted EM field is to beam alignment. Beyond diffractive effects, in Sec. 3.3 we also calculated the modest improvement of a factor 1.4 and 1.3 in the rotation and ellipticity inducement in the polarisation of probe light, in the double-slit and double-shaft case respectively, over single strong-beam + probe collisions. Moreover, by including effects of probe focusing, it was shown that with a finite separation of beams, effects on the probe polarisation oscillate both with beam-separation and detector distance, highlighting once again the sensitivity to beam alignment. We concluded the chapter in Sec. 3.4 with a comprehensive discussion of the approximations used and experimental issues, with particular emphasis on thermal effects and finite vacuum pressure.

In calculating the amplitude for photon scattering in an external EM plane wave, **chapter 4** marked the beginning of the thermal part of the thesis. The QFT derivation of the polarisation operator is also crucial to the development of the thesis, as it is the object that encodes the full detail of the scattering process according to QED, in comparison to the fermionic average given by the effective field theory in **chapter 2**, which is restricted to frequencies $\omega \ll m$. Detailing calculation of the amplitude for plane waves, which was supplemented by steps in **appendix A**, we then specialised to the case of a constant crossed field in Sec. 4.2 whose pertinence to ultra-intense lasers was also clarified, following which we calculated the modification in refractive index in Sec. 4.3, reproducing asymptotic limits, aided by content from **appendix B**. This all formed the basis for calculations in **chapter 5**.

After giving a brief review of mechanisms for incorporating finite temperatures into QFT in **appendix C** and a summary of previous results relevant to the polarised QED vacuum in the opening to **chapter 5**, we began a calculation of the change in thermodynamic properties of a vacuum polarised by a constant crossed field. Interpreting the vacuum at finite temperature as a thermal photon gas, we summed the photon scattering result of the previous chapter over the ensemble, thus incorporating the effect of an external strong field. Concentrating again on the weak-field limit, we calculated an increase in pressure due to vacuum polarisation and posed the original question whether the effect of the polarised vacuum could be measured through macroscopic quantities. Moreover, the calculated relative change was independent of temperature, meaning that even at low temperatures, where the assumption of thermal equilibrium is more valid (due to the small pair-production rate), there would

remain a vacuum signature. In addition, we outlined a preliminary expression for the pair creation rate at finite temperature, which we interpreted as a measure of the potential of the vacuum to decay into pairs, which is also important in verifying thermal equilibrium.

To conclude, both on the applied and theoretical sides, we have contributed important results to the body of work on vacuum polarisation effects.

6.2   Outlook

An outlook on future work can likewise be split into two sections on diffractive and thermal vacuum polarisation effects.

Although we comfortably met our aims in devising a realistic scenario in which to measure elastic real photon-photon scattering, it might be possible to further specify this to experiment by e.g. using more realistically shaped beams. At ultra-high intensities, there is evidence to suggest that the Gaussian assumption becomes less valid, and that the beam profile can be best described by q-Gaussian's of the form $[1 + (\rho/\rho_r)^2]^{-\mu}$, for transverse beam co-ordinate ρ, constants ρ_r and $\mu > 1$ [134]. However, in order to perform this consistently, one would first have to find a solution to Maxwell's equation which had this form, which would probably be less tractable than a Gaussian (which was at least analytically integrable in two dimensions) increasing the numerical calculation effort considerably.

Due to the wide applicability of the operator diagram technique devised by Baier and colleagues [17, 18] and the veritable bounty of potential observables that can be investigated in statistical physics combined with the rich array of potential vacuum polarisation effects, there is plenty of room for further development of thermal results from **chapter 5**. We re-iterate the three most important tasks from that chapter, identified as being the following.

i. Evaluation of the thermal pair creation rate: this would on the one hand allow us to further corroborate the domain of validity of the assumption of thermal equilibrium and on the other provide a crucial comparison with results from the existing thermal field theoretical approaches based on the Matsubara, Keldysh and thermofield formalisms [73, 57, 43]. In the event that the thermal correction is non-zero, which is possible as we have no such limitation that $\omega \ll m$, this would allow us to define a thermally-modified Schwinger pair-production threshold.

ii. Displacement from thermal equilibrium: if we are ever to seriously consider application to experiment, the assumption of thermal equilibrium must be somehow relaxed, especially in situations involving ultra-intense lasers. In addition, this would allow us to better evaluate the equilibrium results of refractive vacuum polarisation effects in chapter 5. An ideal example would be to consider polarisation of the photon gas in a circularly-polarised laser, for which one can also straightforwardly derive the polarisation operator (see e.g. [19]). Again beginning in the parameter regime in which pair-creation is negligible, this would relax the condition that the real photon-scattering be elastic. Circularly-polarised light offers the advantage that, due to conservation of

angular-momentum, the only non-elastic scattering events involve a change in photon momentum of $\pm 2\varkappa$ where $\varkappa$ is the momentum of the laser photon. This would then weakly displace a photon gas from equilibrium, whilst minimising analytical complexity.

iii. Introduction of inhomogeneity: as polarisation effects in the weak-field limit scale with parameter $\kappa^2 = (E_0/E_{\mathrm{cr}})(1 - \cos\theta)\omega/m$, for angle θ between photon of frequency ω with $\varkappa$ in a background field strength E_0, first defined in Eq. (4.70) in Ch. 4, and as most detection apparatus cannot withstand the intense radiation required to observe such effects, it is necessary to introduce some inhomogeneity between the interaction centre and detector. Although difficult to analytically include in four dimensions, a first step could be to specify the solution of polarisation operator in general EM waves to a wide, slowly-varying (in the sense of longer than the thermal equilibration time) sech^2 or Gaussian function. This would on the one hand be closer to EM fields available in the laboratory but on the other provide a better understanding of the role of field inhomogeneities at finite temperature.

It is envisaged that the first two of these tasks will provide important insights, of use in the development of the theoretical framework, in which one may be able to make the first tentative suggestions for experiment.

Appendix A

Results from Quantum Electrodynamics

We collect some useful reference formulae and give brief explanations for some of the main results from QED that we use in the main text. In the second part, we detail the derivation of the key operator disentangling method used in the calculation of the polarisation tensor.

A.1 QED toolbox

Here we collect some useful formulae to accompany discussion in the main text, as well as giving brief explanations for key QED results.

A.1.1 Useful products

In a metric $\eta = \mathrm{diag}(+,-,-,-)$, the *Faraday* or *electromagnetic field strength* tensor $F^{\mu\nu}$ and its dual $F^{*\mu\nu} = (1/2)\varepsilon^{\mu\nu\alpha\beta}F_{\alpha\beta}$ for the fourth-rank totally antisymmetric pseudotensor ε, $\varepsilon^{0123} = 1$, for electric and magnetic fields $\mathbf{E}$, $\mathbf{B}$ respectively and general four-vector l_ν, obey:

$$F^{\mu\nu} = \begin{pmatrix} 0 & -E_1 & -E_2 & -E_3 \\ E_1 & 0 & -B_3 & B_2 \\ E_2 & B_3 & 0 & -B_1 \\ E_3 & -B_2 & B_1 & 0 \end{pmatrix}, \tag{A.1}$$

$$F^{*\mu\nu} = \begin{pmatrix} 0 & -B_1 & -B_2 & -B_3 \\ B_1 & 0 & E_3 & -E_2 \\ B_2 & -E_3 & 0 & E_1 \\ B_3 & E_2 & -E_1 & 0 \end{pmatrix}, \tag{A.2}$$

$$
\begin{aligned}
F^{\mu\nu}l_\nu &= -l_\mu F^{\mu\nu} = \left[\, \mathbf{l}\cdot\mathbf{E},\ (l^0\,\mathbf{E} + \mathbf{l}\wedge\mathbf{B})\,\right]^\mu, &\tag{A.3} \\
F^{*\mu\nu}l_\nu &= -l_\mu F^{*\mu\nu} = \left[\, \mathbf{l}\cdot\mathbf{B},\ (l^0\,\mathbf{B} - \mathbf{l}\wedge\mathbf{E})\,\right]^\mu. &\tag{A.4}
\end{aligned}
$$

Both $F^{\mu\nu}$ and $F^{*\mu\nu}$ are gauge-invariant and can be combined to give Lorentz-invariant scalars, which can be chosen to be:

$$\mathcal{F} := -\frac{1}{4}F_{\mu\nu}F^{\mu\nu} \ = \ \frac{1}{2}(E^2 - B^2), \tag{A.5}$$

$$\mathcal{G} := -\frac{1}{4}F^*_{\mu\nu}F^{\mu\nu} \ = \ \mathbf{E}\cdot\mathbf{B}. \tag{A.6}$$

It is often convenient to construct the positive semi-definite *secular invariants* from these objects, given by:

$$a = \sqrt{\sqrt{\mathcal{F}^2 + \mathcal{G}^2} + \mathcal{F}}, \qquad b = \sqrt{\sqrt{\mathcal{F}^2 + \mathcal{G}^2} - \mathcal{F}}, \tag{A.7}$$

which obey the useful identities:

$$ab = \mathbf{E}\cdot\mathbf{B} = \mathcal{G}, \qquad a^2 - b^2 = E^2 - B^2 = 2\mathcal{F}. \tag{A.8}$$

A.1.2   Traces

Here we compile a list of some useful QED traces. The trick to working out a trace of $n \in \mathbb{N}$ gamma matrices is to pull the first gamma matrix through to the end using:

$$\{\gamma^\mu, \gamma^\nu\} = 2g^{\mu\nu}, \tag{A.9}$$

and then use cyclicity to show that the resulting trace is equal to $(-1)^n$ times the original.

$$\mathbf{Tr}\,\gamma^\mu \ = \ 0, \tag{A.10}$$

$$\mathbf{Tr}\,(\gamma^\mu)^{2n+1} \ = \ 0, \tag{A.11}$$

$$\mathbf{Tr}\,\gamma^\mu\gamma^\nu \ = \ 4g^{\mu\nu}, \tag{A.12}$$

$$\mathbf{Tr}\,\gamma^\mu\gamma^\nu\gamma^\rho\gamma^\sigma \ = \ 4\Big(g^{\mu\nu}g^{\rho\sigma} - g^{\mu\rho}g^{\nu\sigma} + g^{\mu\sigma}g^{\nu\rho}\Big), \tag{A.13}$$

$$\begin{aligned}
\mathbf{Tr}\,\gamma^\mu\gamma^\nu\gamma^\rho\gamma^\sigma\gamma^\alpha\gamma^\beta = \ &4g^{\mu\nu}\Big(g^{\rho\sigma}g^{\alpha\beta} - g^{\rho\alpha}g^{\sigma\beta} + g^{\rho\beta}g^{\sigma\alpha}\Big)\\
&-4g^{\mu\rho}\Big(g^{\nu\sigma}g^{\alpha\beta} - g^{\nu\alpha}g^{\sigma\beta} + g^{\nu\beta}g^{\sigma\alpha}\Big)\\
&+4g^{\mu\sigma}\Big(g^{\nu\rho}g^{\alpha\beta} - g^{\nu\alpha}g^{\rho\beta} + g^{\nu\beta}g^{\rho\alpha}\Big)\\
&-4g^{\mu\alpha}\Big(g^{\nu\rho}g^{\sigma\beta} - g^{\nu\sigma}g^{\rho\beta} + g^{\nu\beta}g^{\rho\sigma}\Big)\\
&+4g^{\mu\beta}\Big(g^{\nu\rho}g^{\sigma\alpha} - g^{\nu\sigma}g^{\rho\alpha} + g^{\nu\alpha}g^{\rho\sigma}\Big),
\end{aligned} \tag{A.14}$$

$$\begin{aligned}
\mathbf{Tr}\,\gamma^a\gamma^b\gamma^c\gamma^d\gamma^e\gamma^f\gamma^g\gamma^h \ = \ &g^{ab}\,\mathbf{Tr}\left(\gamma^c\gamma^d\gamma^e\gamma^f\gamma^g\gamma^h\right) - g^{ac}\,\mathbf{Tr}\left(\gamma^b\gamma^d\gamma^e\gamma^f\gamma^g\gamma^h\right)\\
&+g^{ad}\,\mathbf{Tr}\left(\gamma^b\gamma^c\gamma^e\gamma^f\gamma^g\gamma^h\right) - g^{ae}\,\mathbf{Tr}\left(\gamma^b\gamma^c\gamma^d\gamma^f\gamma^g\gamma^h\right)\\
&+g^{af}\,\mathbf{Tr}\left(\gamma^b\gamma^c\gamma^d\gamma^e\gamma^g\gamma^h\right) - g^{ag}\,\mathbf{Tr}\left(\gamma^b\gamma^c\gamma^d\gamma^e\gamma^f\gamma^h\right)\\
&+g^{ah}\,\mathbf{Tr}\left(\gamma^b\gamma^c\gamma^d\gamma^e\gamma^f\gamma^g\right).
\end{aligned} \tag{A.15}$$

A.1.3   Properties of the polarisation tensor

Furry's theorem

Furry's theorem is the statement that closed fermion loops with an odd number of photon vertices sum to zero and can be neglected. This can be seen to be a consequence of charge conjugation. Utilising notation from the main, ignoring coefficients, and filtering out polarisation vectors, the amplitude for the diagrams Fig. A.1.3 can
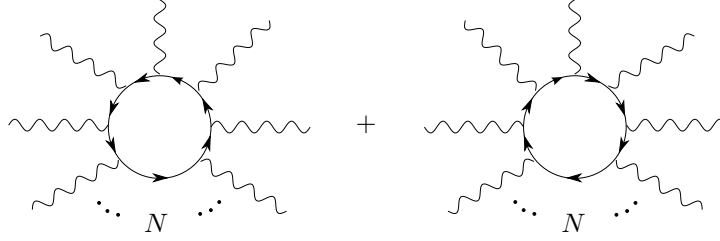

Figure A.1: A closed fermion loop with N photon vertices.

be written as:

$$\int d^4x \Big\{ \mathbf{Tr}\, \langle x | \gamma^{\mu_1} S_F^{(1)}(\hat{p}) \mathrm{e}^{\pm i k_1 \hat{x}} \gamma^{\mu_2} S_F^{(2)}(\hat{p}) \mathrm{e}^{\pm i k_2 \hat{x}} \cdots \gamma^{\mu_N} S_F^{(N)}(\hat{p}) \mathrm{e}^{\pm i k_N \hat{x}} | x \rangle$$

$$+ \mathbf{Tr}\, \langle x | \gamma^{\mu_1} S_F^{(1)}(-\hat{p}) \mathrm{e}^{\pm i k_1 \hat{x}} \gamma^{\mu_N} S_F^{(N)}(-\hat{p}) \mathrm{e}^{\pm i k_N \hat{x}} \cdots \gamma^{\mu_2} S_F^{(2)}(-\hat{p}) \mathrm{e}^{\pm i k_2 \hat{x}} | x \rangle \Big\}$$

$$\text{(A.16)}$$

where $-$ is understood as an incoming and $+$ an outgoing photon in the $\pm$ term in the exponentials and the (n) superscripts for $n \in \mathbb{N}_1$, $1 \le n \le N$, label the propagator and gamma matrices for the corresponding vertex. But since charge conjugation is a symmetry in QED, one can insert $C^{-1}C = \mathbb{1}$, $2N$ times, once on either side of each propagator. Using the property of the the charge conjugation matrix $C\gamma\,C^{-1} = -\gamma^{\mathrm{T}}$ for e.g. a $C = i\gamma^2\gamma^0$ (up to a phase factor), one can also show:

$$S_F(\hat{p}) \;\; = \;\; \frac{1}{\gamma P - m} \;\; = \frac{\gamma P + m}{P^2 - m^2},$$

$$C S_F(\hat{p}) C^{-1} \;\; = \;\; C\frac{1}{\gamma P - m}C^{-1} = \frac{1}{-\gamma^{\mathrm{T}} P - m} = S_F^T(-\hat{p}), \qquad \text{(A.17)}$$

with the third equality of Eq. (A.17) verifiable by Taylor expanding the propagator. Application to e.g. the second term in our amplitude Eq. (A.16) gives:

$$\int d^4x \Big\{ \mathbf{Tr}\, \langle x | \gamma^{\mu_1} S_F^{(1)}(\hat{p}) \mathrm{e}^{\pm i k_1 \hat{x}} \gamma^{\mu_2} S_F^{(2)}(\hat{p}) \mathrm{e}^{\pm i k_2 \hat{x}} \cdots \gamma^{\mu_N} S_F^{(N)}(\hat{p}) \mathrm{e}^{\pm i k_N \hat{x}} | x \rangle$$

$$+ (-1)^N \mathbf{Tr}\, \langle x | (\gamma^{\mu_1})^{\mathrm{T}} \big[S_F^{(1)}(\hat{p}) \big]^{\mathrm{T}} \mathrm{e}^{\pm i k_1 \hat{x}} \cdots (\gamma^{\mu_2})^{\mathrm{T}} \big[S_F^{(2)}(\hat{p}) \big]^{\mathrm{T}} \mathrm{e}^{\pm i k_2 \hat{x}} | x \rangle \Big\},$$

$$\text{(A.18)}$$

which after re-arranging and utilising cyclicity becomes:

$$\Big(1 + (-1)^N \Big) \int d^4x \, \mathbf{Tr}\, \langle x | \gamma^{\mu_1} S_F^{(1)}(\hat{p}) \mathrm{e}^{\pm i k_1 \hat{x}} \cdots \gamma^{\mu_N} S_F^{(N)}(\hat{p}) \mathrm{e}^{\pm i k_N \hat{x}} | x \rangle. \qquad \text{(A.19)}$$

So for odd N, the amplitude for the closed fermion loop diagram Fig. A.1.3 is identically zero.

Pair creation

For an elastic scattering process, we can use Fermi's golden rule in conjunction with the optical theorem to relate the rate of pair creation to the imaginary part of the polarisation operator. For a scattering matrix S_{fi} describing non-trivial elastic scattering of input and output momenta $p_{\mathrm{i}}, p_{\mathrm{f}}$ in the matrix T_{fi} we have:

$$S_{\mathrm{fi}} = \delta_{\mathrm{fi}} + i(2\pi)^4 \delta(p_{\mathrm{f}} - p_{\mathrm{i}})T_{\mathrm{fi}}. \tag{A.20}$$

The probability W_{fi} of this process is the square of the non-trivial part, and dividing by the volume V and time t that occur upon squaring the delta function, we can define a rate:

$$\frac{1}{V}\frac{dW_{\mathrm{fi}}}{dt} = (2\pi)^4 V t\, \delta(p_{\mathrm{f}} - p_{\mathrm{i}})|T_{\mathrm{fi}}|^2, \tag{A.21}$$

which is the statement of Fermi's golden rule. In this notation, the optical theorem becomes [140]:

$$2\,\mathfrak{Im}\, T_{\mathrm{ii}} = i(2\pi)^4 V t \sum_j \delta(p_{\mathrm{i}} - p_{\mathrm{j}})|T_{\mathrm{ij}}|^2. \tag{A.22}$$

Combining Eq. (A.21) and Eq. (A.22) we then have an expression for the rate of elastic scattering in terms of the matrix T:

$$\frac{1}{V}\frac{dW_{\mathrm{fi}}}{dt} = 2\,\mathfrak{Im}\, T_{\mathrm{ii}}. \tag{A.23}$$

In the main text we have the correspondence:

$$T_{\mathrm{fi}} = \frac{\mathrm{e}_1(k_1)}{\sqrt{2\omega_1 V}}\Pi^{\mu\nu}(k_1, k_2)\frac{\mathrm{e}_2(k_2)}{\sqrt{2\omega_2 V}}, \tag{A.24}$$

and if we define the elastic polarisation operator as

$$T^{\mu\nu}(k_1, k_2) = i(2\pi)^4 \delta^{(4)}(k_1 - k_2)\Pi_{\mathrm{e}}^{\mu\nu}(k_1), \tag{A.25}$$

we have a rate:

$$\frac{dW(k_1)}{dt} = \frac{1}{\omega}\mathfrak{Im}\left[\mathrm{e}_1(k_1)\Pi_{\mathrm{e}}^{\mu\nu}(k_1)\mathrm{e}_2(k_1)\right]. \tag{A.26}$$

Transversality

The polarisation tensor $\Pi(k_2, k_1)$ relating incoming and outgoing photons with wavevectors k_1, k_2 respectively, occurs in Maxwell's equations in the form $\Pi^{\mu\nu}(k_2, k_1)A_\nu(k_1)$. Suppose $A_\nu(k_1)$ were the vector potential of a free photon, then we could write it as $A_\nu(\varphi)$, where $\varphi = k_1 x$ as in the text. As the physics must be invariant under a gauge transformation $A_\nu \to A'_\nu = A_\nu + \partial_\nu f(\varphi) = A_\nu + k_{1\nu} f(\varphi)$, for an arbitrary function f, this should have zero effect on Maxwell's equations. The only way this can be fulfilled is if $\Pi^{\mu\nu}(k_2, k_1)k_{1\nu} = k_{2\mu}\Pi^{\mu\nu}(k_2, k_1) = 0$, and hence the necessary transversality of the polarisation tensor.

Regularisation in an external field

We regularise the polarisation tensor in an external field in the following, standard fashion. We know that at zero field, the unrenormalised tensor is infra-red divergent. No extra divergences are introduced into the tensor by the presence of the external field (signified by $_F$), occurring as it does, in the denominator. We can regularise it simply by subtracting off the zero field term as in the following:

$$\Pi_F^{\mu\nu} = \left(\Pi_F^{\mu\nu} - \Pi_{F=0}^{\mu\nu}\right) + \Pi_{F=0}^{\mu\nu} \tag{A.27}$$

$$= \Pi_{\text{ren}}^{\mu\nu} + \Pi_{F=0}^{\mu\nu}. \tag{A.28}$$

Now $\Pi_{\text{ren}}^{\mu\nu}$ is renormalised as $\lim_{F\to 0} \Pi_{\text{ren}}^{\mu\nu} = 0$ and encodes all parts of the polarisation operator that depend on the field and so will be what we call the "polarisation operator" in external field calculations. So for us, terms that are independent of the field disappear. The remaining term $\Pi_{F=0}^{\mu\nu}$, can then be renormalised with standard methods in zero field and won't appear in our analysis.

A.2 Exponential operator method

A.2.1 Disentangling operators between exponentials

We explain the calculations in [18] for the disentangling of exponentials of non-commut-ing operators. We define a transformation of the operator $\hat{M}$ (where again $\hat{P} = \hat{p} + e\hat{A}$):

$$\overline{\hat{M}} \equiv \hat{M}(s) = \exp(is\hat{P}^2)\hat{M}\exp(-is\hat{P}^2). \tag{A.29}$$

When $\hat{M} \to \hat{P}$, the quantity in Eq. (A.29) occurs in loop calculations e.g. the electron mass operator, and in our case will be used in calculation of the polarisation tensor. How do we evaluate such an object? One possibility, which we now investigate, is to differentiate both sides with respect to the parameter s. This then generates a first-order operator differential equation, which can be solved for $\hat{M}(s)$ using the initial condition: $\hat{M}(0) = \hat{M}$. Letting $\hat{M} \to P$ (removing hats for notational simplicity), differentiating Eq. (A.29) gives us:

$$\frac{d\overline{P}_\mu}{ds} = i\overline{\left[P^2, P_\mu\right]} = -2e\overline{P^\lambda F_{\lambda\mu}}. \tag{A.30}$$

Specialising to a plane EM wave, recalling $\varphi = \varkappa x$, for a vector potential $A_\mu(\varphi) = a_\mu\psi(\varphi)$, and $\varkappa a = 0$, we have:

$$F_{\mu\nu} = 2\partial_{[\mu}A_{\nu]} = f_{\mu\nu}\psi'(\varphi), \tag{A.31}$$

which after substitution gives:

$$\frac{d\overline{P}_\mu}{ds} = 2e\left[\varkappa_\mu(\overline{aP}) - a_\mu(\varkappa P)\right]\overline{\psi}'(\varphi). \tag{A.32}$$

In order to solve this, we first solve for both barred terms on the right-hand side using the exact same method. Contracting Eq. (A.32) with a^μ, which is just a function, not an operator, we acquire:

$$\frac{d(\overline{aP})}{ds} = -2ea^2(\varkappa P)\overline{\psi}'(\varphi). \tag{A.33}$$

In order to evaluate $\overline{\psi}'(\varphi)$, we first assume $\psi'(\varphi)$ is analytic, allowing us to Taylor expand and show $\overline{\psi}'(\varphi) = \psi'(\overline{\varphi})$. Then for $\overline{\hat{\varphi}}$, we begin again from Eq. (A.29) but with $M \to x$. Differentiating again with respect to s, using $[x^\mu, P^\nu] = -ig^{\mu\nu}$ and contracting with $\varkappa$, we have:

$$\frac{d\varphi(s)}{ds} = -2(\varkappa P),\tag{A.34}$$

which can be solved with:

$$\varphi(s) = \varphi - 2(\varkappa P)s.\tag{A.35}$$

Substitution of Eq. (A.35) into Eq. (A.33) brings:

$$\overline{(aP)} = aP + ea^2 \Delta(s),\tag{A.36}$$
$$\Delta(s) = \psi\big(\varphi(s)\big) - \psi\big(\varphi\big),\tag{A.37}$$

and then after a final substitution into Eq. (A.30), some algebra and an integration by parts, we arrive at:

$$P_\mu(s) = P_\mu + \frac{e}{\varkappa P}(fP)_\mu \Delta(s) + \frac{e^2 a^2}{2(\varkappa P)}\Delta^2(s).\tag{A.38}$$

A.2.2   Disentangling momentum squared in exponential

This section is split into two parts. We first acquire the form of the momentum squared by rearranging terms in the squared Dirac equation and then consider a similar method to the previous section for disentangling the exponential of operator expressions. We describe the method in [18] with particular reference to spin-1/2 particles in an electromagnetic wave:

$$A^\mu(\varphi) = a_1^\mu f_1(\varphi) + a_2^\mu f_2(\varphi),\tag{A.39}$$

with again $\varphi = \varkappa x$ and $a_1 \cdot a_2 = \varkappa \cdot a = 0$, $\varkappa \cdot \varkappa = 0$ as in the text in Sec. 4.1. We note that the effect of spin becomes manifest when the Dirac equation in an external field:

$$\big[\gamma(p + eA) - m\big]\psi = 0,\tag{A.40}$$

for a bi-spinor ψ, is squared and decomposing $\gamma_\mu \gamma_\nu = g_{\mu\nu} + \sigma_{\mu\nu}$ with the spin part of the operator $\sigma_{\mu\nu} := (\gamma_\mu \gamma_\nu - \gamma_\nu \gamma_\mu)/2$, we acquire:

$$\Big[(p + eA)^2 - m^2 + \frac{ie}{2}\sigma_{\mu\nu}F^{\mu\nu}\Big]\psi = 0.\tag{A.41}$$

Using Eq. (A.31), and noting that $\varkappa\!\!\!/\,a\!\!\!/ = -a\!\!\!/\,\varkappa\!\!\!/$, the spin term can be rewritten as:

$$\frac{ie}{2}\sigma_{\mu\nu}F^{\mu\nu} = -ie a\!\!\!/\,\varkappa\!\!\!/\,\psi'(\varphi).\tag{A.42}$$

It will prove useful to decompose the total momentum squared into its components. With the vector potential defining a preferential direction, we can write:

$$P_F^2 = P^2 - ie a\!\!\!/\,\varkappa\!\!\!/\,\psi'(\varphi) = P_a^2 + P_\perp^2 - ie a\!\!\!/\,\varkappa\!\!\!/\,\psi'(\varphi),\tag{A.43}$$

$$P_a = P_{a,1} + P_{a,2}, \quad P_{a,i} = (a_i P)a_i / a_i^2, \quad P_\perp = P - P_a,$$

where P_a is the sum of four-momenta along the field direction and $P_a^2 = P_{a,1}^2 + P_{a,2}^2$, and the spin term is also a sum over a_1 and a_2. In order to determine how we can use this in an exponential, we consider solving:

$$\exp\big(is(\gamma P_F)\big) = \exp\big(is(a+b)\big) = L(s)\exp\big(isb\big)\exp\big(isa\big), \tag{A.44}$$

for:

$$a = P_\perp^2, \qquad b = P_{a,1}^2 + P_{a,2}^2 - ie\slashed{a}\slashed{k}\psi'(\varphi). \tag{A.45}$$

We apply the same method as in the previous section to Eq. (A.44) and again differentiate with respect to s. Defining $f_F(s) = \exp(isa)b\exp(-isa)$, we multiply both sides of the result from the left by L^{-1} and from the right by $\exp(-isa)\exp(-isb)$ to give:

$$iL^{-1}\frac{dL}{ds} = b - \exp(isb)f_F(s)\exp(-isb). \tag{A.46}$$

We can rewrite $f_F(s)$ with the aid of the Baker-Campbell-Hausdorff formula:

$$f_F(s) = \exp(isa)b\exp(-isa) = b + [a,b] + \frac{1}{2!}\big[a,[a,b]\big] + \dots \tag{A.47}$$

By first verifying $[P_\perp^2, b]\,g = [P^2, b]\,g$ for b given in Eq. (A.45) and test function g, one can then show by induction that:

$$f_F(s) \equiv b(s) = \exp\big(isP^2\big)b\exp\big(-isP^2\big). \tag{A.48}$$

This can be solved with our usual differentiation method. The part of b that contains $(a_i P)a_i/a_i^2$ can be solved immediately by taking the result Eq. (A.36) directly over, and the spin part of b can simply be added with the replacement $\varphi \to \varphi(s)$, all of which gives us:

$$f_F(s) = \frac{\overline{aP}}{a^2} - ie\slashed{a}\slashed{k}\psi'(\varphi(s)). \tag{A.49}$$

By showing $[b, b(s)] = 0$, Eq. (A.46) becomes:

$$iL^{-1}\frac{dL}{ds} = b - b(s), \tag{A.50}$$

which can be simply integrated by separation of variables using the initial condition $L(0) = 1$, which in conjunction with Eq. (A.44) gives:

$$
\begin{aligned}
\exp\Big[iu\big(\gamma P\big)^2\Big] \;=\; & \exp\Big[\frac{-e\slashed{a}_1\slashed{k}\Delta_1(u)}{2\varkappa P}\Big]\exp\Big[\frac{-e\slashed{a}_2\slashed{k}\Delta_2(u)}{2\varkappa P}\Big] \\
& \times \exp\Big\{iu\Big[\int_0^1 dy\,\frac{1}{a_1^2}\big(a_1 P + ea_1^2\Delta_1(uy)\big)^2\Big] \\
& +iu\Big[\int_0^1 dy\,\frac{1}{a_2^2}\big(a_2 P + ea_2^2\Delta_2(uy)\big)^2\Big]\Big\}\exp\big(iuP_\perp^2\big),
\end{aligned}
\tag{A.51}
$$

and hence we have achieved a disentangling of the exponential of the momentum squared, in terms of functions of its components.

A.2.3 Application to polarisation operator

We can rewrite Eq. (4.22) with the above methods, which for convenience, we reproduce here:

$$\widetilde{T}^{\mu\nu} = \int d^4x \exp[i(k_2 - k_1)x]\mathbf{Tr}\left[\langle x|\exp\left\{it(P+k)^2\right\}\gamma^\mu\right.$$
$$\left.\exp\left\{isP^2\right\}\left(\gamma P + m\right)\left(\gamma^\nu \not{k}_2 + 2P^\nu\right)|x\rangle\right]. \tag{A.52}$$

Using Eq. (A.51) in Eq. (A.52) to separate out the spin-dependent terms, we have:

$$\widetilde{T}^{\mu\nu} = \int d^4x \exp[i(k_2 - k_1)x]\mathbf{Tr}\left[\langle x|\exp\left[\frac{-e\not{a}\not{\varkappa}\Delta_1(u)}{2\varkappa(P+k_1)}\right]\exp\left\{it[P+k]^2\right\}\right.$$
$$\left.\gamma^\mu \exp\left[\frac{-e\not{a}\not{\varkappa}\Delta_1(u)}{2(\varkappa P)}\right]\exp\left\{itP^2\right\}(\gamma P + m)(\gamma^\nu \not{k}_2 + 2\gamma P^\nu)|x\rangle\right], \tag{A.53}$$

where expressions involving a represent those in terms of a_1 and a_2 as mentioned previously. First of all, we use the fact that $a\varkappa = 0$ to show $(\not{a}\not{\varkappa})^2 = 0$ and after showing $\{\not{\varkappa}, \not{a}\} = 0$, it follows that exponentials of the first type within the trace can be expanded as linear functions:

$$\exp\left[\frac{-e\not{a}\not{\varkappa}\Delta(u)}{2\varkappa(P+k_1)}\right] = 1 + \frac{e\not{\varkappa}\not{a}}{2\varkappa(P+k_1)}\left[\psi(\varphi - 2(\varkappa P)s) - \psi(\varphi)\right]. \tag{A.54}$$

We would also like to put the exponentials together. Using our result from Eq. (A.37) with $s \to -s$:

$$\exp(-isP^2)\Delta \exp(isP^2) = \Delta(-s) = \psi(\varphi + 2\varkappa Ps) - \psi(\varphi), \tag{A.55}$$

and so simply multiplying on the left by the exponential gives:

$$\Delta \exp(isP^2) = \exp(isP^2)\Big(\psi(\varphi + 2\varkappa Ps) - \psi(\varphi)\Big). \tag{A.56}$$

Applying this in Eq. (A.53) gives:

$$\widetilde{T}^{\mu\nu} = \int d^4x \exp[i(k_2 - k_1)x]\langle x|\exp\left[it(P+k_1)^2\right]\exp\left[isP^2\right]B^{\mu\nu}|x\rangle,$$
$$B^{\mu\nu} = \mathbf{Tr}\left[\gamma^\mu\left(1 - \frac{er^+(s)}{2(\varkappa P)}\not{\varkappa}\not{a}\right)\left(\gamma P + m\right)\left(\gamma^\nu\not{k}_2 + 2P^\nu\right)\left(1 + \frac{er^-(t)}{2\varkappa(P+k)}\not{\varkappa}\not{a}\right)\right], \tag{A.57}$$

where we have defined:

$$r^+(s) = \psi(\varphi + 2(\varkappa P)s) - \psi(\varphi), \quad r^-(t) = \psi(\varphi - 2\varkappa(P+k)t) - \psi(\varphi). \tag{A.58}$$

Appendix B

Airy functions and constant crossed field calculations

We present some basic definitions and plots of the first three Airy functions $\text{Ai}(x)$, $\text{Bi}(x)$, $\text{Gi}(x)$ as well as some results for the Airy derivative function $f'(x)$ that form useful reference for calculation of the polarisation operator in a constant crossed field. In addition, we plot the form factors $\alpha_{3,4}$ that occur in the calculation, and derive useful asymptotic limits.

One of the simplest non-trivial linear second-order ordinary differential equations:

$$\frac{d^2 f}{dx^2} = fx, \qquad x \in \mathbb{R} \tag{B.1}$$

has a solution given by the following *Airy* integral [5]:

$$\text{Ai}(x) = \frac{1}{\pi} \int_0^\infty dt \cos\left(\frac{t^3}{3} + xt\right), \tag{B.2}$$

plotted in Fig. B.1. That $\text{Ai}(x)$ is convergent is due to the $t^3/3$ term initiating ever more rapid oscillations that the linear term. We show this using a standard trick of asymptotic analysis by integrating by parts in the following way:

$$\text{Ai}(x) = \frac{1}{\pi} \int_0^\infty dt \, \frac{1}{t^2 + x} \frac{d}{dt} \sin\left(\frac{t^3}{3} + xt\right) \tag{B.3}$$

$$= \lim_{t' \to \infty} \frac{\sin\left(\frac{t'^3}{3} + xt'\right)}{t'^2 + x} - \int_0^\infty dt \, \frac{t}{\left(t^2 + x\right)^2} \sin\left(\frac{t^3}{3} + xt\right). \tag{B.4}$$

Due to the absence of poles, we could also use Cauchy's theorem to rotate the integration contour by $t \to \exp(i\pi/6)t$ (also known as a Stokes' transformation [180]) giving:

$$\text{Ai}(x) = \mathfrak{Re}\frac{1}{\pi} \int_0^\infty dt \, \exp\left[i\left(\frac{t^3}{3} + xt\right)\right], \tag{B.5}$$

$$= \mathfrak{Re}\frac{\exp\left(i\pi/6\right)}{\pi} \int_0^\infty dt \exp\left(\frac{-t^3}{3} + ixt \, e^{i\pi/6}\right), \tag{B.6}$$
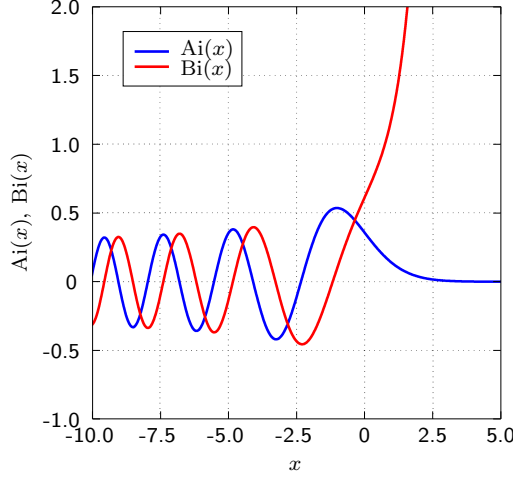
Figure B.1: The two standard Airy functions. For $x > 0$, $\mathrm{Ai}(x)$ converges whereas $\mathrm{Bi}(x)$ diverges.

also clearly showing convergence as $t \to \infty$. The second linearly-independent solution to the Airy equation is $\mathrm{Bi}(x)$, often defined as:

$$\mathrm{Bi}(x) \;=\; \int_0^\infty dt \exp\left(\frac{t^3}{3} + xt\right) + \sin\left(\frac{t^3}{3} + xt\right). \tag{B.7}$$

As the integral of the cosine is a solution, since a phase change only adds a constant that can be cancelled to both sides of the differential equation Eq. (B.1), the integral of the sine is also a solution. As a linear combination is a solution the complex exponential is a solution, and after a contour rotation, one acquires the real exponential, all of which verifies that $\mathrm{Bi}(x)$ is a solution. Both Airy functions can also be written in terms of Bessel functions [137].

Airy derivative function, $f'(x)$

In the text, we encounter Scorer's function $\mathrm{Gi}(x)$ as the integral:

$$\mathrm{Gi}(x) = \frac{1}{\pi} \int_0^\infty dt \sin\left(\frac{t^3}{3} + xt\right), \tag{B.8}$$

which is very similar in form to Airy's function, and can even be rewritten in these terms [137]:

$$\mathrm{Gi}(x) = \mathrm{Bi}(x) \int_x^\infty \mathrm{Ai}(t)dt + \mathrm{Ai}(x) \int_0^x \mathrm{Bi}(t)dt. \tag{B.9}$$

For calculations in a constant-crossed field, we wish to evaluate the combination:

$$f'(z) := \frac{d}{dz}\Big(i\mathrm{Ai}(z) + \mathrm{Gi}(z)\Big) = \int_0^\infty dx\, x \exp\left[-i\left(xz + \frac{x^3}{3}\right)\right]. \tag{B.10}$$

The absence of poles in $f'(z)$ allows us to use Cauchy's theorem again to introduce a rotation in the complex plane of the integration contour: $x \to R\exp(i\theta_0)$ to transform the integral into a radial one. For $\theta_0 = -\pi/6$ we obtain a form with rapid

convergence:

$$f'(z) = \exp(-i\pi/3) \int_0^\infty dx\, x \exp\left[-izxe^{-i\pi/6} - x^3/3 \right], \tag{B.11}$$

which is then suitable for numerical integration. To verify numerical evaluation of the integrand, we can form the asymptotic limits $z \gg 1$, $z \ll 1$, which we will label the *weak* and *strong* limits on account of their usage in the main text. Beginning with the strong limit, one might expect due the asymptotic nature of the oscillating exponential and considering the method of stationary phase that the imaginary part should vanish. Using the original form Eq. (B.10), the cubic term in the exponential can be argued away and by integrating by parts one acquires:

$$\lim_{z\to\infty} f'(z) = \exp\left(-\frac{i\pi}{3} \right) \int_0^\infty dx\, x \exp\left[-izxe^{-i\pi/6} \right] = -\frac{1}{z^2}. \tag{B.12}$$

For the *strong* limit $z \ll 1$, using the rewritten Eq. (B.11) we can approximate the oscillating integrate with unity and with a co-ordinate transformation $x \to t = x^3/3$ we acquire:

$$\lim_{z\to 0} f'(z) = \frac{\exp(-i\pi/3)}{\sqrt[3]{3}} \int_0^\infty dt\, t^{-1/3} e^{-t} = \frac{1 - i\sqrt{3}}{2\sqrt[3]{3}} \Gamma\left(\frac{2}{3} \right). \tag{B.13}$$

The agreement of these asymptotic results as well as numerical evaluation of the real and imaginary parts of $f'(z)$ for general z is plotted in Fig. B.2, from which we note a similarity of the overall form with $\mathrm{Ai}(z)$ Fig. B.2.
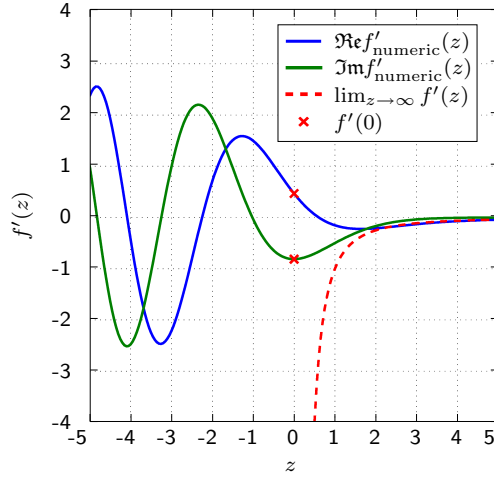

Figure B.2: Numerical evaluation of $f'(z)$, with the analytical asymptotics plotted in red ($\mathfrak{Im} f'_{\text{numerical}}(z) \to 0$ as $z \to \infty$ also agrees with the analytical limit).

Constant external field form factors

The function f' occurs in the following integrand in the calculation of the photon dispersion relation in an external field:

$$\alpha_3(\kappa) = -\frac{2\alpha m^2}{3\pi} \int_4^\infty dv\, \frac{2v - 2}{v\sqrt{v(v-4)}} \left(\frac{\kappa}{v} \right)^{2/3} f'\left(\left[\frac{v}{\kappa} \right]^{2/3} \right), \tag{B.14}$$

$$\alpha_4(\kappa) = -\frac{2\alpha m^2}{3\pi} \int_4^\infty dv\, \frac{2v + 4}{v\sqrt{v(v-4)}} \left(\frac{\kappa}{v} \right)^{2/3} f'\left(\left[\frac{v}{\kappa} \right]^{2/3} \right). \tag{B.15}$$

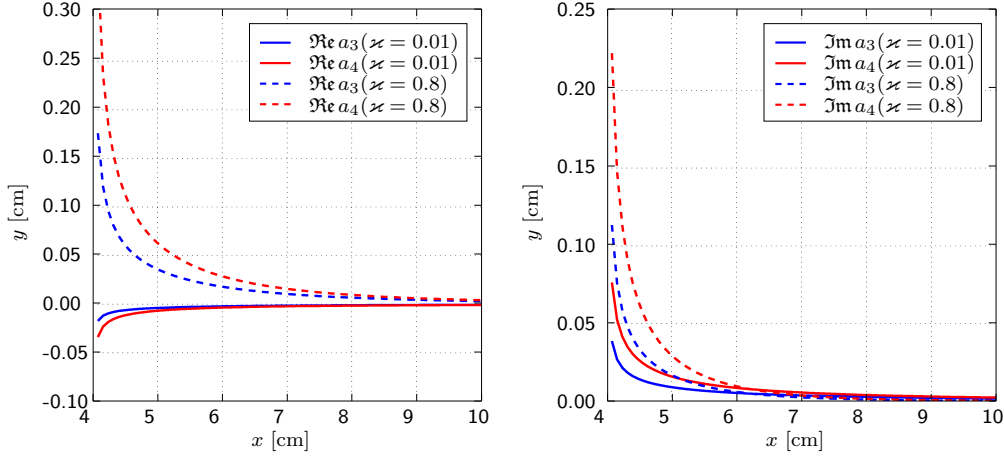Using the definition $\alpha_i(\kappa) = \int_4^\infty dv a_i(\kappa, v)$, we plot these integrands in Fig. B.3

Figure B.3: The integrands of the constant external field form factors α_3, α_4

and notice that the imaginary part of the form factors α_3, α_4 is always positive, corresponding to a positive probability of pair creation. Although initially negative, due to the asymptotic nature of $f'(x)$ Eq. (B.12), the real parts of a_3, a_4 will become positive. We can calculate the strong $\kappa \to 0$ and weak $\kappa \to \infty$ limits of these integrals in the same fashion as for $f'(z)$. Substituting Eqs. (B.12) and (B.13) into the above expressions, and using the results:

$$\int_4^\infty dv \frac{2v + 1 \mp 3}{v^3 \sqrt{v(v-4)}} = \frac{11 \mp 3}{60}, \tag{B.16}$$

$$\int_4^\infty dv \frac{2v + 1 \mp 3}{v^{5/3} \sqrt{v(v-4)}} = \frac{5 \mp 1}{4} \frac{\sqrt{\pi}}{2^{1/3}} \frac{\Gamma(2/3)}{\Gamma(13/6)}, \tag{B.17}$$

as well as:

$$\Gamma(z)\Gamma(z + 1/2) = 2^{\frac{1}{2} - 2z} \sqrt{2\pi} \Gamma(2z), \tag{B.18}$$

$$\Gamma\left(\frac{2}{3}\right)\Gamma\left(\frac{4}{3}\right) = \frac{2\pi}{3\sqrt{3}}, \tag{B.19}$$

where the last formula can be arrived at by substituting the integral form of Γ and switching to polar co-ordinates, we achieve:

$$\lim_{\kappa \to 0} \alpha_{3,4} = -\frac{11 \mp 3}{90} \frac{\alpha m^2}{\pi} \kappa^2, \tag{B.20}$$

$$\lim_{\kappa \to \infty} \alpha_{3,4} = \frac{\sqrt{3}}{28} \frac{\alpha m^2}{\pi^2} (5 \mp 1)(1 - i\sqrt{3}) \Gamma^4\left(\frac{2}{3}\right) (3\kappa)^{2/3}. \tag{B.21}$$

We note, it is also possible to derive a non-zero imaginary limit for $\kappa \to 0$ which we quote as [151]:

$$\lim_{\kappa \to 0} \mathfrak{Im}\, \alpha_{3,4} = -\alpha m^2 \sqrt{\frac{3}{2}} \frac{3 \mp 1}{16} \kappa e^{-\frac{8}{3\kappa}}. \tag{B.22}$$

Appendix C

Quantum field theory at finite temperature

> There are a multitude of ways to describe physics at finite temperature. To complement the discussion of the direct ensemble method used in the text, in this chapter, we review the basics of the the imaginary- and real-time formalisms in an equilibrium context. In the final section we explain the necessary *hard thermal loop resummation* required when considering ultra-relativistic temperatures.

Finite temperature and non-equilibrium field theory have long enjoyed many applications in condensed matter physics. From calculating the properties of an electron gas [72, 145], to DC conductivity (electron scattering in metals) [111, 112], explaining the resistivity minimum of magnetic impurities in metal with temperature [107] (Kondo effect) as well as the properties of superconductors [1]. Due to the short timescales and often very far-from-equilibrium processes involved, usage in the particle physics community has taken more time to develop. The last couple of decades however, have seen an increase in the application and development of finite-temperature methods in relativistic settings[1]. Unresolved questions in QCD from calculation of the phase diagram of the QGP have renewed interest in finite-temperature methods. The quality of our understanding in this non-equilibrium domain will be tested in current and near-future heavy-ion collision experiments like ALICE [38] at CERN, RHIC [33] at Brookhaven and FAIR [79] at GSI. In addition, finite-temperature QFT finds widespread use in astrophysics: in leptogenesis, which seeks to explain the matter-antimatter asymmetry of the universe, from which it has been deduced, the universe must have been out of thermal equilibrium at some point [153]; in non-equilibrium electron-positron-photon astrophysical plasmas [7], in active galactic nuclei [179] as well as to describe gamma-ray bursts [77]. Finally, as explained in the main text Sec. 5, finite-temperature methods have also been utilised in strong-field QED in the processes of pair-production [41, 117, 71, 57, 49], photon-splitting [58] and photon-photon-scattering [168]. We begin by reviewing quantum statistical mechanics.

---

[1]For example, the famous hard thermal loop resummation paper by Braaten and Pisarski [29] has obtained more than 20 citations every year since 1996 (source: Scopus)

C.1   Quantum statistical mechanics

Thermodynamics, being a macroscopic phenomenon, must be reproduced by the quantum version of classical statistical mechanics. In the classical version, each phase-space volume $dpdq$ is occupied with a probability proportional to the *Boltzmann factor* $e^{-\beta\mathcal{E}(p,q)}$, for Boltzmann's constant k_B at temperature T, energy $\mathcal{E}$, momentum and position p, q. All thermodynamic quantities can be derived from the partition function Z, which for a closed system is equal to the sum over all configurations of the Boltzmann factor:

$$Z_{\rm cl}(\beta) = \int dpdq\, g(p,q) e^{-\beta\mathcal{E}(p,q)}, \tag{C.1}$$

where $g(p,q)$ is the density of classical states and p, q are momentum and position respectively. This also acts as the normalisation of the Boltzmann factor, giving the probability that a given phase-space volume is occupied.

Quantum statistics, as the name suggests, are discrete, and the continuous phase space of classical mechanics is replaced by the Hilbert space of quantum states. The quantum-statistical partition function $Z(T)$, becomes then a trace of the operator corresponding to the classical Boltzmann factor acting on the Hilbert space:

$$Z(\beta) = \mathbf{Tr}\, e^{-\beta\hat{H}(\hat{p},\hat{x})} \tag{C.2}$$

We note that this discrete sum is convertible to an integral when a density of energy states $g(\epsilon) = \sum_n \delta(\epsilon - E_n)$ is introduced, and the integral proceeds over ϵ. Some thermodynamical quantities given in terms of $Z(T)$ are the following [67]:

$$
\begin{aligned}
F &= -\frac{N}{\beta}\ln Z, & P &= -\left(\frac{\partial F}{\partial V}\right)_T \\
S &= -\beta^2\left(\frac{\partial \ln Z}{\partial \beta}\right)_V, & \mathrm{C}_V &= -\beta\left(\frac{\partial S}{\partial \beta}\right)_V,
\end{aligned}
\tag{C.3}
$$

where F denotes the free energy, N the number of particles, P the pressure, S the entropy and C_V is the specific heat at constant volume. We note that for a photon gas, $(\partial F/\partial N)_S = 0$ and in this case the free energy is defined $F = -(\ln Z)/\beta$. With a view to vacuum polarisation we would like to allow for open systems in which particles may be added or removed such as via pair-production. Therefore it is useful to define the chemical potential [67]:

$$\mu = \left.\frac{\partial U}{\partial N}\right|_{S,V} = \left.\frac{\partial F}{\partial N}\right|_{V,T} = \left.\frac{\partial G}{\partial N}\right|_{T,P}, \tag{C.4}$$

for internal energy U, free energy F, Gibbs free energy G, entropy S, volume V and pressure P, equal to the energy the system acquires by the addition of a particle under fixed conditions. This gives the *grand canonical quantum-statistical partition function* [105]:

$$Z_{\mathbf{G}}(T,\mu) = \mathbf{Tr}\, e^{-\beta(\hat{H}-\mu\hat{N})}, \tag{C.5}$$

where $\hat{N}$ is the number operator for the state in the Hilbert space on which it is acting. If we define a density matrix[2]:

$$\hat{\rho}(T) := \mathbf{Tr}\, \frac{e^{-\beta\hat{H}_G}}{Z(T)}, \tag{C.6}$$

---

[2]If $\hat{\rho}$ satisfies i) $\hat{\rho}^\dagger = \hat{\rho}$; ii) $\mathbf{Tr}\,\rho = 1$; iii) $\hat{\rho}$ is positive semi-definite i.e. $\langle\psi|\hat{\rho}|\psi\rangle \geq 0$; then $\hat{\rho}$ is a *density matrix* [91].

for $\hat{H}_G = \hat{H} - \mu\hat{N}$, which represents the classical probability of finding a particle in a specific state at a given temperature, then outcomes of measurements of an observable $\hat{A}$ are given by [91]:

$$\langle \hat{A} \rangle = \mathbf{Tr}\, \hat{\rho}\hat{A} = \frac{1}{Z}\sum_n \mathrm{e}^{-\beta E_n}\langle n|\hat{A}|n\rangle, \tag{C.7}$$

for non-degenerate energy eigenvalues and eigenvectors satisfying $\hat{H}_G|n\rangle = E_n|n\rangle$.

One can in addition define a path-integral formulation of quantum statistical mechanics by making the *key* observation which underlies both the real and imaginary formalisms that follow, namely that when the time variable is analytically continued to imaginary values in the quantum-mechanical partition function Z_{QM}:

$$Z_{\mathrm{QM}} = \mathbf{Tr}\, \mathrm{e}^{-i(t_b - t_a)\hat{H}/\hbar}, \tag{C.8}$$

and the association $t_b - t_a = -i\hbar\beta$ is made, we recover the quantum-statistical partition function Z. Then by discretising the co-ordinates, (for details see [105]). Finally, one is left with:

$$Z = \int \mathcal{D}x \int \frac{1}{2\pi\hbar}\mathcal{D}p\, \mathrm{e}^{-S_{\mathrm{E}}[p,x]/\hbar}, \qquad S_{\mathrm{E}} = \int_0^\beta d\tau\, L(x), \tag{C.9}$$

where since $t \to -i\hbar\beta = -i\hbar\tau$, $-(dt)^2 \to (d\tau)^2$, we have a Euclidean action S_{E} over $(dx)^2 = (cd\tau)^2 + d\mathbf{x}\cdot d\mathbf{x}$ and $\mathcal{D}x$, $\mathcal{D}p$ are path integral measures. This provides a direct link with amplitudes from quantum theory when recalling that the typical path integral involves an action:

$$S(t_b, t_a) = \int_{t_a}^{t_b} dt\, L(x). \tag{C.10}$$

Therefore by imposing $t_b - t_a = -i\hbar\beta$ and making a Euclidean rotation $t \to -i\hbar\beta$, a path-integral can be turned into the partition function.

Quantum statistical mechanics is the theoretical starting point of finite temperature formalisms and provides the crucial link to classical macroscopic thermodynamic quantities, that are of use when dealing with predictions of ensembles. This will be achieved either as above by substituting the time variable for an imaginary temperature or by doubling the degrees of freedom and introducing a thermal field.

C.2   Matsubara (imaginary-time) formalism

The seminal work by Takeo Matsubara [124] over fifty years ago, first showed this analytical continuation of time to complex inverse temperature. Our interest is in understanding how to calculate Green's functions, being the basis for calculation of many other quantities in a quantum field theory. The imaginary-time formalism allows one to take over the machinery of $T = 0$ quantum field theory with, in many cases, a factor T and an additional sum over Matsubara frequencies to be performed. We begin by splitting the total Hamiltonian H into a sum of free H_0 and interaction H_1 parts $H = H_0 + H_1$, where in the Schrödinger picture, states $|\psi(t)\rangle$ evolve by:

$$|\psi(t)\rangle \;\; = \;\; \mathrm{e}^{-i\hat{H}(t-t_0)/\hbar}|\psi(t_0)\rangle. \tag{C.11}$$

Representing the density matrix $\hat{\rho}(t)$ as the special projection $\hat{\rho}(t) = |\psi(t)\rangle\langle\psi(t)|$, differentiating both sides of Eq. (C.11), using the spectral theory for self-adjoint operators on the Hamiltonian, one can show that the density matrix must satisfy the following *von Neumann* equation:

$$i\hbar\frac{d\hat{\rho}(t)}{dt} = [H, \hat{\rho}(t)]. \tag{C.12}$$

In order to accommodate the thermal density matrix, we make the continuation $t \to -i\hbar\beta(T)$. With $\hat{\rho}$ given by Eq. (C.6) we then have:

$$-\frac{d\rho(T)}{d\beta} = [H, \rho(T)], \tag{C.13}$$

which can be verified by evaluation of both sides. Following [124], it turns out to be useful to consider the Boltzmann factor, for which we make the ansatz $\exp(-\beta H) = \exp(-\beta H_0)S(\beta)^3$. Differentiating both sides with respect to β gives the *Bloch* equation:

$$-\frac{\partial S(\beta)}{\partial\beta} = H_1(\beta)S(\beta), \tag{C.14}$$

with $H_1(\beta) = \exp(-\beta H_0)H_1\exp(\beta H_0)$, which we recognise as the Schrödinger equation in complex time. Defining $-i\hbar\tau = t$, one can solve Eq. (C.14) by iteration in the standard way to produce a Dyson series (see e.g. [120]), giving:

$$S(\beta) = S(\beta, 0) = \hat{\mathcal{T}}_\tau e^{-\int_0^\beta d\tau H_1(\tau)}, \tag{C.15}$$

where $\hat{\mathcal{T}}_\tau$ is the τ-ordering operator, and the exponential is understood as a mnemonic for the Maclaurin expansion. The object $S(\beta)$, although not being unitary like the standard S-matrix, satisfies all the semi-group properties required of an evolution matrix for quantum fields in complex time, namely i) $S(\tau, \tau) = 1$; ii) $S^{-1}(\tau, \tau') = S(\tau', \tau)$ and iii) $S(\tau, \tau')S(\tau', \tau'') = S(\tau, \tau'')$.

Let us turn to the Heisenberg picture to show some useful properties of thermal Green's functions. We introduce thermal Green's functions as the following:

$$\begin{aligned} G_\beta(\tau, \tau') &= -\langle\mathcal{T}_\tau\hat{\psi}(\tau)\hat{\psi}^\dagger(\tau')\rangle, & \text{(C.16)} \\ G_\beta(\tau - \tau') &= -Z^{-1}\mathbf{Tr}\left[e^{-\beta H}\mathcal{T}_\tau e^{-\beta\tau}\hat{\psi}e^{\beta\tau}e^{-\beta\tau'}\hat{\psi}^\dagger e^{\beta\tau'}\right], & \text{(C.17)} \end{aligned}$$

where $\hat{\psi} = \hat{\psi}(\tau = 0)$ and where we have explicitly separated out the time-dependence from the field operators and using cyclicity of the trace, can justify writing the Green's function in terms of just one variable $\tau - \tau'$. The absence of a factor i in Eq. (C.16), originates from the reassignment $iT_t \to T_\tau$. We can then split Eq. (C.16) into its causal and anti-causal parts:

$$\begin{aligned} G_\beta(\tau - \tau') &= -\theta(\tau - \tau')Z^{-1}\mathbf{Tr}\left[e^{-\beta H}e^{-\tau H}\hat{\psi}e^{-(\tau'-\tau)H}\hat{\psi}^\dagger e^{\tau'H}\right], \\ &\pm\theta(\tau' - \tau)Z^{-1}\mathbf{Tr}\left[e^{-\beta H}e^{-\tau'H}\hat{\psi}^\dagger e^{-(\tau-\tau')H}\hat{\psi}e^{\tau H}\right], \end{aligned} \tag{C.18}$$

where the + sign is for fermions and the − sign for bosons. Let $\tau > \tau' > 0$, and $G^>$ ($G^<$) represent the Green's function evaluated at positive (negative) argument, then we can use trace cyclicity to give:

$$G_\beta^>(\tau - \tau') = -Z^{-1}\mathbf{Tr}\left[e^{-\tau'H}\hat{\psi}^\dagger e^{-(\tau-\tau')H}e^{-\beta H}\hat{\psi}e^{\tau H}\right]. \tag{C.19}$$

---

[3]This is *not* a density matrix, contrary to the label given in [124] and [43]

By judiciously introducing a factor $e^{-\beta H}e^{\beta H}$ and again using cyclicity, we have:

$$G_\beta^>(\tau - \tau') \;=\; -Z^{-1}\mathbf{Tr}\left[e^{-\beta H}e^{-\tau' H}\hat{\psi}^\dagger e^{-((\tau-\beta)-\tau')H}\hat{\psi}e^{(\tau-\beta)H}\right], \qquad (C.20)$$

$$G_\beta^>(\tau - \tau') \;=\; \mp G_\beta^<(\tau - \tau' - \beta). \qquad\qquad\qquad (C.21)$$

Eq. (C.21) is the famous KMS (Kubo-Martin-Schwinger) equation, which can be used to describe thermal equilibrium. Insertion into the Green's function definition Eq. (C.16) shows how this also places a periodicity on the fields: for $\tau'' < 0$ $\hat{\psi}(\tau'' + \beta) = \pm\hat{\psi}(\tau'')$, again with a change of sign for the fermion case. The bounding of $\tau \in [-\beta, \beta]$ has implications for the Fourier transformation of the Green's function. As is routine for calculations of the leading-order contribution to the self-energy Feymann graph (e.g. in QED for the calculation of the polarisation operator), virtual propagators occurring in loops must be integrated over all possible (four)-momenta. As the Fourier transform is over a finite τ interval, the inverse Fourier transform will be over discrete frequencies. In general, these are the so-called *Matsubara frequencies*, ω_n:

$$G(i\omega_n) \;=\; \int_0^\beta G(\tau)e^{i\tau\omega_n}, \qquad\qquad\qquad (C.22)$$

$$G(\tau) \;=\; \frac{1}{\beta}\sum_n e^{-i\omega_n\tau}G(i\omega_n), \qquad\qquad (C.23)$$

$\omega_n = n\pi/\beta$, $n \in \mathbb{Z}$. One can then use the KMS condition to show that for the fermion (boson) fields, the Matsubara frequencies are given by $\omega_n = (2n + 1)\pi/\beta$ ($\omega_n = 2n\pi/\beta$).

The Matsubara formalism is an equilibrium method and perfectly applicable when there is a well-defined temperature and only time-averaged quantities are of interest. Having widely been used in QCD, it is however inapplicable to any situations involving evolution such as phase transitions.

C.3   Keldysh (real-time) formalism

Although the Matsubara formalism adequately describes many finite-temperature phenomena, it does so by sacrificing the evolution variable. When dealing with general processes involving heat, we envisage being able to describe systems which, once at a well-defined temperature, have been driven out of thermal equilibrium by interactions with external fields. In order to describe effects on the time scale of collisions due to an external interaction, or dissipative and transient behaviour, one requires an evolution parameter. In the 1960s, L. V. Keldysh developed a general real-time formalism that can be used when a statistical system under the action of an external field "deviates to any arbitrary extent" from thermal equilibrium [99] and is applicable to the aforementioned situation. The real-time or closed-loop formalism is characterised by the ordering of field operators along a complex contour in time. We begin by defining the evolution matrix, explaining the contour and then how non-equilibrium methods can be used with perturbative Feynman diagrams. A fuller treatment of this method is given in [146] and [119].

Consider first a Hamiltonian $\hat{H}$ split into free and interaction terms $\hat{H} = \hat{H}^0 + \hat{H}^I$. In the Heisenberg picture, the time evolution of operators with initial condition

$\hat{A} = \hat{A}(t_0)$, can be described with a unitary evolution operator $\hat{U}(t, t_0)$ as:

$$\hat{A}_H(t) = \hat{U}_H^\dagger(t, t_0)\hat{A}\hat{U}_H(t, t_0), \quad \text{with} \tag{C.24}$$

$$\hat{U}_H(t, t_0) := \exp\left[-\frac{i}{\hbar}\hat{H}(t - t_0)\right], \tag{C.25}$$

and $\hat{A}_H(t)$ being the operator $\hat{A}$ in the Heisenberg picture with respect to $\hat{H}$. If we instead considered a time-dependent perturbation $\hat{H}'(t)$ giving a time-dependent Hamiltonian $\hat{\mathcal{H}}(t) = \hat{H}^0 + \hat{H}^I + \hat{H}'(t)$, the evolution would be given by:

$$\hat{A}_\mathcal{H}(t) = \hat{U}_\mathcal{H}^\dagger(t, t_0)\hat{A}\hat{U}_\mathcal{H}(t, t_0), \quad \text{with} \tag{C.26}$$

$$\hat{U}_\mathcal{H}(t, t_0) := \hat{T}\exp\left[-\frac{i}{\hbar}\int_{t_0}^t dt'\mathcal{H}(t')\right], \tag{C.27}$$

with $\hat{T}$ the time-ordering operator. We can combine these two equations to relate an operator in the Heisenberg picture with respect to $\mathcal{H}$ to one with respect to $\hat{H}$ with:

$$\hat{A}_\mathcal{H}(t) = \hat{U}_\mathcal{H}^\dagger(t, t_0)\hat{U}_H(t, t_0)\hat{A}_H(t)\hat{U}_H^\dagger(t, t_0)\hat{U}_\mathcal{H}(t, t_0), \tag{C.28}$$

i.e. by first transforming out the dependence on $\hat{H}$ and transforming in that on $\hat{\mathcal{H}}$. It is possible to show that a combined operator $V(t, t_0)$ representing the above transformation obeys[4]:

$$\hat{V}(t, t_0) := \hat{U}_H^\dagger(t, t_0)\hat{U}_\mathcal{H}(t, t_0) \tag{C.29}$$

$$= \hat{T}\exp\left[-\frac{i}{\hbar}\int_{t_0}^t dt'\,\hat{H}'_H(t')\right], \quad \text{where} \tag{C.30}$$

$$\hat{H}'_H(t) = \hat{U}_H^\dagger(t, t_0)\hat{H}'(t)\hat{U}_H(t, t_0). \tag{C.31}$$

By expansion, one can then prove the crucial rewriting [146]

$$\hat{A}_\mathcal{H}(t) = T_c\left\{\exp\left[-\frac{i}{\hbar}\left(\int_c dt'\hat{H}'_H(t')\right)\right]\hat{A}_H(t)\right\}, \tag{C.32}$$

where the subscript $_c$ represents the first "transformation" contour given in Fig. C.1 **a**.
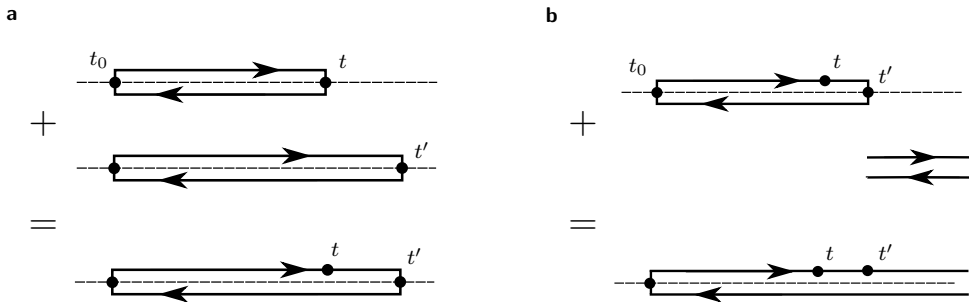
Figure C.1: Development of the Schwinger-Keldysh contour.

When this is applied to Green's functions, $G(t, t')$ (where we sporadically omit writing the spatial dependence), which consist of a pair of ordered operators, we then have

---

[4]The perturbation $\hat{H}'(t)$ is time-dependent and therefore also changes under the various pictures unlike in the usual time-independent case, where conservation of energy is explicit and ensures the constancy of the Hamiltonian $\hat{H}$, which is the same in all pictures.

the situation given in Fig. C.1 **a**, in which we depict that, due to the overlap of integrations in opposite directions on the t-axis, the two separate contours can be written as one. So the contour Green's function becomes:

$$
\begin{aligned}
G(t,t') &= -i\langle T_{\mathrm{c}}\big(\psi_{\mathcal{H}}(t)\psi_{\mathcal{H}}^{\dagger}(t')\big)\rangle, && \text{(C.33)} \\
&= i\Big\langle T_{\mathrm{c}}\Big\{ \exp\Big[-\frac{i}{\hbar}\Big(\int_{\mathrm{c}} dt'\, \hat{H}'_{H}(t')\Big)\Big]\psi_{H}(t)\psi_{H}^{\dagger}(t')\Big\}\Big\rangle. && \text{(C.34)}
\end{aligned}
$$

In addition, using the property $V(t,\infty)V^{\dagger}(t,\infty) = \mathbb{1}$ we can add a contour from $\sup\{t,t'\}$ to $+\infty$ and back as depicted in Fig. C.1 **b**.

Now suppose we also consider time-dependent interactions i.e. a Hamiltonian of the form $\hat{\mathcal{H}} = \hat{H}^0 + \hat{H}^{\mathrm{I}}(t) + \hat{H}'(t)$. Since our goal is the perturbation method, we transfer to the interaction representation in the same manner, now with just the free-field:

$$
G(t,t') = \Big\langle T_{\mathrm{c}}\Big\{\exp\Big[-\frac{i}{\hbar}\Big(\int_{\mathrm{c}} d\tilde{t}\,\big(\hat{H}^{I}_{H_0}(\tilde{t}) + \hat{H}'_{H_0}(\tilde{t})\big)\psi_{H_0}(t)\psi_{H_0}^{\dagger}(t')\Big]\Big\}\Big\rangle. \quad \text{(C.35)}
$$

What about the statistical averaging $\langle\rangle$? For our purposes we mention a crucial assumption, that the system was in thermal equilibrium at some point in the distant past t_0. Again appealing to the adiabatic theorem, this then allows the density matrix Eq. (C.6) to be written at this reference time in terms of $\hat{H}_0$, independent of interactions. The effect of the density matrix can then be represented by an additional contour beginning at t_0 and continuing straight to $t_0 - i\beta$, in a similar way to in the Matsubara formalism. However, when our main focus is on average quantities and time-independent effects, we can take $t_0 \to -\infty$ without loss of generality. If one of the Green's function's arguments were on this contour, then due to thermal fluctuations, any initial condition should be annulled when it is moved to the distant past, and the result should be equivalent to putting the argument on the real axis. This is an assumption that Green's functions fall off rapidly enough for a sufficiently large separation of their temporal components, a point which has been discussed in the literature [128]. This then gives us the *Schwinger-Keldysh closed time path* running from $-\infty$ to $+\infty$ and back.

Using Eq. (C.35) one can expand the exponential and formulate a non-equilibrium version of Wick's theorem which then yields perturbative Feynman rules [146]. These can be used in conjunction with a diagrammatic form of the possible Green's functions. We can define for instance:

$$
\begin{aligned}
G(t,t') &= \theta(t-t')G^{>}(t,t') + \theta(t'-t)G^{<}(t,t'), \quad \text{with} && \text{(C.36)} \\
G^{>}(t,t') &= -i\langle\psi(t)\psi^{\dagger}(t')\rangle, && \text{(C.37)} \\
G^{<}(t',t) &= \mp i\langle\psi^{\dagger}(t')\psi(t)\rangle, && \text{(C.38)}
\end{aligned}
$$

where the $\mp$ is for bosons and fermions respectively. The definite ordering implied by $G^{<}$, $G^{>}$ is depicted on the contour by having the earliest time occur on the increasing t branch, and the latest on the decreasing one. Likewise one can define an anti-time-ordered Green's function:

$$
\widetilde{G}(t,t') = -i\langle\widetilde{\mathcal{T}}\big(\psi(t)\psi^{\dagger}(t')\big)\rangle, \quad \text{(C.39)}
$$

for anti-time ordering operator $\widetilde{\mathcal{T}}$, which then has $G^{<}$, $G^{>}$ with points on the contour in the opposite fashion. Contrary to $G(t,t')$, which is depicted by both points

occurring on the upper branch, $\widetilde{G}(t,t')$ is represented by both points occurring on the lower branch and all four Green's functions occur naturally in the contour prescription. It proves useful to define a general Green's function in *Schwinger-Keldysh* space:

$$\hat{G}(t,t') = \begin{pmatrix} G(t,t') & G^<(t,t') \\ G^>(t,t') & \widetilde{G}(t,t') \end{pmatrix}. \tag{C.40}$$

All the different parts of this matrix are important. For example, $G^<(t,t')$ will turn out to be trivially related to the Wigner distribution function, the equation of motion of which is the *quantum Boltzmann equation*. We can develop this for an interaction with e.g. a scalar potential $V(\mathbf{x}',t')$ Fig. C.2, with the combined Green's function on the contour, parametrised by t':

$$G_{ik}^{(1)}(\mathbf{x},\mathbf{x}'',t,t') = \int d\mathbf{x}' \int dt' G_{ij}^{(0)}(\mathbf{x},\mathbf{x}',t,t') V_{jj'}(\mathbf{x}',t') G_{j'k}^{(0)}(\mathbf{x}',\mathbf{x}'',t',t''). \tag{C.41}$$

As time runs opposite on the reverse contour, this equation is consistent when:

$$V(\mathbf{x}',t')_{jj'} := V(\mathbf{x}',t')\sigma_{3\,jj'}, \tag{C.42}$$

for σ_3 the third Pauli matrix $\mathrm{diag}(1,-1)$. Then the Green's function for the tree-level scalar field interaction becomes:

$$\hat{G}^{(1)} = \hat{G}^{(0)} \otimes V\hat{G}^{(0)} = \hat{G}^{(0)}V \otimes \hat{G}^{(0)}, \tag{C.43}$$

where $\otimes$ represents matrix multiplication and spacetime integration. This formalism
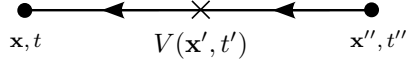

Figure C.2: Scattering off a classical potential.

is then further generalisable to interactions with e.g. fermion-boson vertices and eventually in a similar vein, non-equilibrium Feynman rules can be derived (see e.g. [147]). To finish this brief introduction, we mention a key observation that $G(t,t') + \widetilde{G}(t,t') - G^<(t,t') - G^>(t,t') = 0$. This allows a rotation in Schwinger-Keldysh space to reduce $\hat{G}$ to:

$$\hat{G}(t,t') = \begin{pmatrix} 0 & G^A \\ G^R & G^K \end{pmatrix}, \tag{C.44}$$

where:

$$\begin{aligned} G^R(t,t') &:= G(t,t') - G^<(t,t') &&= -i\theta(t-t')\langle[\psi(\mathbf{x},t),\psi^\dagger(\mathbf{x}',t')]_\mp\rangle, \\ G^A(t,t') &:= G(t,t') - G^>(t,t') &&= i\theta(t'-t)\langle[\psi(\mathbf{x},t),\psi^\dagger(\mathbf{x}',t')]_\mp\rangle, \\ G^K(t,t') &:= G^<(t,t') + G^>(t,t') &&= i\langle[\psi(\mathbf{x},t),\psi^\dagger(\mathbf{x}',t')]_\pm\rangle, \end{aligned} \tag{C.45}$$

are the *retarded* (and hence causal), *advanced* and *kinetic* Green's functions respectively, and the commutator $[]_\mp$ becomes an anti-commutator when dealing with fermions and vice versa for $[]_\pm$. Many physical quantities are retarded correlation functions, making $G^R(t,t')$ particularly important.

The Keldysh formalism is the most versatile discussed here and can even deal with initial correlations. It can be used in conjunction with the Matsubara technique e.g.

the substitution $i\omega_n \to \omega + i\delta$ in the Matsubara Green's function is an easier way to derive G^R in the Keldysh formalism [119]. However, it is unsuccessful at describing high-density, strongly-interacting, correlated systems such as liquid helium ^{3}He, ^{4}He, for which other methods have been developed. Since VPEs generally occur in weakly-correlated, weakly-interacting systems however, the Keldysh formalism should be suitable to describe such situations.

C.4   Hard Thermal Loops

After some inconsistent results from perturbation theory applied in high-temperature backgrounds ($T \gg m$, for a typical mass occurring in the theory m), such as a gauge-dependency of the damping rate of a plasma wave in a QGP (see references [3] in [29]), a breakthrough was made in the early 1990s [29, 28, 30], which showed how perturbation theory should be applied in the high-temperature limit. Some of the techniques of *hard thermal loop resummation* are reviewed in [97, 167], and we give a brief outline in this section.

Whenever heat is present in a quantum field theory, the standard quantum vacuum picture must be replaced by an *electron-positron-photon* plasma, due to the photon gas carrying the heat. This brings about the important change that such self-energy quantities as the polarisation operator, which have otherwise null vacuum expectation values, are finite in a plasma. The physical reason for this is similar to that for an external field. A photon can in principle decay into an electron-positron pair (see Fig. C.3), but in order to preserve four-momentum conservation, requires an additional photon to "seed" the process. In a photon gas or in other words, in a vacuum at finite temperature, both these requirements are fulfilled. As the pair creation amplitude is related to the imaginary part of the polarisation tensor (as shown in Eq. (A.23) in App. A.1.3), the polarisation tensor must be non-zero. As shown

Figure C.3: Pair creation from a photon of energy $\omega > 2m$ in an external field.

in Eq. (4.8) in Sec. 4.1, a non-zero polarisation operator implies that gauge bosons acquire a mass, in this case a *thermal mass*, $m_{\text{th}} \sim \sqrt{\Pi}$ (where the square root is understood as pertaining to the eigenvalues). Its presence in the exact propagator can be seen from the Dyson equation for the full photon self-energy Eq. (4.7). Considering the limit $T \gg m$, it can be shown that the leading-order QED photon self-energy is $\Pi^{(1)} = e^2 T^2 / 3$ [162, 73]. As mentioned in the introduction to Ch. 5, calculation of the polarisation operator runs into problems when the plasma frequency drops below that associated with virtual pairs (m), equivalent to $T \sim \sqrt{\alpha} m$. We show this by specifically considering the fermionic propagator we had at low temperature Eq. (4.3) in Ch. 4 for an external photon of initial momentum k_1:

$$S_F(P + k_1) = \frac{1}{[\gamma(\hat{P} + k_1)]^2 - m^2} \cdot \big(\gamma(\hat{P} + k_1) + m\big). \qquad (C.46)$$

We consider what occurs in the high-temperature limit $T \gg m$. First, masses should be inconsequential and so we set $m = 0$ in Eq. (C.46), and secondly at high temperature, we should make the replacement $k^2 \rightarrow k^2 + m_{\mathrm{th}}^2$. We notice:

$$\frac{\gamma(\hat{P} + k_1)}{\gamma[\hat{P} + k_1]^2 + m_{\mathrm{th}}^2} = \frac{\gamma(\hat{P} + k_1)}{\gamma[\hat{P} + k_1]^2} - \frac{m_{\mathrm{th}}^2}{\gamma[\hat{P} + k_1]^2 + m_{\mathrm{th}}^2} \frac{\gamma(\hat{P} + k_1)}{\gamma[\hat{P} + k_1]^2}, \qquad \text{(C.47)}$$

and so for small k_1 and large enough m_{th}^2, the correction due to the thermal mass becomes as large as the original term itself, meaning a breakdown in the perturbation approach, leading to an infra-red divergence. This is essentially because the approximation $\Pi \approx \Pi^{(1)}$ we make at $T \ll \sqrt{\alpha}m$ is no longer an approximate solution to the Dyson equation at high temperature.

In reality, in a thermal distribution at temperature $T \gg m$, the contribution from *soft* momenta ($k \sim \sqrt{\alpha}T$) to the polarisation operator should be negligible[5]. Braaten and Pisarski devised a method to solve this problem called *hard thermal loop resummation* that consists of replacing bare propagators that carry soft momenta with ones with a self-energy insertion, in which the momentum integral is restricted to *hard momenta* $\sim T$, i.e. to the actual dominant physical contribution. So in the high-temperature limit, for soft external momenta, a contribution to our polarisation diagram, in which we don't consider the change in vertices which in general would also have to be resummed, would become Fig. C.4 (see also [12]), in which the sum over soft fermion momenta S involves effective propagators. These effective propagators then correspond to self-energy insertions with an integral only over hard momenta, H. vertices and fermionic propagators have been replaced by effective versions (an example of this is also found in [166]). This corresponds in the case of the
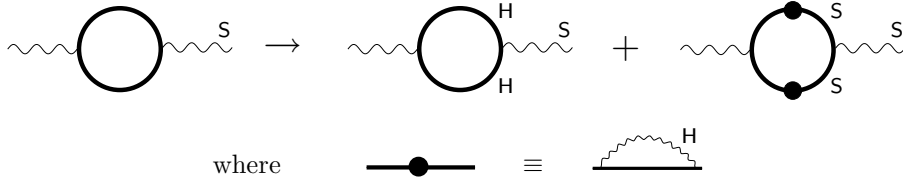

Figure C.4: Polarisation operator with HTL-resummed internal propagators involving hard momenta H and soft momenta S.

fermionic propagator to:

$$\begin{aligned} S_F(P + k) &\rightarrow S_F(P + k)\Big[\int d^4k' S_F(P + k + k')\gamma D_F(k')\gamma\Big] S_F(P + k) \\ &\rightarrow S_F(P + k)\Big[\int d^4k' S_F(k')\gamma D_F(k')\gamma\Big] S_F(P + k). \end{aligned} \qquad \text{(C.48)}$$

Although hard thermal loop resummation has been successfully used for $T \gg m$, there lacks an approach which deals with the transition between the soft and hard regimes.

HTL resummation has been successful in removing infra-red divergences in the high-temperature limit, and restoring gauge-invariance to amplitudes involving soft

---

[5]The assumption is that the distribution function drops off sufficiently quickly on the lower side of the average photon energy. For thermal ensembles, this seems realistic, but the assumption can also be used to describe non-equilibrium phenomena [166].

external momenta. Quantities that are sensitive to *super-soft* external momenta ($T \sim \alpha^2 m$) however, such as damping rates of hard partons in the QGP [114] have to be tackled by further developing the Braaten-Pisarski method. For the QED polarisation operator, if the external momenta are hard, bare propagators can be used. To include soft external momenta, HTL resummation must be employed.

Bibliography

[1] A. A. Abrikosov, L. P. Gorkov, and I. E. Dzyaloshinski, *Methods of quantum field theory in statistical physics*, Prentice-Hall, Engelwood Cliffs, N. J., 1963.

[2] S. L. Adler, *Photon splitting and photon dispersion in a strong magnetic field*, Ann. Phys. **67** (1971), 2, 599–647.

[3] M. Ahlers et al., *Light from the hidden sector: Experimental signatures of paraphotons*, Phys. Rev. D **76** (2007), 115005.

[4] ———, *Laser experiments explore the hidden sector*, Phys. Rev. D **77** (2008), 095001.

[5] G. B. Airy, Trans. Camb. Phil. Soc. vi (1838), 379–402.

[6] Sh. Zh. Akhmadaliev et al., *Experimental investigation of high-energy photon splitting in atomic fields*, Phys. Rev. A **89** (2002), 061802.

[7] A. G. Aksenov, R. Ruffini, and G. V. Vereshchagin, *Thermalization of nonequilibrium electron-positron-photon plasmas*, Phys. Rev. Lett. **99** (2007), 125003.

[8] ANDOR technology, *X-ray cameras*, http://www.andor.com/scientific_cameras/xray/, (2008).

[9] M. R. Andrews et al., *Observation of interference between two Bose condensates*, Science **275** (1997), 637.

[10] G. S. Anufriev, B. S. Boltenkov, and A. I. Ryabinkov, *High-resolution mass spectra of the residual gas in a metallic vacuum system*, Technical Physics **51** (2006), 1, 100–111.

[11] M. Arndt et al., *Wave-particle duality of C60 molecules*, Nature **401** (1999), 680–682.

[12] M. Le Ballac, *Thermal field theory*, Cambridge, The Pitt Building, Trumpington Street, Cambridge, United Kingdom, 2000.

[13] M. A. Bandres and J. C. Gutierrez-Vega, *Ince Gaussian beams*, Opt. Lett. **29** (2004), 2, 144–146.

[14] M. G. Baring, *Photon splitting and pair conversion in strong magnetic fields*, AIP Conf. Proc. **1051** (2008), 53–64.

[15] I. A. Batalin and A. E. Shabad, Sov. Phys. JETP **33** (1971), 483.

[16] V. N. Baǐer, V. M. Katkov, A. I. Mil'shteǐn, and V. M. Strakhovenko, *The theory of quantum processes in the field of a strong electromagnetic wave*, Sov. Phys. JETP **42** (1976), 3, 400–407.

[17] V. N. Baǐer, V. M. Katkov, and V. M. Strakhovenko, Sov. Phys. JETP **40** (1975), 225.

[18] ———, Sov. Phys. JETP **41** (1975), 198.

[19] V. N. Baǐer, A. I. Mil'shteǐn, and V. M. Strakhovenko, *Interaction between a photon and an intense elctromagnetic wave*, Sov. Phys. JETP **42** (1976), 6, 961–965.

[20] A. R. Bell and John G. Kirk, *Possibility of prolific pair production with high-power lasers*, Phys. Rev. Lett. **101** (2008), 200403.

[21] C. M. Bender, *Introduction to nonlinear waves and shocks*, University of Heidelberg, unpublished lectures, (2009).

[22] C. M. Bender and S. A. Orszag, *Advanced mathematical methods for scientists and engineers*, Springer, 1978.

[23] V. B. Berestetskii, E. M. Lifshitz, and L. P. Pitaevskii, *Quantum electrodynamics (second edition)*, Butterworth-Heinemann, Linacre House, Jordan Hill, Oxford OX2 8DP, UK, 1982.

[24] D. Bernard et al., *Search for stimulated photon-photon scattering in vacuum*, Eur. Phys. J. D **10** (2000), 141–145.

[25] M. S. Bessell, *UBVRI Passbands*, Publications of the Astronomical Society of the Pacific **102** (1990), 1181–1199.

[26] Z. Bialynicka-Birula and I. Bialynicka-Birula, *Nonlinear effects in quantum electrodynamics. photon propagation and photon splitting in an external field*, Phys. Rev. D **2** (1970), 10, 2341–2345.

[27] N. N. Bogolyubov and D. V. Shirkov, *Introduction to the theory of quantized fields*, Nauka, 1973.

[28] E. Braaten and R. D. Pisarski, *Deducing hard thermal loops from Ward identities*, Nucl. Phys. B **339** (1990), 310–324.

[29] ———, *Soft amplitudes in hot gauge theories: A general analysis*, Nucl. Phys. B **337** (1990), 569–634.

[30] ———, *Simple effective Lagrangian for hard thermal loops*, Phys. Rev. D **45** (1992), R1827.

[31] M. Bregant, G. Zavattini, et al., Phys. Rev. D **78** (2008), 032006.

[32] G. Brodin et al., *Quantum-electrodynamical photon splitting in magnetized nonlinear pair plasmas*, Phys. Rev. Lett. **98** (2007), 125001.

[33] Brookhaven National Laboratory, *RHIC — Relativistic Heavy Ion Collider*, http://www.bnl.gov/rhic/, (2010).

[34] D. L. Burke et al., *Positron production in multiphoton light-by-light scattering*, Phys. Rev. Lett. **79** (1997), 1626.

[35] P. Candelas, *Vacuum polarization in Schwarzschild spacetime*, Phys. Rev. D **21** (1980), 8, 2185–2202.

[36] O. Carnal and J. Mlynek, *Young's double-slit experiment with atoms: A simple atom interferometer*, Phys. Rev. Lett. **66** (1991), 21, 2689–2692.

[37] Stanford Linear Accelerator Center, Lawrence Livermore National Laboratory, and Argonne National Laboratory, *Linac Coherent Light Source (LCLS) Conceptual Design Report*, http://www-ssrl.slac.stanford.edu/lcls/cdr/, (2002).

[38] CERN, *A Large Ion Collider Experiment*, http://aliceinfo.cern.ch/, (2010).

[39] C-F. Chang, K. Cheung, and T-C. Yuan, *Unparticle effects in photon-photon scattering*, Phys. Lett. B **4** (2008), 646, 291–294.

[40] R. A. Cover and G. Kalman, *Longitudinal, Massive Photon in an External Magnetic Field*, Phys. Rev. Lett. **33** (1974), 1113.

[41] P. H. Cox, W. S. Hellman, and A. Yildiz, *Finite temperature corrections to field theory: Electron mass and magnetic moment, and vacuum energy*, Ann. Phys. **154** (1984), 1, 211–228.

[42] C. G. Darwin, *The wave equations of the electron*, Z. Phys. **118** (1928), 654–680.

[43] A. Das, *Finite temperature field theory*, World Scientific, P O Box 128, Farrer Road, Singapore 912805, 1999.

[44] A. Das and J. Frenkel, *Thermal operator and dispersion relation in qed at finite temperature and chemical potential*, Phys. Rev. D **76** (2007), 087701.

[45] C. Davisson and L. H. Germer, *The scattering of electrons by a single crystal of nickel*, Nature **119** (1927), 558–560.

[46] S. P. Dawson and C. J. Fewster, *An explicit quantum weak energy inequality for dirac fields in curved spacetimes*, arXiv:gr-qc/0604106v2, 2006.

[47] P. A. M. Dirac, *The principles of quantum mechanics (4th edition)*, Oxford University Press, 1958.

[48] W. Dittrich, *Effective Lagrangians at finite temperature*, Phys. Rev. D **19** (1979), 8, 2385–2390.

[49] W. Dittrich and H. Gies, *Probing the quantum vacuum*, Springer-Verlag, Berlin, Germany, 2000.

[50] W. Dittrich and M. Reuter, *Effective Lagrangians in Quantum Dynamics*, Springer-Verlag, Berlin, 1985.

[51] W. Dittrich and R. Shaisultanov, *Vacuum polarization in QED with world-line methods*, Phys. Rev. D **62** (2000), 4, 045024.

[52] G. V. Dunne, *Functional determinants in quantum field theory*, 14th Saalburg Summer School, unpublished lectures, 2008.

[53] G. V. Dunne, H. Gies, and R. Schützhold, *Catalysis of Schwinger vacuum pair production*, Phys. Rev. D **80** (2009), 111301.

[54] G. V. Dunne and C. Schubert, *Two-loop Euler-Heisenberg QED pair-production rate*, Nucl. Phys. B **564** (2000), 3, 591–604.

[55] F. J. Dyson, *The S matrix in quantum electrodynamics*, Phys. Rev. **75** (1949), 1736–1755.

[56] ——, *Divergence of perturbation theory in quantum electrodynamics*, Phys. Rev. **85** (1952), 4, 631–632.

[57] P. Elmfors and B-S. Skagerstam, *Electromagnetic fields in a thermal background*, Phys. Lett. B **348** (1995), 141–148.

[58] ——, *Thermally induced photon splitting*, Phys. Lett. B **427** (1998), 197–205.

[59] J. Enderlein and F. Pampaloni, *Unified operator approach for deriving Hermite-Gaussian and Laguerre-Gaussian laser modes*, J. Opt. Soc. Am. A **21** (2004), 8, 1553–1558.

[60] European Light Infrastructure (ELI), *ELI Scientific Case*, http://www.extreme-light-infrastructure.eu/Publications_2_4.php, (2007).

[61] T. S. Evans, *What is being calculated with thermal field theory?*, http://arXiv:hep-ph/9404262v2, 1994.

[62] A. M. Fedotov and N. B. Narozhny, *Generation of harmonics by a focused laser beam in the vacuum*, Phys. Lett. A **362** (2006), 1–5.

[63] A. Ferrando et al., *Nonlinear phase shift from photon-photon scattering in vacuum*, Phys. Rev. Lett. **99** (2007), 150404.

[64] P. C. Ferreira and J. D. de Deus, *QCD corrections to QED vacuum polarization*, Eur. Phys. J. C **54** (2008), 539–545.

[65] R. P. Feynman, *Space-time approach to quantum electrodynamics*, Phys. Rev. **76** (1949), 769–789.

[66] ——, *Statistical mechanics*, Addison-Wesley, California, USA, 1988.

[67] C. B. P. Finn, *Thermal physics (second edition)*, Chapman & Hall, 2-6 Boundary Row, London SE1 8HN, 1993.

[68] Free electron LASer in Hamburg, *Flash*, http://flash.desy.de, (2009).

[69] K. Fredenhagen, K-H. Rehren, and E. Seiler, *Quantum field theory: Where we are*, Lec. Notes Phys. **721** (2007), 61–87.

[70] W. H. Furry, *On bound states and scattering in positron theory*, Phys. Rev. **81** (1951), 115–124.

[71] A. J. Ganguly, P. K. Kaw, and J. C. Parikh, *Thermal tunneling of $q\bar{q}$ pairs in A-A collisions*, Phys. Rev. C **51** (1995), 2091.

[72] M. Gell-Mann and K. Brueckner, *Correlation energy of an electron gas at high density*, Phys. Rev. **106** (1957), 364–368.

[73] H. Gies, *QED effective action at finite temperature*, Phys. Rev. D **60** (1999), 105002.

[74] ———, *QED effective action at finite temperature: Two-loop dominance*, Phys. Rev. D **61** (2000), 085021.

[75] ———, *Strong laser fields as a probe for fundamental physics*, Eur. Phys. J. D **55** (2009), 311–317.

[76] N. K. Glendenning, *Vacuum polarization effects on nuclear matter and neutron stars*, Nucl. Phys. A **493** (1989), 3–4, 521.

[77] J. Goodman, Astrophys. J. **308** (1986), L47.

[78] W. Gordon, Z. Phys. **48** (1928), 3–4, 180–191.

[79] GSI Helmholtzzentrum für Schwerionenforschung GmbH, *FAIR - Facility for Antiproton and Ion Research*, http://www.gsi.de/fair/index_e.html, (2010).

[80] E. I. Guendelman, *Photon and axion splitting in an inhomogeneous magnetic field*, Phys. Lett. B **662** (2008), 445–448.

[81] L. Hackermüller et al., *Wave nature of biomolecules and fluorofullerenes*, Phys. Rev. Lett. **91** (2003), 9.

[82] T. Heinzl et al., *On the observation of vacuum birefringence*, Opt. Commun. **267** (2006), 318–321.

[83] W. Heisenberg, *Der Teil und das Ganze*, R. Piper & Co Verlag, Munich, 1981.

[84] W. Heisenberg and H. Euler, *Photon acceleration in vacuum*, Z. Phys. **98** (1936), 714.

[85] J. S. Heyl and L. Hernquist, *Birefringence and dichroism of the QED vacuum*, J. Phys. A: Math. Gen. **30** (1997), 6485–6492.

[86] High Power laser Energy Research (HiPER), *HiPER Technical Background and Conceptual Design Report*, http://www.hiperlaser.org/docs/tdr/HiPERTDR2.pdf, (2007).

[87] W. A. Hiscock and D. A. Konkowski, *Quantum vacuum energy in Taub-NUT (Newman-Unti-Tamburino)-type cosmologies*, Phys. Rev. D **26** (1982), 6, 1225–1230.

[88] W. C. G. Ho and D. Lai, *Atmospheres and spectra of strongly magnetized neutron stars - II. the effect of vacuum polarization*, Monthly Notices of the Royal Astronomical Society **338** (1982), 1, 232–252.

[89] K. Hornberger et al., *Collisional decoherence observed in matter wave interferometry*, Phys. Rev. Lett. **90** (2003), 160401.

[90] J. F. Hua et al., *High-order corrected fields of ultrashort, tightly focused laser pulses*, Applied Physics Letters **85** (2004), 17, 3705–3707.

[91] C. J. Isham, *Lectures on quantum theory*, Imperial College Press, 57 Shelton Street, Covent Garden, London WC2H 9HE, 2008.

[92] C. Itzykson and J-B. Zuber, *Quantum field theory*, McGraw-Hill, New York, 1980.

[93] J. D. Jackson, *Classical electrodynamics (3rd edition)*, John Wiley & Sons, Inc., New York, 1999.

[94] C. Jönsson, Z. Phys. **161** (1961), 454–474.

[95] M. Kac, *Can one hear the shape of a drum?*, Amer. Math. Monthly **73** (1966), 1–23.

[96] M. Kamionkowski and J. N. Bahcall, *The rate of the proton-proton reaction*, the Astrophysical Journal (1993), 420, 884–891.

[97] J. I. Kapusta and C. Gale, *Finite-temperature field theory (second edition)*, Cambridge University Press, The Edinburgh Building, Cambridge CB2 2RU, UK, 2006.

[98] E. Karimi et al., *Hypergeometric-Gaussian beams*, Opt. Lett. **32** (2004), 21, 3053–3055.

[99] L. V. Keldysh, *Diagram technique for nonequilbrium processes*, Sov. Phys. JETP **20** (1965), 4, 1018–1026.

[100] M. Kiffner, J. Evers, and C. H. Keitel, *Quantum interference enforced by time-energy complementarity*, Phys. Rev. Lett. **96** (2006), 100403.

[101] B. King, A. Di Piazza, and C. H. Keitel, *Double-slit vacuum polarisation effects in ultra-intense laser fields*, (to be submitted).

[102] ———, *A matterless double-slit*, Nature Photon. **4** (2010), 92–94.

[103] J. G. Kirk, A. R. Bell, and I. Arka, *Pair production in counter-propagating laser beams*, Plasma Phys. Control. Fusion **51** (2009), 085008.

[104] O. Klein, *Die Reflexion von Elektronen an einem Potentialsprung nach der relativistischen Dynamik von Dirac*, Z. Phys. **53** (1929), 3–4, 157–165.

[105] H. Kleinert, *Path integrals in quantum mechanics, statistics, polymer physics, and financial markets (3rd edition)*, World Scientific Publishing, 2004.

[106] B. A. Kniehl, *Two-loop corrections to the vacuum polarizations in perturbative QCD*, Nucl. Phys. B **347** (1990), 1–2, 86–104.

[107] J. Kondo, *Resistance minimum in dilute magnetic alloys*, Prog. Theo. Phys. **32** (1964), 1, 37–49.

[108] V. V. Kotlyar et al., *Hypergeometric modes*, Opt. Lett. **32** (2007), 742–744.

[109] W. E. Lamb and R. C. Retherford, *Fine structure of hydrogen by a microwave method*, Phys. Rev. **72** (1947), 241–243.

[110] L. D. Landau, E. M. Lifshitz, and L. P. Pitaevskii, *Statistical physics*, Butterworth-Heinemann, Linacre House, Jordan Hill, Oxford OX2 8DP, UK, 1996.

[111] J. S. Langer, *Theory of impurity resistance in metals*, Phys. Rev. **120** (1960), 714.

[112] _____, *Some considerations of analyticity in the many-fermion problem*, Phys. Rev. **124** (1961), 997.

[113] I. D. Lawrie, *On the relationship between thermo field dynamics and quantum statistical dynamics*, J. Phys. A: Math. Gen. **27** (1994), 1435–1452.

[114] S. Leupold and M. H. Thoma, *Soft thermal loops in scalar quantum electrodynamics*, Phys. Lett. B (1999), 465, 249–253.

[115] L. Levi, *Applied optics*, John Wiley & Sons, Inc., New York, 1968.

[116] F. Lindner et al., *Attosecond double-slit experiment*, Phys. Rev. Lett. **95** (2005), 040401.

[117] M. Loewe and J. C. Rojas, *Thermal effects and the effective action of quantum electrodynamics*, Phys. Rev. D **46** (1992), 6, 2689–2693.

[118] E. Lundström et al., *Using high-power lasers for detection of elastic photon-photon scattering*, Phys. Rev. Lett. **96** (2006), 8, 083602.

[119] G. D. Mahan, *Many-particle physics*, Plenum Press, 233 Spring Street, New York, N.Y. 10013, 1990.

[120] F. Mandl and G. Shaw, *Quantum field theory*, John Wiley & Sons, 1986.

[121] M. Marklund, G. Brodin, and L. Stenflo, *Electromagnetic wave collapse in a radiation background*, Phys. Rev. Lett. **91** (2003), 163601.

[122] M. Marklund, B. Eliasson, and P. K. Shukla, Sov. Phys. JETP **79** (2004), 208.

[123] M. Marklund and P. K. Shukla, *Nonlinear collective effects in photon-photon and photon-plasma interactions*, Rev. Mod. Phys. **78** (2006), 591.

[124] T. Matsubara, *A new approach to quantum-statistical mechanics*, Prog. Theo. Phys. **14** (1955), 351.

[125] J. A. Mendez et al., *A Multi-Frame, Megahertz CCD Imager*, IEEE Transaction on Nuclear Science **56** (2009), 3, 1188–1192.

[126] J. T. Mendonca et al., *Photon acceleration in vacuum*, Phys. Lett. A **359** (2006), 700–704.

[127] P. G. Merli, G. F. Missiroli, and G. Pozzi, Am. J. Phys. **44** (1976), 306–307.

[128] R. Mills, *Propagators for many-particle systems*, Gordon and Breach, New York, 1969.

[129] A. I. Milstein et al., *Laser-dressed vacuum polarization in a Coulomb field*, Phys. Rev. A **72** (2005), 052104.

[130] A. I. Milstein and M. Schumacher, *Present status of Delbrück scattering*, Phys. Rep. **243** (1994), 183–214.

[131] H. Mimura et al., *Breaking the 10nm barrier in hard-X-ray focusing*, Nature Photon. **6** (2010), 2, 122–124.

[132] A. Minguzzi, Nuovo Cimento **4** (1956), 476.

[133] M. H. Mittleman and F. A. Wolf, *Coherent scattering of photons by atomic hydrogen*, Phys. Rep. **128** (1962), 2686.

[134] M. Nakatsutsumi et al., *Space and time resolved measurements of the heating of solids to ten million kelvin by a petawatt laser*, New J. Phys. **10** (2008), 043046.

[135] N. B. Narozhny et al., *e^+e^--pair production by a focused laser pulse in vacuum*, Phys. Lett. A **330** (2004), 1–6.

[136] N. B. Narozhnyǐ, *Propagation of plane electromagnetic waves in a constant field*, Sov. Phys. JETP **28** (1969), 2, 371–374.

[137] F. W. J. Olver, *Asymptotics and special functions*, AKP Classics, A K Peters Ltd., 63 South Avenue, Natick, MA 01760, 1997.

[138] F. Özel, *Surface emission properties of strongly magnetic neutron stars*, Astrophys. J. (2001), 563, 276–288.

[139] P. K. Patel et al., *Integrated laser-target interaction experiments on the RAL petawatt laser*, Controlled Fusion **47** (2005), B833.

[140] M. E. Peskin and D. V. Schroeder, *An introduction to quantum field theory*, Westview, 1995.

[141] A. Di Piazza, K. Z. Hatsagortsyan, and C. H. Keitel, *Harmonic generation from laser-driven vacuum*, Phys. Rev. D **72** (2005), 085005.

[142] _____, *Light diffraction by a strong standing electromagnetic wave*, Phys. Rev. Lett. **97** (2006), 083603.

[143] Princeton Instruments, *Imaging applications*, http://www.princetoninstruments.com/products/imcam/, 2010.

[144] T. Prokopec and R. Woodard, *Photon mass from inflation*, Phys. Rev. Lett. **89** (2002), 10, 101301.

[145] J. J. Quinn and R. A. Ferrell, *Electron self-energy approach to correlation in a degenerate electron gas*, Phys. Rev. **112** (1958), 812.

[146] J. Rammer, *Quantum field thoery of non-equilibrium states*, Cambridge University Press, The Edinburgh building, Cambridge CB2 8RU, UK, 2007.

[147] J. Rammer and H. Smith, *Quantum field-theoretical methods in transport theory of metals*, Rev. Mod. Phys. **58** (1986), 2, 323–359.

[148] P. J. Redmond, *Solution of the Klein-Gordon and Dirac equations for a particle with a plane electromagnetic wave and a parallel magnetic field*, J. Math. Phys. **6** (1965), 1163.

[149] L. E. Reichl, *A modern course in statistical physics (second edition)*, John Wiley & Sons, Inc., 605 Third Avenue, New York, NY 10158-0012, 1998.

[150] V. I. Ritus, *Radiative corrections in quantum electrodynamics with intense field and their analytical properties*, Ann. Phys. **69** (1972), 555–582.

[151] _____, *Quantum effects of the interaction of elementary particles with an intense electromagnetic field*, J. Russ. Laser Res. **6** (1985), 5, 497–617.

[152] L. H. Ryder, *Quantum field theory (second edition)*, Cambridge, 1996.

[153] A. D. Sakharov, *Violation of CP invariance, C asymmetry, and baryon asymmetry of the universe*, Sov. Phys. JETP **5** (2007), 1, 24–27.

[154] Y. I. Salamin, *Fields of a Gaussian beam beyond the paraxial approximation*, Appl. Phys. B **86** (2007), 319–326.

[155] Y. I. Salamin and others, *Relativistic high-power laser-matter interactions*, Phys. Rep. **427** (2006), 2–3, 41–155.

[156] F. Sauter, Z. Phys. **69** (1931), 742.

[157] J. Schwinger, *Quantum electrodynamics. I. A covariant formulation*, Phys. Rev. **74** (1948), 1439–1461.

[158] _____, *On gauge invariance and vacuum polarization*, Phys. Rev. **82** (1951), 664–679.

[159] M. O. Scully, B-G. Englert, and H. Walther, *Quantum optical tests of complementarity*, Nature (London) **351** (1991), 111.

[160] A. E. Shabad, Ann. Phys. **90** (1975), 166.

[161] P. K. Shukla and B. Eliasson, *Modulational and filamentational instabilities of intense photon pulses and their dynamics in a photon gas*, Phys. Rev. Lett. **92** (2004), 073601.

[162] E. V. Shuryak, Sov. Phys. JETP **47** (1978), 212.

[163] Y. Takahashi and H. Umezawa, *Thermo field dynamics*, Collective Phenomena **2** (1975), 55.

[164] _____, *Thermo field dynamics*, IJMPB **10** (1996), 13–14, 1755–1805.

[165] G. I. Taylor, Proc. Cam. Philos. Soc. **15** (1909), 114–115.

[166] M. H. Thoma, *Ward identities in nonequilibrium QED*, Phys. Rev. D **58** (1998), 085025.

[167] _____, *New developments and applications of thermal field theory*, arXiv:hep-ph/0010164v1, 2000.

[168] _____, *Photon-photon interaction in a photon gas*, Europhys. Lett. **52** (2000), 5, 498–503.

[169] D. Tommasini et al., *Detecting photon-photon scattering in vacuum at exawatt lasers*, Phys. Rev. A **77** (2008), 042101.

[170] _____, *Precision tests of QED and non-standard models by searching photon-photon scattering in vacuum with high power lasers*, JHIP (2009), 11, 43.

[171] A. Tonomura et al., *Demonstration of single-electron build-up of an interference pattern*, Am. J. Phys. **57** (1989), 117–120.

[172] W. Tsai and T. Erber, *Photon pair creation in intense magnetic fields*, Phys. Rev. D **10** (1974), 2, 492–499.

[173] _____ , *Propagation of photons in homogeneous magnetic fields: Index of refraction*, Phys. Rev. D **12** (1975), 4.

[174] _____ , Acta Phys. Austriaca **45** (1976), 245.

[175] L. F. Urrutia, *Vacuum polarization in parallel homogeneous electric and magnetic fields*, Phys. Rev. D **17** (1978), 8, 1977–1984.

[176] A. A. Varfolomeev, Sov. Phys. JETP **23** (1966), 681.

[177] D. M. Volkov, Z. Phys. **94** (1935), 250.

[178] CLF Facilities Vulcan, *Vulcan glass laser*, http://www.clf.rl.ac.uk/Facilities/vulcan/index.htm, (2010).

[179] J. F. C. Wardle et al., *Electronpositron jets associated with the quasar 3C279*, Nature (London) **395** (1998), 457.

[180] G. N. Watson, *Theory of bessel functions*, Cambridge, 200 Euston Road, London, NW1, 1951.

[181] V. Weisskopf, *Über die Elektrodynamik des Vakuums auf Grund der Quantentheorie des Elektrons*, Mat.-fys. Medd. **14** (1936), 6, 6.

[182] H. A. Weldon, *Covariant calculations at finite temperature: The relativistic plasma*, Phys. Rev. D **26** (1982), 6, 1394–1407.

[183] R. R. Wilson, *Scattering of 1.3³ MeV Gamma-Rays by an Electric Field*, Phys. Rev. **90** (1953), 720–721.

[184] H. Wiseman and F. Harrison, *Uncertainty over complementarity?*, Nature (London) **377** (1995), 584.

[185] X-Ray Free-Electron Laser (XFEL), *The European X-Ray Free-Electron Laser Technical Design Report*, http://xfel.desy.de/tdr/tdr, (July 2007).

[186] Z. Yan et al., *Accurate description of ultra-short tightly focused Gaussian laser pulses and vacuum laser acceleration*, Appl. Phys. B **81** (2005), 813–819.

[187] V. Yanovsky et al., *Ultra-high intensity- 300-TW laser at 0.1 Hz repetition rate*, Opt. Express **16** (2008), 2109–2114.

[188] T. Young, *Experiments and calculations relative to physical optics*, Philos. Trans. R. Soc. London **94** (1804), 1.

[189] E. Zavattini et al., Phys. Rev. D **77** (2008), 032006.

[190] A. Zeilinger et al., *Single- and double-slit diffraction of neutrons*, Rev. Mod. Phys. **60** (1988), 4, 1067–1073.

Acknowledgments

There seems to be two schools of thought of how science and human understanding progresses. One hypothesis deems the revolutionary paradigm shifts introduced by a very few to be the driving component with other scientists simply filling in the gaps, whilst the Ortega hypothesis actually views the smaller contributions made by the scientific masses to be quintessential to progress. I like to think that the process of "research" is no dissimilar to that of ocean waves eroding the cliffs of great land masses, a scale-free phenomenon that permeates the entire natural world from the distribution of sizes of raindrops to the magnitude of earthquakes. In a similar vein, I wish to thank the many people whose contribution were crucial to the development and production of this thesis.

First thanks go to Prof. Christoph H. Keitel for accepting me as a student in his theoretical quantum dynamics department and providing crucial seasoned guidance during difficult stages of the project. I am indebted to Antonino Di Piazza, whose enthusiasm, creativity and expert physical intuition were the trigger for some very interesting work.

I thank Peter Brunner for the excellent technical support who helped remove various obstacles in the way of progress and also for his generally refreshing good nature and positive influence and I also acknowledge the logistical support from Sibel Babacan and Vera Beyer in efficiently guiding me round the eccentricity of German bureaucracy.

I acknowledge Antonino Di Piazza's helpful proof-reading and suggestions for sections of the thesis and also thank the guidance from Markus Thoma through the intricacies of finite temperature field field theory and the tips from Andreas Ipp on hard thermal loops. I also wish to thank Prof. Carl Bender for his inspiring lectures and uplifting discussions.

Many thanks go to Robert Fleischhaker for the games of go and his refreshing view of the world, which has at many times allowed me to find my way again after being blown off course by the turmoils a PhD student seems to necessarily undergo. I also thank Michael Ruggenthaler and Matthias Ruf for their openness to questions on the finer parts of mathematics and to Erik Lötstedt for his infectious enthusiasm for all things QED-related. I give a nod in the direction of members of my former office, who created such a positive working atmosphere and helped me settle in: Henrik Hetzheim also for the productive laser-based discussions, Hosein Ebadi, Mario Verschl and Martin Kiffner and to members of my current office who have always been open to scientific discussion, participating in the revival of the once forlorn journal club: Anis Dadi, Benjamin Galow and Octavian Postavaru. I also thank